LUND UNIVERSITY

Methods of characterization of pore structure

Fagerlund, Göran

1973

Citation for published version (APA):
Fagerlund, G. (1973). *Methods of characterization of pore structure.* (Report 41). Tid. Institutionen för byggnadsteknik, Tekniska högskolan i Lund.

Total number of authors:
1

METHODS OF CHARACTERIZA- TION OF PORE STRUCTURE

3 CONTRIBUTIONS TO RILEM COMMITTEE PORE STRUCTURE AND PROPERTIES OF MATERIALS

GÖRAN FAGERLUND

C O N T E N T S

PREFACE

PREFACE

The three reports included in this volume are my main contribution to the work within the RILEM-committee "Pore Structure and Properties of Materials". The reports will be published in the RILEM paper "Materials and Structures" presumably during 1973 together with about 20 other reports also dealing with methods of characterization of pore structure.

The committee was initiated by mr Tenho Sneck from Finland and started its work in the summer 1970. It will conclude its work in september 1973 by a symposium in Prague sponsored by the two international organizations RILEM and IUPAC (International Union for Pure and Applied Chemistry). The name of the Symposium is the same as that of the committee.

The aim of the committee was drawn up by mr Sneck. It can be divided in two parts

1. Collecting and discussing methods of investigating pore properties.

2. Analysis of connections between pore structure and materials properties.

So far the main activities have been concentrated on part 1.

Part 2 was considered to be the most important part by mr Sneck and many others myself included. However the committee participants are in general more interested and able in pore structure analysis.

Part 2 has however not been completely neglected. It has resulted in a report (1), which is "performance oriented". Besides the symposium in Prague will be divided in two parts in the same way as parts 1 and 2 above.

I myself has published a work (2) on connections between pore structure and mechanical properties. This work is directly initiated by the work within the committee.

I want to thank mr Tenho Sneck who invited me to become member in the committee, professor Sven G Bergström, who always encouraged me in the work and the Swedish Council for Building Research, which has made it financially possible for me to participate in the committee meetings.

Lund 23 January 1973

Göran Fagerlund

LITERATURE

(1) J M Haynes & T Sneck: "Pore Properties in the Evaluation of Materials". Proceedings vol 1 from the joint RILEM-ASTM-CIB Symposium "Performance concept in Buildings" in Philadelphia 1972. (NBS Special Publication 361. US Department of Commerce).

(2) G Fagerlund: "Connections between Porosity and Mechanical Properties of Materials". Report 26. Division of Build. Technol. Lund Inst. of Technol. Lund 1972. (In Swedish).

I

DETERMINATION OF PORE-SIZE DISTRIBUTION BY SUCTION POROSIMETRY

Contribution to RILEM committee

"Pore Structure and Properties of Materials (PM)"

by

Göran Fagerlund

CONTENTS

Lund, September 1972

INTRODUCTION

The concept "suction porosimetry" is used as a joint concept for all
methods where a wetting liquid is involved in the measurements. Conse-
quently not only pure suction experiments are taken into account but
also methods based upon centrifugation and displacement from the pores
of a wetting liquid by another liquid or a gas.

The basic equation is the same as for mercury porosimetry, viz the Laplace
equation for the pressure difference across the curved interface liquid-
gas or liquid-liquid.

$$\Delta p = -\sigma_{ij} \cdot \cos \theta \left(\frac{1}{r_1} + \frac{1}{r_2}\right) = \frac{-2 \cdot \sigma_{ij} \cdot \cos \theta}{r} \qquad (1)$$

where r_1 and r_2 are the principal radii of curvature of the menisci while
r is a sort of mean radius. The negative value of Δp indicates that the
pressure is lower on the convex side of the meniscus.

The only essential difference between suction porosimetry and mercury
porosimetry is the effect of the contact angle liquid-pore wall, θ.
Mercury is almost nonwetting, for which reason it must be forced into
the pores. In suction porosimetry the liquid is wetting and therefore
penetrating the pore system itself and consequently must be forced out
of the specimen.

The suction porosimetry is applicable in the same pore-size range as
the mercury porosimetry. That is, in the intermediate range between very
coarse pores, where visual phase integration is the only possible method,
and very small pores, where the Kelvin equation for capillary condensation
is suitable.

However suction porosimetry brings certain additional advantages:

- The surface tension of a liquid like water is substantially lower than
  for mercury. Hence the pressures exerted on the specimen at determina-
  tion are considerably smaller.
- Methods can easily be designed where anisotropy of a specimen is taken
  into account.
- Water can be used as measuring fluid which from a principal point of
  view is a great advantage since the interaction water - pores influences
  most materials properties, and it is a known fact that the measuring
  fluid has a considerable effect on the pore - size measurements.
- Information on the pore shape can be obtained by determinations of pore
  size distributions from desorption as well as from absorption curves.

The materials often exhibit considerable hysteresis in calculation of pore-size distributions from wetting of a material or from drying of the same material. No final answer can be given to whether the "wetting curve" or the "drying curve" gives the best information on the pore structure. Hence it is recommended to use both types of methods at the determination.

General works dealing with determination of pore-size distributions,where also the problem hysteresis wetting-drying is discussed,are Dullen & Batra /10/ with a comprehensive bibliography, Sewell & Watson /24/, Minnen & Vos /19/, Vos & Tammes /26/, Bomberg /5/ also with a comprehensive bibliography, de Boer /4/.

2 DIRECT SUCTION MEASUREMENTS

2.1 Theory

As a consequence of the occurence of a pressure difference between the liquid and the ambient medium according to eq (1), the liquid will rise in a capillary in contact with bulk liquid as long as the contact angle meniscus-capillary wall is less than 90°. Since the pressure under the meniscus is less than that at a plane surface (eq (1)) the liquid column balances the pressure difference. The expression is at equilibrium

$$h = \frac{2 \cdot \sigma_{ij} \cdot \cos \theta}{(\rho - \rho_0) \cdot g \cdot r} \tag{2}$$

where ρ_0 is the density of the ambient medium. When this is a vapour as at water uptake in a porous material ρ_0 is negligable compared to ρ:

$$h = \frac{2 \cdot \sigma_{ij} \cdot \cos \theta}{\rho \cdot g \cdot r} \tag{3}$$

Hence the capillary rise is a measure of the pressure difference across the curved interface and consequently of the pore radius.

Another effect of the pressure difference across the curved interface is the phenomenon capillary condensation; This is expressed by Thomson´s law (Kelvin´s law);

$$\ln p/p_s = - \frac{2 \cdot \sigma_{ij} \cdot M}{\rho \cdot r \cdot R \cdot T} \cdot \cos \theta \tag{4}$$

By combination of eq:s (1), (3) and (4) a connection between pressure difference, capillary rise and relative vapour pressure can easily be derived

$$\Delta p = - \rho \cdot g \cdot h = \frac{R \cdot T \cdot \rho}{M} \cdot \ln (p/p_s) \tag{5}$$

In eq (5) the pore radius is included through eq:s (3) and (4).

The pressure difference Δp is called the "suction" of the capillary or the material.

Schofield /22/ introduced the concept pF as a measure of the suction of water of a material. pF is defined as the Briggian logarithm of the possible capillary rise in a capillary or a material.

$$pF = {}^{10}log(h \cdot 10^2) \tag{6}$$

The pF-concept may of course also be used at other types of liquids.

Eq (5) expresses the "capillary potential" at the interface. For a horisontal capillary in rest the same potential is acting throughout the filled part of the capillary. For a vertical capillary at rest the potential according to eq (5) gradually decreases downwards from the interface because of gravitation.

$$W = -\Delta p - g \cdot x \cdot \rho \tag{7}$$

However this effect is of importance only at coarse capillaries. According to Luikow /17/ it is negligible if the pores are smaller than 0,01 mm, when water is the measuring fluid. Besides the specimen used is normally so small that it can be assumed that at equilibrium all pore liquid has the same capillary pressure.

At centrifugation on the other hand the additional effect of outer forces are essential. See section 2.4.

So far all equations are derived for single capillaries. A porous material however consists of a complex system of capillaries of a wide range of sizes. The capillaries are interconnected in a complicated way. It can be proved (for instance by Hansen /19/) that at equilibrium with a certain suction value all pores larger than that corresponding to the actual suction value according to eq (5) are empty,while all pores smaller than the "equilibrium pore"are filled with liquid of the same pressure. Hence the pore liquid pressure at equilibrium with a certain suction value is the same despite pore radius and determined by the radius of the largest filled pore.

It is now easy to calculate the mutually connected values Δp, pF, h, p/p_s, r for a certain measuring fluid. This has been done for water at $+20^\circ$C in table 1.

TABLE 1

Δp (N/m^2)	pF	h (m)	P/P_s (%)	r μ	r Å	Methods of measurements
-0	-∞	0	100	∞		
$-9,8\cdot10^1$	0	10^{-2}	~100	1530		suction porosimetry
$-9,8\cdot10^2$	1	10^{-1}	~100	153		
$-9,8\cdot10^3$	2	1	99,99	15,3		
$-9,8\cdot10^4$	3	10^1	99,92	1,53		
$-9,8\cdot10^5$	4	10^2	99,27		1530	
$-9,8\cdot10^6$	5	10^3	93,00		153	Kelvin's law
$-9,8\cdot10^7$	6	10^4	48,43		15,3	
$-9,8\cdot10^8$	7	10^5	0,07		1,53	

Similar tables can be calculated for other fluids or for combinations of nonmixable fluids.

At the measurement the suction is expressed as a pressure, Δp, as a capillary rise, h, or a relative vapour pressure, P/P_s. The amount of liquid retained in the specimen at each suction value is measured.

The connection suction-liquid content at a certain temperature is called an absorption or desorption isotherm when the suction is expressed as a relative vapour pressure, and a capillary equilibrium curve when the suction is expressed in pF-degrees or as capillary rise.

By use of the connection between capillary pressure, Δp, and pore radius, eq (1), the pore size distribution can be calculated from the equilibrium curve.

Evidently even calculation of pore-size distribution (and also calculation from freezing point depression) from Kelvin's eq (4) is a sort of suction porosimetry. However it is suitable to make a distinction between the two types of porosimetry for the following reasons.

- Methods of determination; Calculation by Kelvin's law is based upon the sorption isotherm. Suction porosimetry is based upon measurements of capillary pressure, that is capillary equilibrium curves.
- At suction measurements no consideration must be taken to the adsorbed molecules on the pore wall. At use of Kelvin's law this consideration is essential.

However the two methods overlap at the upper part of the relative vapour pressure range which is shown in table 1. In this pore-size range the two methods give exactly the same results.

The hysteresis wetting drying can be extremely great. Fig 1 shows an example of this, Penner /21/. The hysteresis is to a great extent an effect of the pore shape. The wood cells are in principle parallell short cylinders with constrictions in each end. The cells are interconnected by a fine-porous membrane. Fig 2.

The filling of the cell system is in principle determined by the radius at center of the cylinder. The emptying of a saturated cell system is determined by the radius of the pores in the membrane.

Hence a good information on the shape of the pore system can only be obtained by determination of wetting curves as well as of drying curves.

The fact that hysteresis occurs must be taken into careful consideration at use of the suction tests described below. If a wetting curve shall be obtained, the specimen must always have a greater suction than the porous plate on which it is put. If not the specimen will have a certain drying out before the test starts which means that the measured curve will be a scanning curve between the wetting and drying curves.

An excellent review of traditional methods of suction measurements is given by Croney, Coleman & Bridge /9/.

2.2 Suction Plate, pF0-pF3

Main reference is Croney et al /9/. Normally water is used as measuring fluid.

Range pF1-pF3; Fig 3

A typical apparatus is shown in fig 3. The porous specimen with or without water is placed on a porous plate, a sort of filter. This contains moisture, since it is in direct contact with bulk water. If the suction of the porous plate is less than that of the material this takes up water. At inverse conditions the material gives away water until equilibrium conditions are restored.

The suction is regulated by a vacuumpump. When the air pressure in the flask is reduced an equal reduction of the suction of the porous plate occurs. The resulting suction can be expressed

$$pF = {}^{10}\log(z \cdot 10^2 + 1354 \cdot Z) \qquad (8)$$

where z is the distance between the upper surface of the porous plate and the water surface in the flask. Maximum pF is 3 since this corresponds to complete vacuum.

Range_pF0-pF1_à_2;_Fig_4_and_5

In this low range a simplified version of the method can be used
The suction is obtained by variation of the depth z of the water surface
below the specimen. At these small suctions a certain effect of the spe-
cimen thickness will occur. cf eq (7). The suction will be

$$pF = {}^{10}log(z \cdot 10^2) \qquad (9)$$

Both methods mentioned are relatively slow. Measurements of water content
can first be made when equilibrium is reached. A complete capillary
equilibrium curve can be an affair of weeks or months.

Modified_suction_plate_apparatus_for_rapid_measurements._Range_pF0-pF3;
Fig_6

In fig 6 a modified suction plate apparatus is shown.

The specimen is adapted to a certain water content and placed on the
porous plate. The specimen will draw water from the water reservoir in
contact with the flow-tube. By decreasing the pressure in the flow-tube
the meniscus in this is kept fixed. The suction is obtained from eq (8).
The method is rapid since there is almost no moisture transport specimen-
porous plate involved.

Some practical aspects of the method are given in Croney et al /9/.

General_discussion

The porous plate must fulfil certain requirements.

- The pore size must be so small that air cannot pass through when the
  maximum pressure difference is reached. (cf eq (1) which gives a pore
  diameter <3μ).
- The external surface must be plane so that intimate contact is achie-
  ved between the specimen and the plate.

The change of temperature and atmospheric pressure influence the measure-
ments. This is of special importance at small suctions.

2.3 Pressure membrane: pF0-pF4 à 6

The suction plate method is limited to pF≈3, at which suction water boils
at room-temperature.

The method can be extended to pF=6,2 by putting the specimen chamber
under pressure up till $1,5 \cdot 10^8$ N/m^2 (1500 atms). This pressure membrane
method has been described by Croney et al /9/, Penner /21/ and Bomberg /5/.

An apparatus according to Penner is shown in fig 7.

The porous plate consists of a fineporous pressure membrane which can be supported by a coarseporous metal filter. The maximum pore-size of the membrane can be calculated from eq (1).

The suction in an ordinary suction plate apparatus, fig 3, is now obtained as the pressure difference across the pressure membrane.

Starting with a fully saturated sample and increasing the suction gives the drying curve. The wetting curve is obtained by reducing the pressure on a initially dry specimen.

Water expulsion and water intake are measured by the change of the meniscus in the pipet.

2.4 Centrifuge: pF3-pF4,5

The methods,showed in figs 4 and 5, are limited to pF=1 à 2 which corresponds to a water column of 0,1 à 1 m. The suction is determined by the gravitational field.

By increasing the outer field of forces, for instance by centrifugation, a certain water column signifies a greater suction. Eqs (3), (5) and (6) are transformed to

$$h = \frac{2 \cdot \sigma_{ij} \cdot \cos \theta}{\rho \cdot n \cdot g \cdot r} \tag{10}$$

$$\Delta p = -\rho \cdot n \cdot g \cdot h \tag{11}$$

$$pF = {}^{10}\log(n \cdot h \cdot 10^2) \tag{12}$$

Where n is the intensity of the centrifugal field expressed as multiples of the gravitational field.

The centrifuge method has been described by Croney et al /9/ and by Ksenzhek et al /16/.

The methods are principally different. A principle of an apparatus according to Croney et al /9/ is shown in fig 8. The specimen is supported by a porous cylinder which is in contact with bulk water.

It is essential to keep the water level constant. This is done by means of a drain hole in the specimen jacket.

Normally only desorption tests are performed. This means,that the water is drawn from the specimen into the porous cylinder. This is a relatively slow process,viz in the case of a coarse-porous cylinder this moisture transport from the specimen is merely a vapour phase transport since the ambient medium is almost dry. On the other hand, at use of a fine-porous cylinder this is certainly wet. However the permeability is low. Measurements of moisture content can not be done until the moisture distribution throughout the cylinder corresponds to equilibrium conditions.

The authors recommend hard chalk as a suitable material and a length of the cylinder of 6 cm.

The mean acceleration is at the distance $\dfrac{R_2 + R_1}{2}$ from the center of rotation

$$n \cdot g = \frac{R_2 + R_1}{2} \cdot \omega^2 \tag{13}$$

and the height of capillary rise.

$$h = R_2 - R_1 \tag{14}$$

Hence the suction is

$$pF = {}^{10}\log\left(\frac{R_2^2 - R_1^2}{2} \cdot \frac{\omega^2}{g} \cdot 10^2\right) \tag{15}$$

The capillary equilibrium curve is obtained by weighing the specimen after each increase in suction. Drying curves as well as wetting curves can be obtained.

The suction at rest is about 1 pF. Hence a specimen having initially a greater suction will increase its moisture content when it is placed upon the cylinder. This water is removed at acceleration but it may have a considerable effect on the results because of the hysteresis wetting-drying.

In the same way a change in equilibrium may occur when the centrifuge is stopped.

The specimen thickness has an influence on the results, cf eq (7) . Hence it must not exceed 5 mm.

Ksentzhek et al /16/ have refined the centrifugal method considerably. In their method consideration can also be taken to distribution of liquid throughout the specimen thickness . Besides the method is fastened up considerably. Only desorption curves can be obtained however.

The authors use a cuvett as specimen support. Fig 9. Hence the specimen is not in direct contact with a water column as in fig 8. The water displaced from the specimen at centrifugation is collected in the cuvette where it is measured after stopping the centrifuge. It can also be measured during the run in a very elegant way. The specimen is impregnated with an electrically conducting liquid. The amount of liquid entering the ring-formed cuvette is measured by the electric resistance between two platinum electrodes.

Since the specimen thickness is small the acceleration can be assumed to be the same in all cross-sections of the specimen.

All pores are assumed to be cylindrical and parallell to the radius of rotation.

At saturation all pores are completely filled. When the centrifugal acceleration is increased the capillary rise in the coarsest pore is gradually decreased according to eq (10).

A certain acceleration corresponds to a certain pore radius, r_n, where the capillary rise h is equal to the specimen thickness, H.

The radius r_n is obtained from eq (10)

$$r_n = \frac{2 \cdot \sigma_{ij} \cdot \cos \theta}{\rho \cdot n \cdot g \cdot H} \tag{16}$$

Pores of radius $r > r_n$ are partly filled to an extent obtained from eq (10).

However the authors show theoretically that the pore-size distribution funktion, $f(r)$, is independent on the thickness of the specimen.

$$f(r) = -(\frac{r_n}{\varepsilon_0}) \cdot \frac{d^2 \varepsilon_n}{dr_n^2} \tag{17}$$

where ε_0 is the pore-volume and ε_n is the liquid retained in the specimen at a certain acceleration.

Hence by determination of ε_n at a certain acceleration, $n \cdot g$, as function of the pore-radius, r_n, calculated from eq (16), the pore-size distribution can easily determined by eq (17) for instance by use of a simple graphical method.

The method has been compared to mercury porosimeter. The agreement was satisfactory.

3 PENETRATION OF WETTING LIQUIDS

The pore-size distribution can also be determined by measurements of penetration of liquids in a porous specimen.

The connection between time and capillary rise at a capillary uptake of liquid in a straight cylindrical capillary is at laminar flow

$$t = \frac{2 \cdot \mu \cdot l^2}{\sigma_{ij} \cdot r \cdot \cos \theta} \tag{18}$$

Hence by measurements of time, t, and dept of penetration, l, the pore-size cen be determined.

This model can also be applied to a porous material in which case a pore-size distribution can be evaluated. The complications at application to real materials are:

- The pores are not straight cylindres but each capillary has a random variation of pore radius along its axis.
- The pores have an axial "tortuosity" or "meandering".
- The pores are interconnected.
- The method is accompanied by difficulties of measurements of penetration.

Astbury /2, 3/ has elaborated a method where consideration is taken all complications listed above except the interconnection of individual pores.

The pore model is shown in fig 10. Its main characteristics are:

- All pores are geometrically alike. However they differ in size.
- All pores are meandering. Their tortuosity (effective length) is $\beta \cdot H$ where $\beta > 1$ and H is the thickness of the specimen. (in his work /2/ Astbury assumes all pores to be straight).
- All pores are cylindrical. The radius is varying along the pore axis.
- The appearance of radius variation is the same in all random pore sectors.
- The pore-walls are completely wettened by the fluid and Hagen-Poiseulle's law is valid.

The principle of the apparatus is shown in fig 11. The dried prismatic specimen is placed in a plastics box. The outer surface of the specimen is painted with a silver paint which creates a porous electrode. Another electrode is placed in the box. The resistivity of the specimen is measured after which an electrolyte (eg decinormal aqueous solution of $Ca\ Cl_2$ or K_2SO_4) is introduced into the box. According to eq (18) the rate of capillary rise is higher the coarser the capillary. Hence when the electrolyte in the coarsest connection through the specimen has reached the silver electrode the resistivity is changed. A curve conductance-time is obtained.

The amount of electrolyte absorbed is measured by maintaining the electrolyte at a fixed level by filling from a burette.
The measurements are going on until steady a state is reached.
The apparatus is shown more in detail in Astbury /3/.

If all capillaries were straight cylinders it would be possible to calculate the pore-size distribution from eq (18) and the conductance time curve. However Astbury /2/ shows that this assumption is erroneous.
Instead he evaluates a pore-size distribution from his own pore model.
The basis of calculation is three theoretical expressions (eq:s 19, 21, 22) describing the pore model.

The first expression is the time to fill a single capillary

$$t = \frac{2\mu \cdot (\beta \cdot H)^2}{\sigma_{ij} \cdot a} \cdot k_3 \cdot k_{-4} \tag{19}$$

Where $k_i = \bar{\xi}^i$ (mean value of ξ^i)   (20)
       a is the smallest radius in the pore and $\xi \cdot a$ is the radius of the pore at a certain point. The largest radius in the pore is Xa. The constants k_3 and k_{-4} can be quite large for some materials which explains why eq (18) is inapplicable.

The second expression is the total accessible pore volume of the specimen;

$$\varepsilon = \pi \cdot (\beta \cdot H) \cdot k_2 \int a^2 \cdot f(a) \cdot da \tag{21}$$

$f(a) \cdot da$ is the number of pores with smallest radii between a and a+da.
Thus its expresses the distribution of smallest accessible radii.

The third expression is the permeability at saturation which is according to Hagen Poiseulles' law

$$B = \frac{\pi}{8 \cdot \mu \cdot (\beta \cdot H) \cdot k_{-4}} \cdot \int a^4 f(a) \cdot da \tag{22}$$

Thus the needed measurements are two
- The time function of capillary uptake of liquid.
- The permeability.

As mentioned earlier all measurements are made as conductivity measurements. Eqs (19), (21) and (22) must therefore be transformed to measured quantities.

dC is the contribution to electrical conductivity by the pores with smallest radii within interval da; Then it is valid.

$$dC = \frac{di_t}{V} = \frac{1}{R_t} = \frac{\pi \cdot c \cdot a^2}{(\beta \cdot H) \cdot k_2} \cdot f(a) \cdot da \qquad (23)$$

Now the conductance-time curve can be transformed to a distribution of smallest accessible radii through eq (24), Astbury /2/

$$\int f(a)da = \frac{(\beta \cdot H) \cdot k_{-2}}{\pi \cdot c \cdot D^2} \cdot \int t^2 \cdot dC \qquad (24)$$

where $D = t \cdot a = \dfrac{2 \cdot \mu \cdot (\beta \cdot H)^2}{\sigma_{ij}} \cdot k_3 \cdot k_{-4}$ \qquad (19)

Eq (21) can be transformed to, Astbury /3/;

$$c \cdot \varepsilon_t \cdot R_t = (\beta \cdot H)^2 \cdot k_2 \cdot k_{-2} \qquad (25)$$

where ε_t is the amount of liquid absorbed at a certain stage.
And eq (22) transformed to , Astbury /3/;

$$B_t = \frac{D^2}{8 \cdot \mu \cdot c \cdot V} \cdot \frac{k_{-2}}{k_{-4}} \int \frac{1}{t^2} \cdot di_t \qquad (26)$$

where B_t is the permeability at a certain stage.
By use of eqs (24), (25) and (26) it is now possible to solve the values of ß(tortuosity), X(ratio of smallest and coarsest part of capillary) $\int f(a)da$ (distribution of smallest accessible radii) and X (ratio of coarsest and smallest part of a capillary which gives the distribution of coarsest accessible radii).
It is however at first necessary to evaluate the k-factors which depend on the way in which the radial variations are distributed along the capillary.

Astbury /3/ suggests a rectangular distribution,which means that any radius between a and X·a (smallest and largest radius) is equally probable. Then k_i is only dependent on the value of X;

$$k_i = \frac{(X^{i+1} - 1)}{(X-1)(i+1)} \qquad (27)$$

The extreme pore radius X·a can now be obtained from eq (25) after insertion of eq (27).

$$X \cdot a = \frac{3 \cdot c \cdot \varepsilon \cdot R_{t_1}}{(\beta H)^2} \cdot a \qquad (28)$$

with the pore shape indicated above.

The extreme pore radius a can be obtained if eq (25) is inserted in eq (19).

$$a = \frac{2 \cdot \mu \cdot c \cdot \varepsilon \cdot R_{t_1}}{\sigma_{ij} \cdot t_1} \cdot \frac{k_3 \cdot k_{-4}}{k_2 \cdot k_{-2}} \qquad (29)$$

or

$$a = \frac{1}{2} \cdot \frac{\mu \cdot c \cdot \varepsilon \cdot R_{t_1}}{\sigma_{ij} \cdot t_1} \quad X \qquad (30)$$

with the pore shape indicated above. t_1 is the time at steady state. Tortuosity β is obtained from eq (26).

The evaluation of parameters is discussed more in detail in /3/.

The distribution of extreme pore radii are then calculated from eq (24).

The result is two radii distributions which constitutes on area within which the real pore-size distribution is situated, see fig 12.

The real pore-size distribution can now be calculated. All pores with a radius less than r will contain all pores with smallest radius, a, less than r/X and a certain fraction of pores with mean radius between r/X and r. This fraction is /3/;

$$fr = \frac{1}{X^3 - 1} \cdot \frac{1}{i_{t_1}} \int \frac{r^3 - a^3}{a^3} \cdot di_t \qquad (31)$$

The principle of obtaining the real pore-size distribution is shown in fig 13. The real pore-size distribution lies closer to the curve X·a than to a which is reasonable since the coarser pores represent more pore volume.

It is of course also possible to calculate the specific surface from the same measurements.

The method is applicable to pore radii down to $0,05\mu$ according to Astbury /3/.

The method has been compared with water expulsion method and mercury porosimeter by Astbury /2, 3/ and Clements & Vyse /8/.

In general it indicates a coarser pore-size distribution than do the other methods. This is logical since in the other two methods the pore-size is determined by the most narrow passage into the pore.
It is interesting to notice that the mercury porosimeter distribution often agrees very well with Astbury's distribution of smallest accessible radii /3/. Astbury's method on the other hand, gives a more true pore-size

distribution since "radial tortuosity"is considered.

Astbury writes:"The present model is no easier to accept than others which have proceeded it. It does, however, introduce a new dimension into the problem and it does predict the existence of large cavities⁻ not shown by the water-exulsion and mercury-penetration models."

The penetration of the water front can also be detected by other methods, for instance by radioisotopes, Gêmesi /13/.

4 DISPLACEMENT METHODS

4.1 Introduction

Eq (1) also indicates the pressure needed in order to displace the liquid in a cylindrical capillary by another liquid or a gas.

$$\Delta p = \frac{-2 \cdot \sigma_{ij} \cos \theta}{r} \tag{1}$$

Hence the pore-size distribution can be obtained by succesive displacement of liquid form a saturated material.

This is the basis of the so called displacement methods.

Normally the medium used for displacement is a gas (air) but it is also possible to use a liquid which is nonmiaxable with the liquid in the pores.

The flow must be uni-directional. Hence the faces of the specimen parallell to the flow must be sealed.

The method is especially suitable at indicating anisotropy of the pore system. This can be done by determination of pore-size distributions in three perpendicular directions of the same specimen.

The displacement methods are by nature desorption methods only.

4.2 Static methods

Clements & Vyse /8/ report a method where water is expelled by air from an initially saturated specimen.

The amount of water expelled after each increase in air-pressure is measured by weighing. The apparatus is shown in fig 14.

The method is compared to detetermination by mercury pprosimeter. The two methods give roughly similar results in the pore diameter range 20μ-85μ, when applied to refractories.

However the mercury porosimeter underestimates the amount of pores <20μ. This is certainly an effect of hysteresis wetting-drying. Hence the two methods supplement each other.

The authors also discuss the effect of time of blow on the pore-size distribution. "Since the rate of water movement through a pore is infinitely small when the applied pressure is just equal to the surface tension force, water will exude from a test specimen for infinite time".

The authors find the time of blow 1 minute to give an error in pore radius of as much as 0,3μ for a specimen 2,5 cm thick. The effect of time of blow has been theoretically studied by Manegold et al /18/. Some experimental data are shown in fig 20.

4.3 Dynamic methods

The amount of fluid expelled from the specimen and thus the pore-size distribution can also be obtained indiredly by measurements of change in permeability.

Such methods have been suggested and described by Erbe /11/, Grabar & Nikitine /14/, Manegold et al /18/, Zagar /27, 28, 29/, Schwiete & Ludwig /23/, Alviset & Liger /1/ and Ohnemüller /20/.

The methods can be divided in two groups:
- The displacement medium is a liquid
- The displacement medium is a gas

Since the calculation of pore-sizes is based upon data of permeability the structure of the pore-system has a great effect on the resulting pore-size distribution. A comprehensive discussion of permeability of porous materials together with 134 literature references is provided by Timofeev/25/.

4.3.1 Displacement liquid - liquid

The method is described in detail by Manegold et al /18/.

The principle is simple. Consider a material with parallell cylindrical capillaries of three separate sizes, radii $r_1 > r_2 > r_3$. The material is saturated with a liquid. This liquid will be displaced by another liquid. The two liquids are non mixable. Suitable liquids are for instance water-isobutylalkohol or water-methyl-isobutylalkohol (Manegold et al /18/).

A hypothetical diagram flow rate-pressure is shown in fig 15. The pressure of the displacement medium is gradually increased. The permeability is zero until a pressure Δ_{p1} corresponding to pore radius r_1 according to eq (1) is reached. Then the pores of radius r_1 are emptied and there is a "sudden" increase in permeability. Then the coefficient of permeability is constant until the pressure Δ_{p2} corresponding to pores of radius r_2 are reached and there is a new sudden increase in permeability and so on.

Between each jump in permeability the connection flow rate-pressure is a line through origo. The slope of the line or coefficient of permeability is determined by Hagen-Poiseulles´ law

$$v = \sum_i \frac{r_i^{4} \cdot \pi \cdot N_i}{8 \cdot H \cdot \mu} \cdot \Delta P \qquad (32)$$

or

$$v = B_i \cdot \Delta P \qquad (33)$$

In a real material the pores are of all sizes and certainly not parallell. Therefore a continous curve will be obtained.

Fig 16 shows an example of a real curve. It has a typical S-shape. At high pressures the curve is linear and parallell to the curve of an initially dry material. The point where this line begins corresponds to the smallest permeable capillary and the intersection with the ΔP-axis corresponds to the coarsest permeable pore.

The real curve can be transformed to a stajr-formed curve according to the figure. The coefficient of permeability at each step is calculated from the slope of a line from origo to the actual point of the curve. The pores are divided in pressure classes $\Delta P_i - \Delta P_{i+1}$ etc.

By transforming the pressure into a radius according to eq (1) the amount of pores of each size class $r_i - r_{i+1}$ etc can be calculated from the coefficients of permeability. If all pores are assumed to be cylindrical, parallell to the flow and as long as the specimen thickness eq (34) can be used for calculation of cumulative pore size distribution. It is assumed that the difference $r_i - r_{i+1}$ is small

$$\frac{1}{\varepsilon_0} \sum \varepsilon_i = \frac{1}{\varepsilon_0} \sum B_i \frac{8 \cdot \mu \cdot H^2}{r_i^{2}} \qquad (34)$$

The calculation starts with the coarsest pore. The amount of pores of class $r_i - r_{i+1}$ can also be obtained from the <u>change</u> of the slope of the line between segments $r_{i-1} - r_i$ and $r_i - r_{i+1}$. This change is $B_i - B_{i-1}$ and the amount of pores are when the intervals $r_i - r_{i+1}$ is small;

$$\varepsilon_i = \frac{(B_i - B_{i-1}) \cdot 8 \cdot \mu \cdot H^2}{r_i^2} \tag{35}$$

The foregoing discussion implies that the interface liquid-liquid has penetrated the entire pore. During the penetrating period the coefficent of permeability is determined by viscosities of both liquids. Reliable measurements can not be made until this first period has passed. Manegold et al /18/ give comprehensive information on the length of the "waiting period" which can be very long in the case of long capillaries and low pressures. Hence even at a constant pressure difference across the specimen the flow rate is never quite constant. It will only approach a limiting value asymptotically. The significance of this phenomenon is discussed in detail by Mangegold et al /18/. c.f. Experimental data at displacement water-air. Fig 20. An apparatus is shown in fig 17.

4.3.2 Displacement liquid-gas

Normally water is expelled by air. If the displaced water is removed from the specimen surface the curve flow rate - pressure will be of the same type as when a liquid is displaced by a liquid. This is a S-shaped curve. At high pressures the curve is a line intersecting origo. See fig 16.

However if the free specimen surface is covered by a layer of water the flow rate-pressure curve will have another shape, viz the air cannot leave the specimen until a bubble can be formed at the end of the capillary. The air pressure in the bubble necessary is obtained from eq (1)

$$\Delta P_B = \frac{2 \cdot \sigma_{ij} \cos \theta}{r} \tag{1}$$

This pressure is the same as that necessary in displacing the liquid from the pore. Consider the same material as in fig 15.

The specimen is completely sealed by the water until the pressure ΔP_1 is reached. At a pressure $\Delta P \gtrless \Delta P_1$ air flows through the pore of radius r_1. However because of the necessary bubble pressure ΔP_B the flow rate-pressure line intersects the pressure axis at $\Delta P = \Delta P_1$.

When the pressure is increased further until $\Delta P=\Delta P_2$ air begins to flow even through the capillaries with radius r_2. The line flow rate-pressure through those capillaries intersect the pressure axis at $\Delta P=\Delta P_2$. When the flows in both types of capillaries are added the result is an abrupt increase in slope at $\Delta P=\Delta P_2$. Fig 18.

The result of a test will be a curve which is concave. See fig 19. At $\Delta P>\Delta P_{MAX}$ the curve will be linear. The slope of the line is equal to the air permeability of a dry specimen.

$\Delta P=\Delta P_{MAX}$ corresponds to the smallest permeable pore while $\Delta P=\Delta P_{MIN}$ (intersection with the ΔP-axis) corresponds to the coarsest permeable pore.

The intersection of the linear part of the curve ($\Delta P>\Delta P_{MAX}$) on the ΔP-axis signifies an "equivalent pore-size", Žagar /27/.

Žagar /28/ makes a profound discussion of the method. The author shows theoretically that r_{min} is equal to the "effective pore radius", r_{eff}, which in turn is a pore radius that in a hypothetical equal-pore-sized material gives the same permeability as in the real material when consideration is taken to the fact that only a part, ε_{eff}, of the total porosity, ε_0, is permeable.

By this derivation the author also gives possibilities of a characterization of the pore system. So for instance, permeable and non permeable porosities, "pore shape factor" and effective pore length can be calculated.

The calculation of pore-size distribution from the flow rate-pressure curve can be made graphically, Žagar /28/ or analytically, Alviset & Liger /1/.

A short review of the analytical method is given below. The principle is essentially the same as that given on page 20 for calculation from liquid-liquid displacement.

The curve is divided in segments, fig 19. Consider the interval ΔP_i; $r_i -$
$- \Delta P_{i+1}$; r_{i+1}. The equivalent radius $(r_i)_{equ}$ is obtained at the intersection of tangents to the curve in points i and i+1. The contribution of the pores of size $(r_i)_{equ}$ to permeability is determined from the change is slope of the two tangents.

It is now possible to calculate the pore-volumes of pores of different

sizes. In this calculation it can be necessary to take even molecular slip flow (Knudsen flow) into consideration. This is essential at pores $<1\mu$.

Hagen-Poiseuille's law corrected for slip takes the form

$$v = \frac{\pi \cdot r^4 \cdot N}{8 \cdot \mu \cdot H} \cdot \frac{\bar{P}}{P_o} \cdot \Delta P(1+4\frac{\zeta}{r}) \tag{36}$$

Where ζ is the coefficient of slip. This coefficient is dependent on the gas used, its pressure and temperature, since it is $= 2/3$ of the mean free path of gas molecules. Timofeev /25/ gives further information of the value of ζ. Eq (36) shows that the slip correction is considerable when the pores are small.

The factor $\bar{P}/P_o$ is introduced to correct for change in density of the gas within the capillary

$$\bar{P} = P_o + \frac{\Delta P}{2} \tag{37}$$

The coefficient of permeability in a small interval $r_i - r_{i+1}$ can now be expressed

$$B_i = \sum_i \frac{\pi \cdot r_i^4 \cdot N_i}{8 \cdot \mu \cdot H} \cdot \frac{\bar{P}_i}{P_o} (1+4\frac{\zeta}{r_i}) \tag{38}$$

If all capillaries are cylindrical and have a length equal to the thickness of the specimen, the number of capillaries N_i can be changed to a pore-volume ε_i

$$N_i = \frac{\varepsilon_i}{\pi \cdot r_i^2 \cdot H} \tag{39}$$

B_i is measured from the curve as the slope of the tangent in point i, r_i, is calculated from eq (1). Hence the cumulative pore-size distribution, $\frac{1}{\varepsilon_o} \Sigma \varepsilon_i$, can be calculated by insertion of eq (39) in eq (38).

$$\frac{1}{\varepsilon_o} \sum_i \varepsilon_i = \frac{1}{\varepsilon_o} \cdot \sum_i B_i \cdot \frac{8 \cdot \mu \cdot H^2}{r_i^2} \cdot \frac{P_o}{\bar{P}_i} \cdot \frac{1}{(1 + 4 \frac{\zeta}{r_i})} \tag{40}$$

The amount of pore volume, ε_i, with pore radius $(r_i)_{equ}$ can be calculated by insertion in eq (38) the difference in slope of the tangents in points i and i+1.

Hence:

$$\varepsilon_i = (B_{i+1} - B_i) \frac{8 \cdot \mu \cdot H^2}{(r_i)^2_{equ}} \cdot \frac{P_o}{\bar{P}_i} \cdot \frac{1}{(1 + 4 \frac{\zeta}{(r_i)_{equ}})} \qquad (41)$$

Žagar /28/ takes no consideration to Knudsen flow in his graphical treatment which can be reasonable as long as the measured pores are relatively coarse($\geq 1\mu$). Besides the effect on flow rate of change in density of the gas is neglected by both Žagar /28/ and Alviset & Liger /1/.

Žagar /28/, /29/ discuss reproducibility and effect of thickness of specimen. The reproducibility was satisfactory. The measured r_{min} was smaller the thinner the specimens. However the effect was less than 4 %.

The waiting period before reliable measurements can be made is determined theoretically by Manegold et al /18/. They found that the waiting period in displacement of water by air is considerably shorter than at displacement liquid-liquid which depends on the high surface tension. On the other hand the high surface tension water-air makes the pressures needed very high. The author of this contribution has made own experiments in order to find out absolute values on the waiting period. Some results are shown in fig 20. The material is a well burnt clay brick with thickness 30 mm and surface area 30 cm^2.

Normally the pressure difference, ΔP, is increased without relief of the earlier pressure difference. Despite this a reasonable waiting period at low pressures might be as long as half an hour, shorter at higher pressures. Equilibrium conditions are not assured even after 2 hours.

In three cases the earlier pressure was relieved for some hours before appliance of the new pressure (broken lines). In these cases the waiting periods are very long. This method must therefore be refrained from.

The fact that the waiting times are quite large means, that it takes a long time to obtain a complete curve. This is a disadvantage of the method.

The author has also made experiments in order to find out the effect of degree of saturation of the specimen. Some results for the clay brick mentioned above are shown in fig 21. Such experiments make it possible to find out in which pores water is located at different degrees of saturation. This is an advantage of the method.

Apparatus are described by Žagar /27, 29/, Schwiete & Ludwig /23/ and
Alviset & Liger /1/. An apparatus built at our institution is shown in
fig 22, Fagerlund /12/. The principles of measurements are described by
Žagar /27/. The specimen holder is however adopted to angular specimens.
Besides the apparatus can be used for pure permeability measurements of
liquid or gas.

5 SYMBOLS

B permeability (slope of flow rate-pressure line) $(\frac{m^4 \cdot s}{kg})$

B_t permeability at time t $(\frac{m^4 \cdot s}{kg})$

C conductance between electrodes $(\frac{1}{ohm})$

D defined in eq (19)

H thickness of specimen parallell to flow (m)

M molecular weight (kg/k mole)

N number of capillaries

P_o pressure under which the volume of the penetrating gas is measured eq (36) (N/m^2)

$\bar{P}$ mean pressure across a specimen, eq (37) (N/m^2)

R gas constant $(\frac{j}{^oK \cdot k\ mole})$

R_t electrical resistance of specimen at time t (ohm)

R_{t_1} resistance in steady state (ohm)

R_1 and R_2 distance from center of rotation at centrifugation, eq (13), fig 8 (m)

T absolute temperature (^oK)

X ratio of maximum and minimum radius of one capillary

V voltage across specimen (V)

W capillary potential eq (7) (N/m^2)

Z vacuum read on a Hg-manometer (m Hg)

a minimum pore radius of one capillary (m)

c conductivity of electrolyte $(\frac{1}{ohm \cdot m})$

$f(a)$ distribution function of smallest assessible radii of capillaries

fr fraction of pores with mean radius between r/X and r, eq (31)

g gravitational constant (m/s^2)

h   capillary rise (m)

i_t current through specimen at time t (A)

k_2; k_3;
k_4^2; k_4^3;
k_{-3}^4; k_{-4}^2 mean values of different powers of ξ, eqs (20), (27)

l   depth of penetration, eq (18) (m)

n   centrifugal acceleration divided by g (gravitational constant)

p   vapour pressure (N/m^2)

p_s vapour pressure at saturation (N/m^2)

p/p_s relative vapour pressure

pF   Briggian logarithm of the possible capillary rise of water in a
         porous material expressed in cm eq (6)

r   pore radius (m)

r_1; r_2; principal radii of meniscus (m)

t   time (s)

v   flow rate (m^3/s)

x   vertical distance from the meniscus to a point in a capillary
         eq (7) (m)

z   distance between free water surface and upper surface of the
         porous plate in suction methods (m)

β tortuosity of a capillary. Fig 10.

ΔP pressure difference across a specimen eq (32) (N/m^2)

Δp pressure difference across a curved interface (N/m^2)

ΔP_B pressure needed in order to create a gas bubble of radius r in
         a liquid (N/m^2)

ε volume of accessible pores (m^3)

ε_o pore volume (m^3)

ε_i volume of pores of size r_i - r_i + Δr_i (m^3)

ε_n volume of liquid-filled pores (m^3)

ε_t porosity filled with liquid at time t

ρ density of fluid rising in a capillary, eq (2) (Kg/m^3)

ρ_0 density of displaced medium at capillary rise, eq (2) (Kg/m^3)

σ_{ij} surface tension between substance i and j (N/m)

θ contact angle

μ viscosity of penetrating fluid, eq (18) $(\frac{Ns}{m^2})$

ξ ratio of actual pore radius in the capillary and minimum pore radius of the same capillary

ζ coefficient of slip (m)

ω angular velocity at centrifugation $(\frac{radians}{s})$

6 LITERATURE

1   Alviset L   La mesure de la repartition des capillaires dans un
    Liger C   tesson de terre cuite et les applications que l'on
                     peut en faire. Proc VI Int Ceram Congr, Wiesbaden
                     1958, p 401.

2   Astbury N F   A Model for Connected Porosity in Ceramic Bodies.
                     Trans Brit Ceram Soc, Aug 1968.

3   Astbury N F   Neues Verfahren zur Untersuchung der Poren-Grössen-
                     verteilung. Ber Deut Keram Ges, 49 (1972) Nr 2.

4   de Boer J H   Everett & Stone (Editors). The Structure and Proper-
                     ties of Porous Materials, Tenth Colston Symp,
                     Bristol 1958, Butterworth, London 1958.

5-7 Bomberg M   Water Flow through Porous Material.

                     Part I: Methods of Water Transport Measurements.
                        Report 19, Lund Inst of Techn 1971.

                     Part II: Relative Suction Model. Report 20, Lund Inst
                        of Techn 1971.

                     Part III: Applications of the Relative Suction Model.
                        Report 21, Lund Inst of Techn 1972.

8   Clements J F   A Comparison of Methods of Measuring Pore-Size
    Vyse J   Distribution in Refractories. Trans Brit Ceram Soc
                     67/1968/p 285.

9   Croney D   The Suction of Moisture Held in Soil and other Porous
    Coleman J D   Materials. Road Res Techn Paper No 24, Her Majesty's
    Bridge P M   Stationery Office, London 1952.

10 Dullien F A L   Determination of the Structure of Porous Media.
    Batra V K   Ind and Eng Chem, 62/1970/p 25.

11 Erbe F   Die Bestimmung der Porenverteilung nach ihrer Grösse
                     in Filtern und Ultrafiltern. Kolloid Z 63/1933/
                     p 277.

12 Fagerlund G   Frost Resistance of Porous and Brittle Materials in
                     Relation to their Structure-Theory and Experiments.
                     Report 30, Div of Build Techn at Lund Inst of Techn
                     1972 (in Swedish).

13 Gèmesi J   Untersuchung der Kapillarerscheinungen in Beton mit
                     Zerstörungsfreien Methoden. Wissensch Zeitschr
                     Hochsch f Bauwesen, Leipzig H3 1969 p 175.

14 Grabar P   Sur le diamètre des pores des membranes en collodion
    Nikitine S   utilisées en ultrafiltration. J Chim Phys 33/1936/p 721.

15 Hansen T C   Drying Shrinkage of Concrete due to Capillary Action.
                     Techn Rep No 1. Techn Univ of Denmark, Dept Civil
                     Eng, 1967.

16 Ksenzhek O S   Centrifugal Method for Finding Pore-Size Distribu-
    Kalinovskii E A tion Function in Porous Media. Russian J of Phys
    Petrova S A   Chem, 41/1967/p 856.
    Litvinova V J

17 Luikow A V   Heat and Mass Transfer in Capillary-porous Bodies.
                        Pergamon Press Ltd, Oxford 1966.

18 Manegold E   Über Kapillarsysteme, XIX. Kolloid Zeitschr Band
    Komagata S   93/1940/p 166.
    Albrecht E

19 van Minnen J   Distribution and Transport of Water in Porous Mate-
    Vos B H   rials. Report No II-8 TNO, Delft 1965.

20 Ohnemüller W   Die Bestimmung der Frostempfindlichkeit poröser ke-
                        ramischer Werkstoffe mit Hilfe physikalischen Mess-
                        grössen. Diss Fakultat für Bergbau und Hüttenwesen
                        der Bergakademie Claustal, 1960.

21 Penner E   Suction and its Use as Measure of Moisture Contents
                        and Potentials in Porous Materials. Humidity & Mois-
                        ture Vol 4 p 245. Reinhold Publ Corp NY 1965.

22 Schofield R K   The pF of Water in Soil. Trans 3rd Int Congr of Soil
                        Sci No 2, Oxford 1935.

23 Schwiete H-E   Uber die Bestimmung der offenen Porosität im Zement-
    Ludwig U   stein. Tonind Ztg,90/1966/p 562.

24 Sewell C   Hysteresis in the Moisture Characteristics of Ideal
    Watson E W   Bodies. Bull Rilem No 29 Dec 1965.

25 Timofeev D P   The Mechanism of Transport of Matter in Porous Sor-
                        bents. Russian Chemical Reviews, 29/1960/p 180.

26 Vos B H   Moisture and Moisture Transfer in Porous Materials.
    Tammes E   Report No B I-69-96 TNO, Delft 1969.

27 Žagar L   Ermittlung der Grössenverteilung von Poren in Feuern-
                        festen Baustoffen. Archiv f das Eisenhüttenwesen
                        26/1955/H 9/p 561.

28 Žagar L   Ermittlung der Grössenverteilung von Poren in Feuern-
                        festen Baustoffen und Glasnutschen. Teil II, Archiv
                        f das Eisenhüttenwesen 27/1956/h 10/p 657.

29 Žagar L   Über die Textur von Feuernfesten Baustoffen. Ber
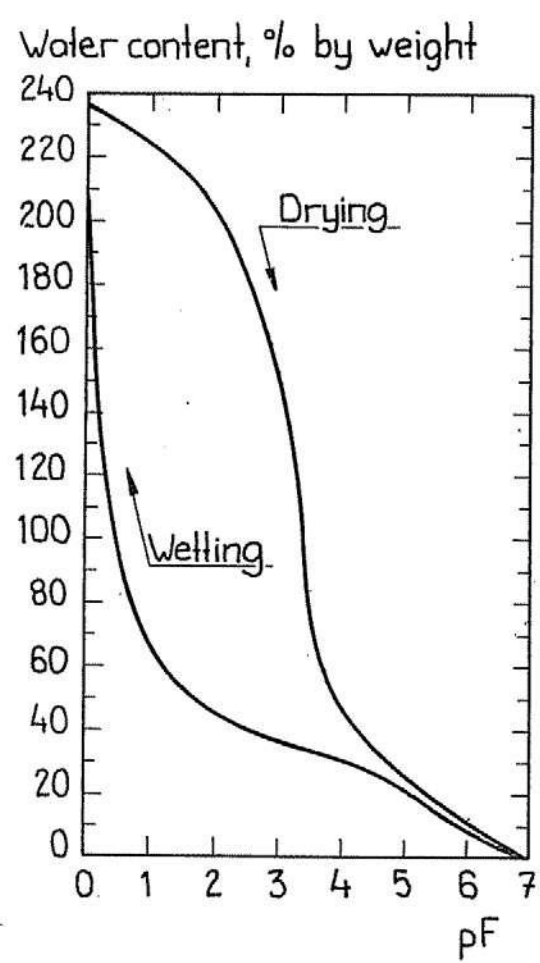   Deut Keram Ges 35/1958/p 294.

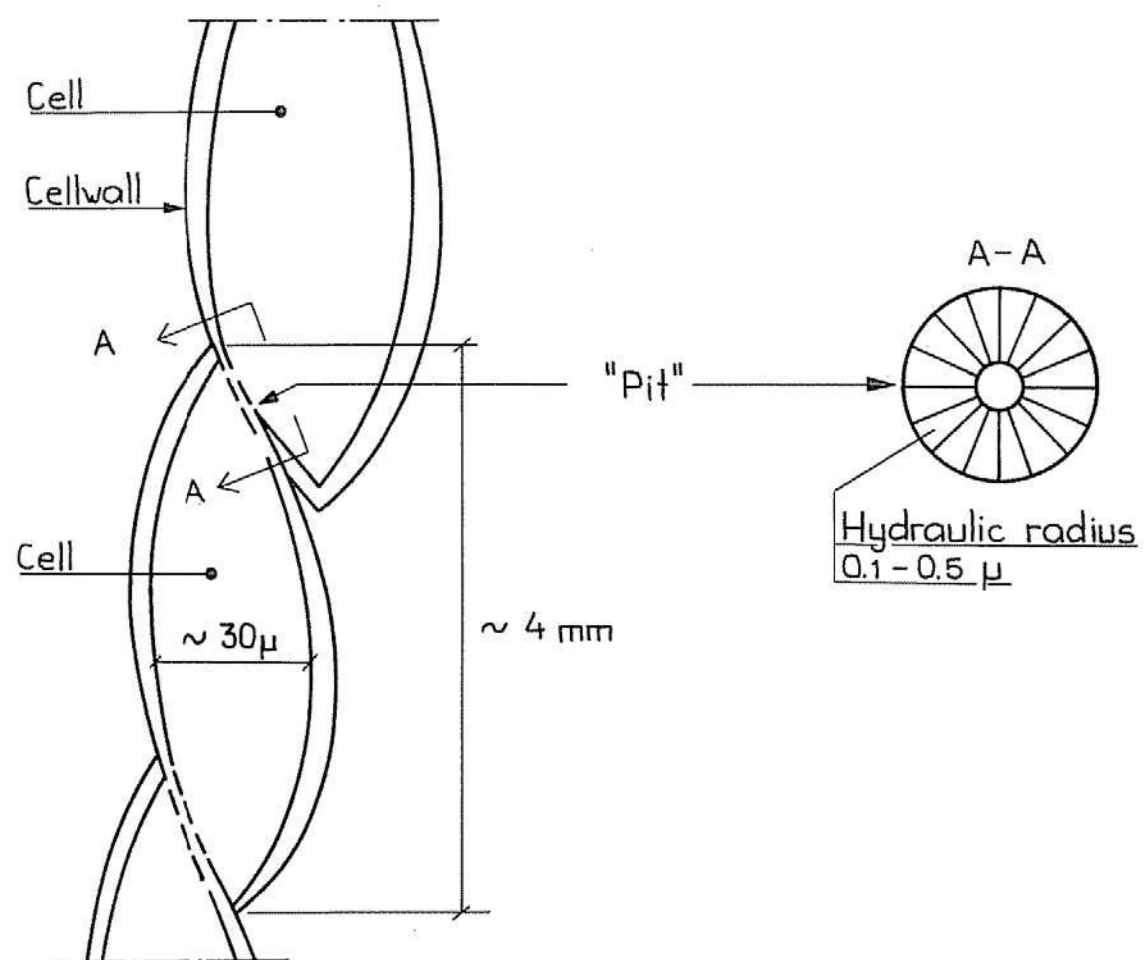FIG 1 Suction-water content curve for spruce at 20°C. /21/.

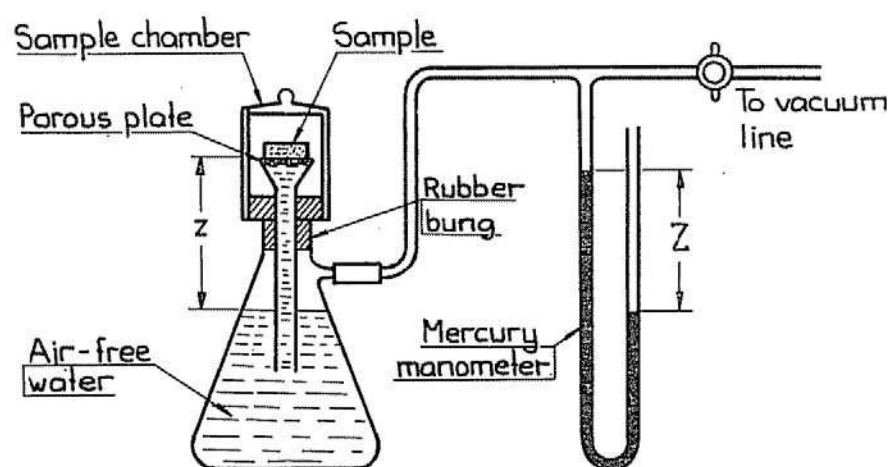FIG 2 Schematic structure of spruce.

FIG 3 Suction apparatus. Range pF1-pF3. /9/.
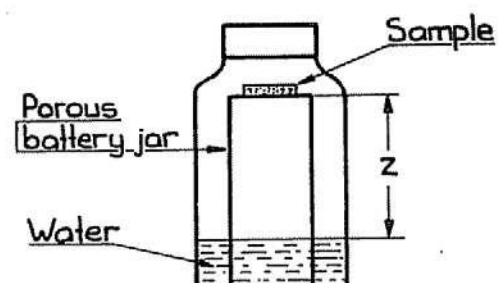
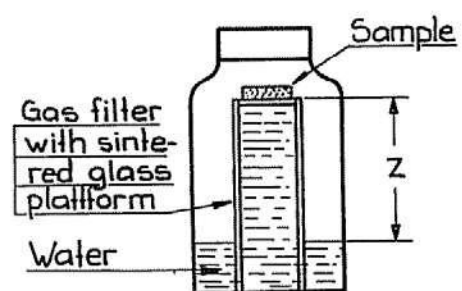FIG 4   Suction apparatus. Range pF0-pF 1 à 2.   /9/.

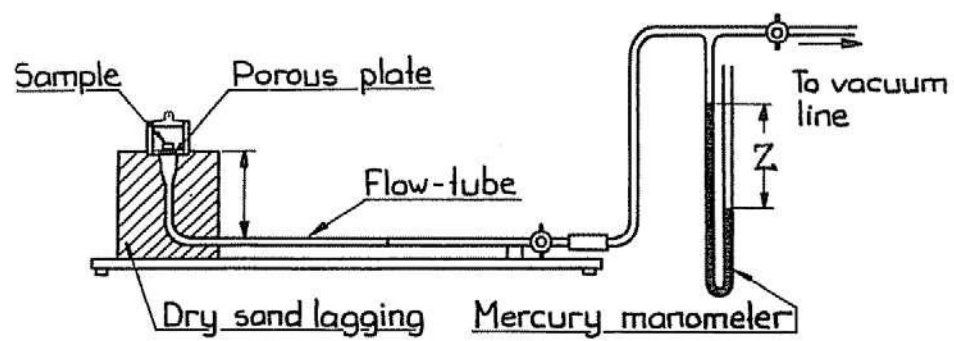FIG 5   Suction apparatus. Range pF0-pF 1 à 2.   /9/.

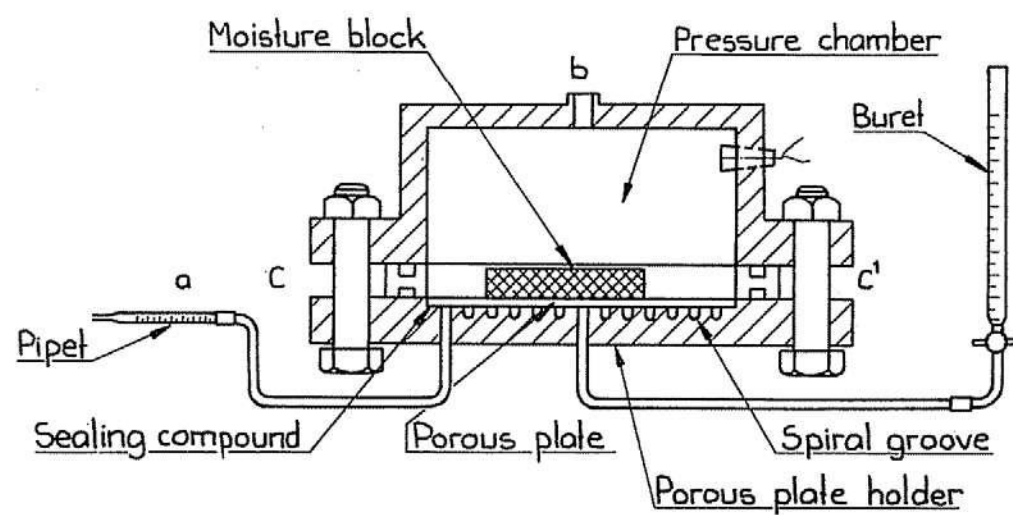FIG 6   Modified suction apparatus for rapid measurements. pF 0-3;   /9/

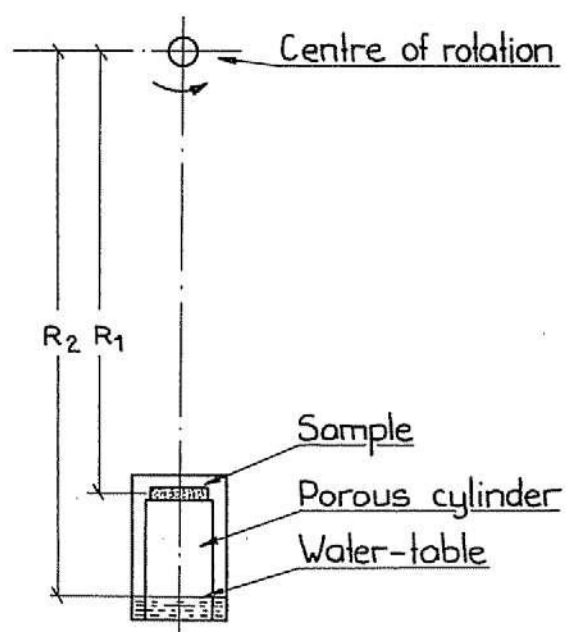FIG 7   Pressure membrane apparatus. /21/.
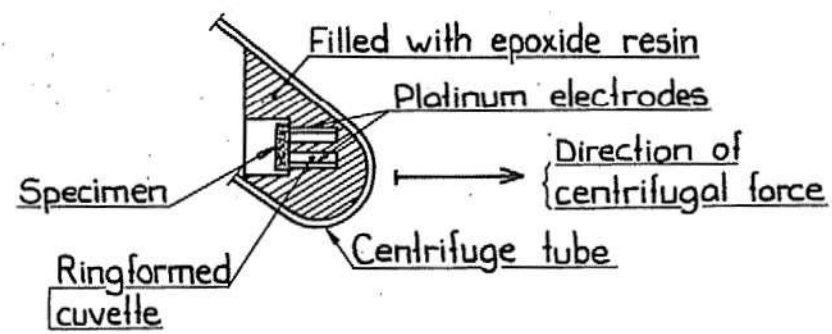

FIG 8   Centrifuge according to Croney et al. /9/.

FIG 9   Specimen cell for investigating pore-size distribution by
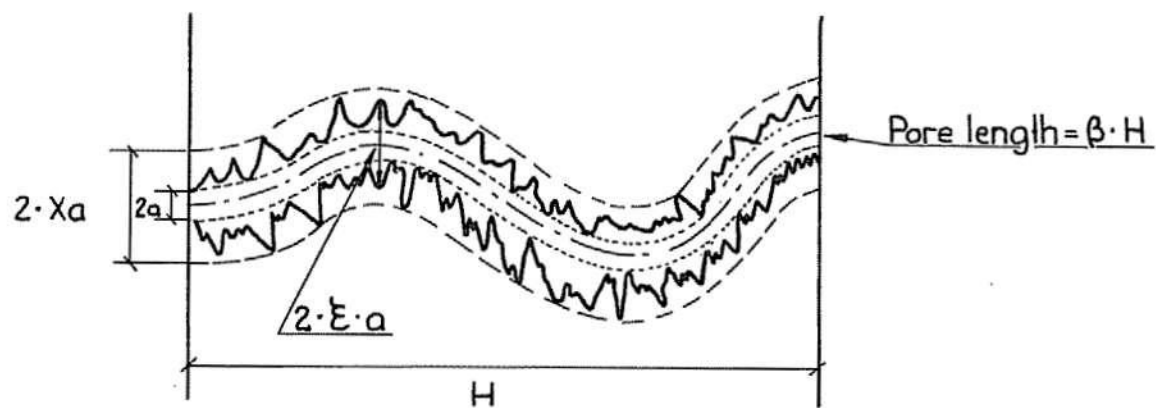   centrifugal method. /16/.
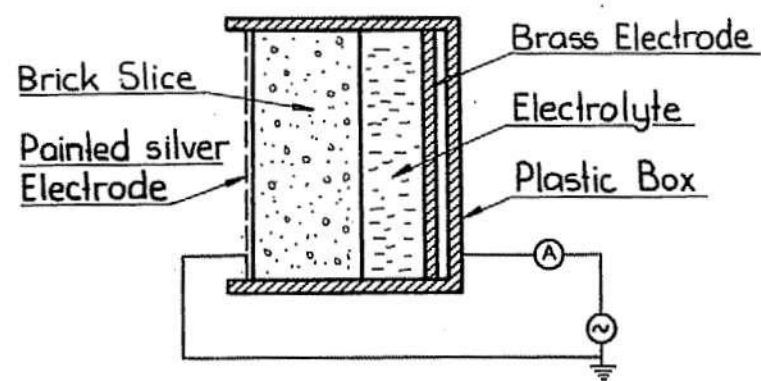

FIG 10 Astbury's pore model. /3/.

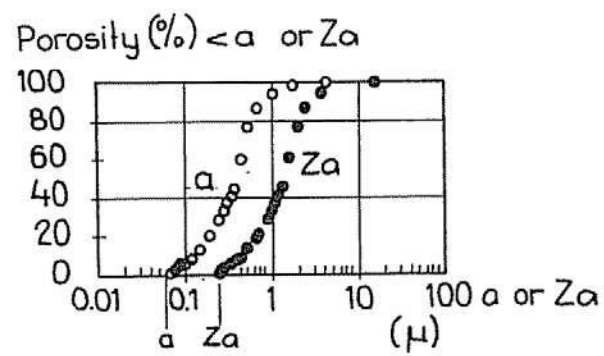FIG 11 Principle of apparatus according to Astbury. /2/.

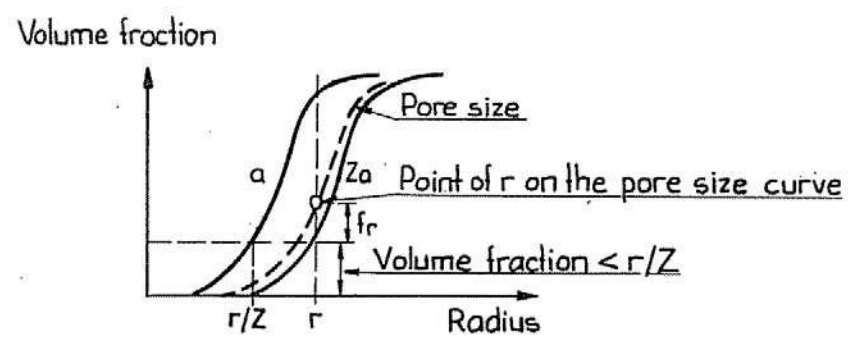FIG 12 Distribution of smallest and coarsest accessible radii. /3/.

FIG 13 Real pore size distribution and distribution of smallest and coarsest accessible radii. /3/.
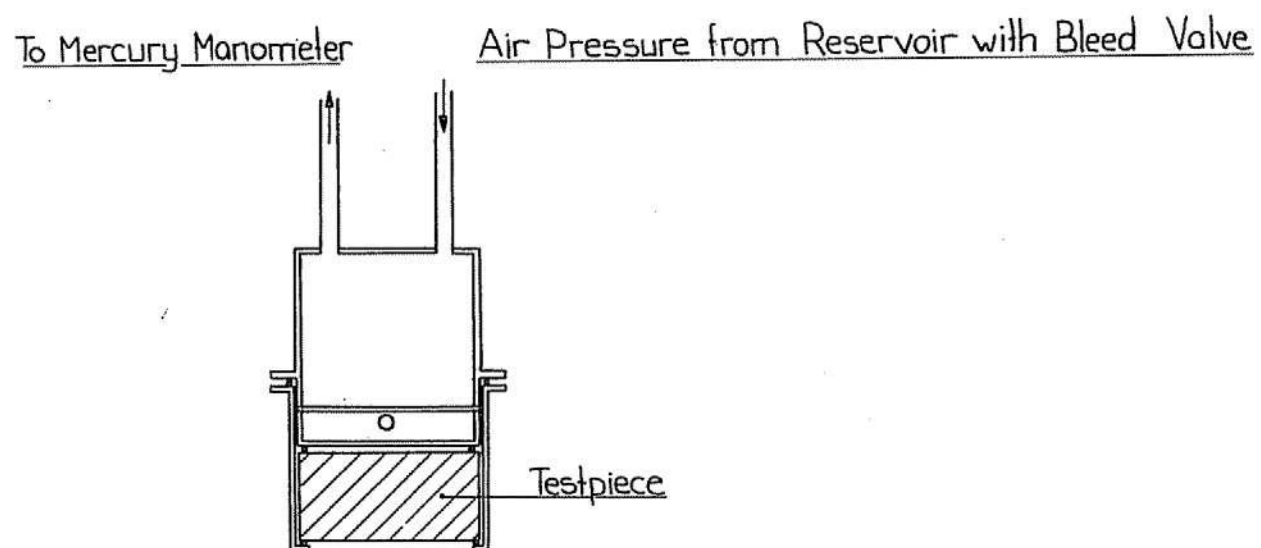

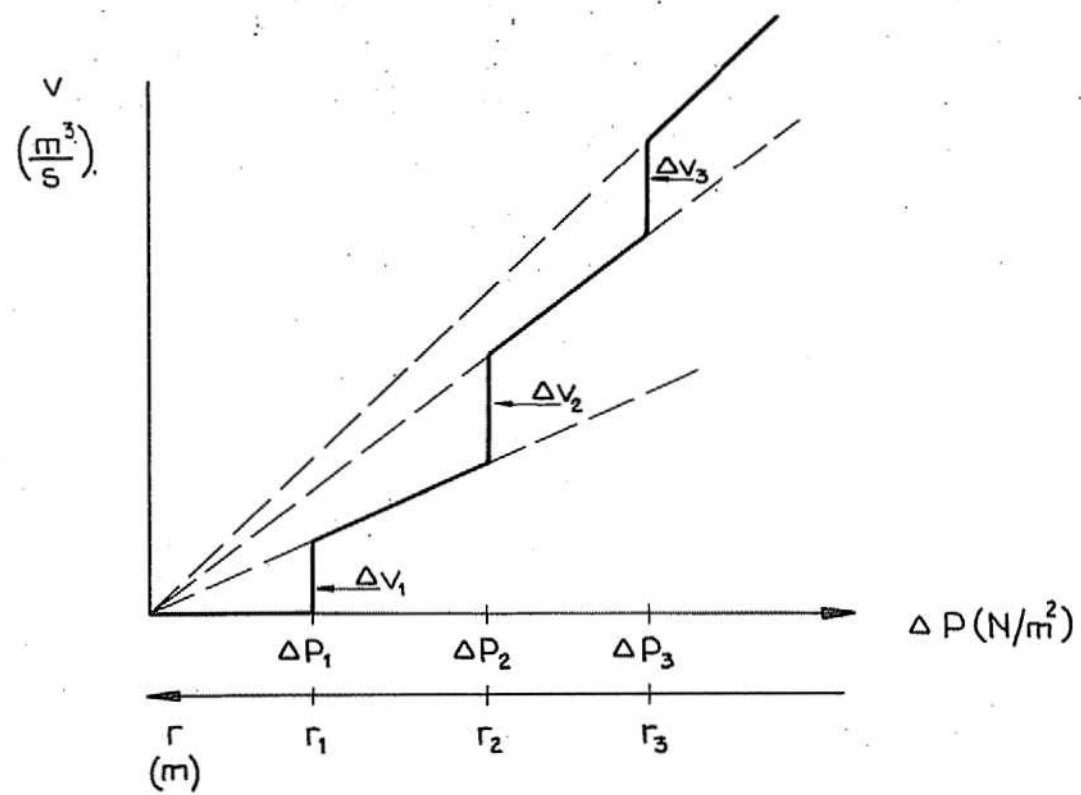FIG 14 Holder for static water-expulsion method. /8/.

FIG 15 Flow rate pressure curve at displacement liquid-liquid in a
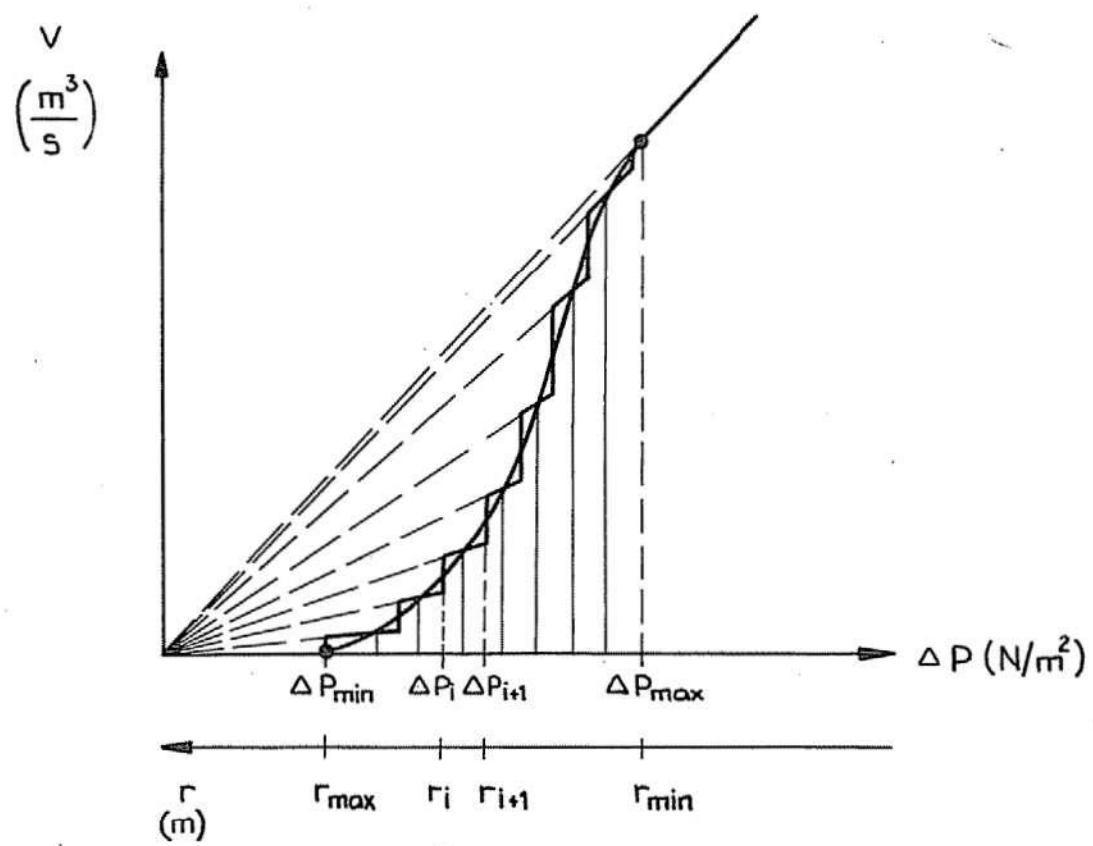material with three pores of different size.

FIG 16 Flow rate-pressure curve at displacement liquid-liquid in
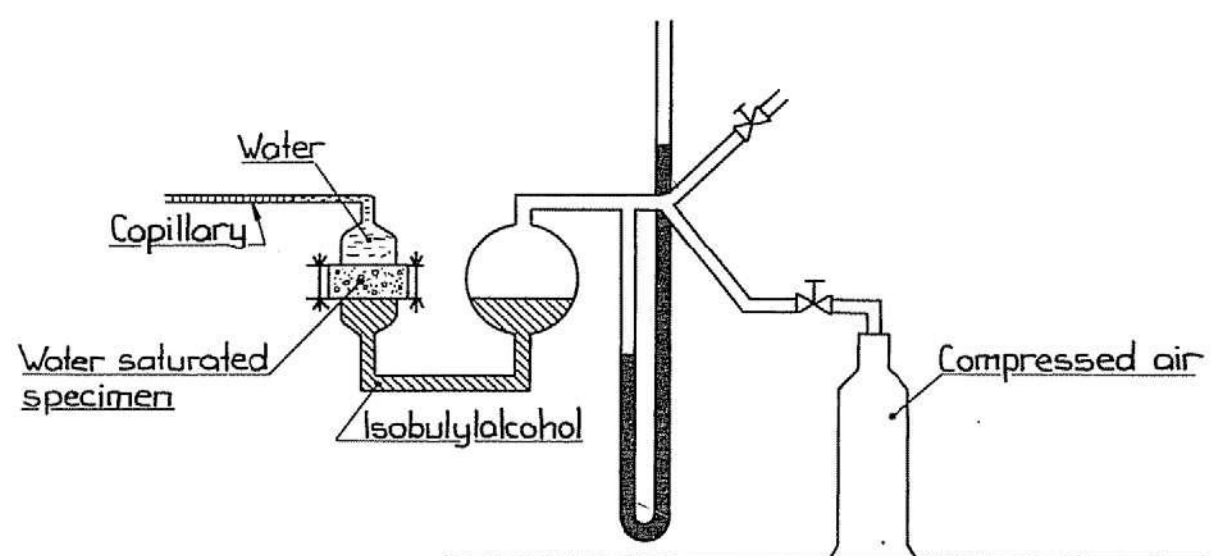a real material.

FIG 17 Apparatus for displacement liquid-liquid. /18/.
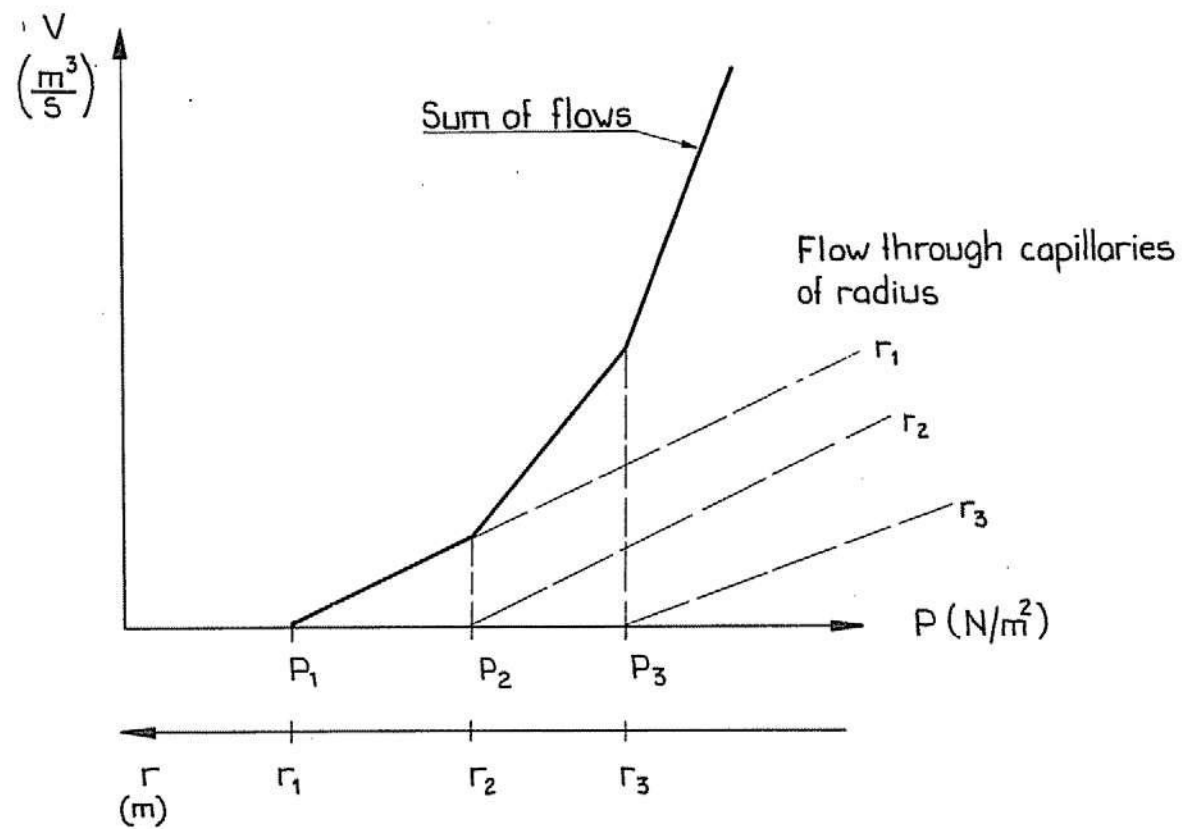
FIG 18 Flow rate-pressure curve at displacement liquid-gas in a
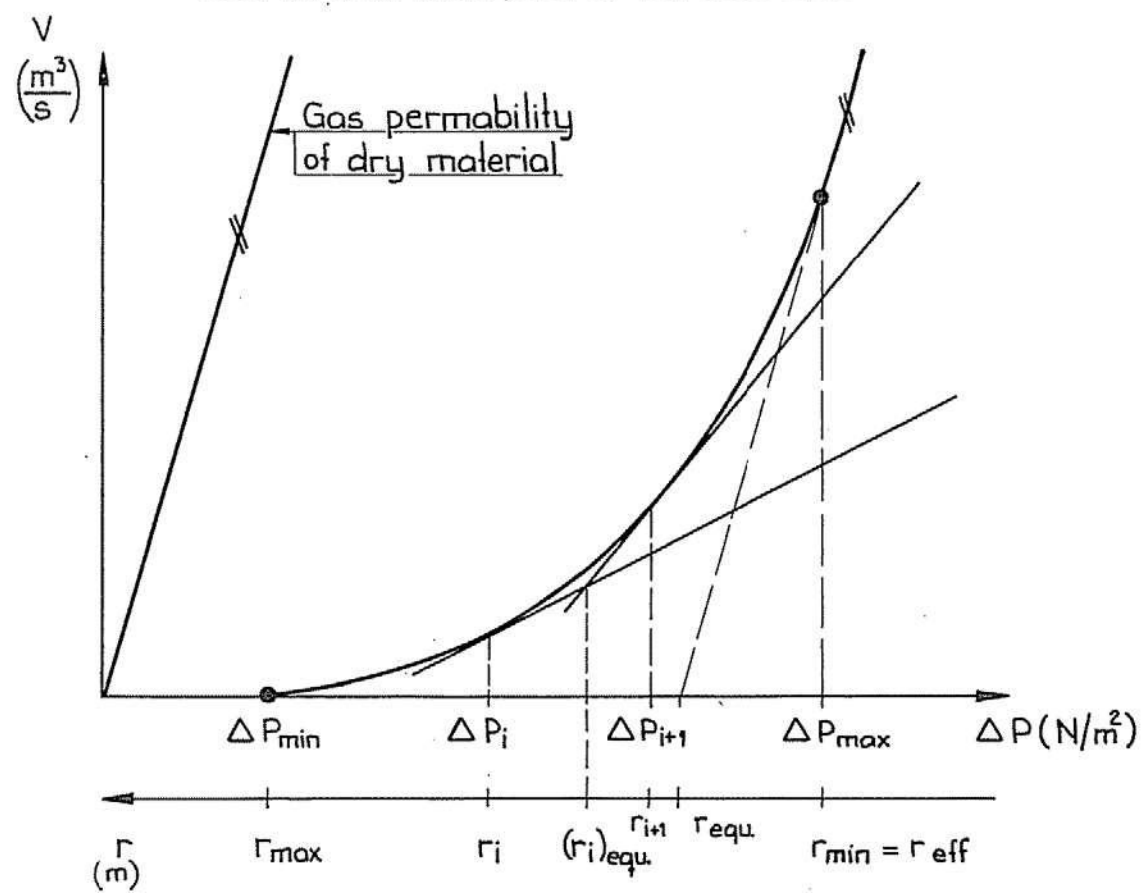material with three pores of different size.

FIG 19 Flow rate pressure curve at displacement liquid-gas in a real
material.

Flow rate = const·permeability

$\Delta P = 3.25 \cdot 10^5 \, N/m^2$

$\Delta P = 2.75 \cdot 10^5 \, N/m^2$

—————— Continous increase in pressure

– – – – – Earlier pressure, ΔP_i relieved before applying new pressure

$\Delta P = 2.00 \cdot 10^5 \, N/m^2$

$\Delta P = 1.75 \cdot 10^5 \, N/m^2$

$\Delta P = 1.50 \cdot 10^5 \, N/m^2$

$\Delta P = 1.25 \cdot 10^5 \, N/m^2$

$\Delta P = 1.00 \cdot 10^5 \, N/m^2$
$\Delta P = 0.75 \cdot 10^5 \, N/m^2$

0

0   1   2   Waiting time (h)

This part magnified below

Flow rate = const · permeability

$\Delta P = 1.25 \cdot 10^5 \, N/m^2$

$\Delta P = 1.00 \cdot 10^5 \, N/m^2$
$\Delta P = 0.75 \cdot 10^5 \, N/m^2$
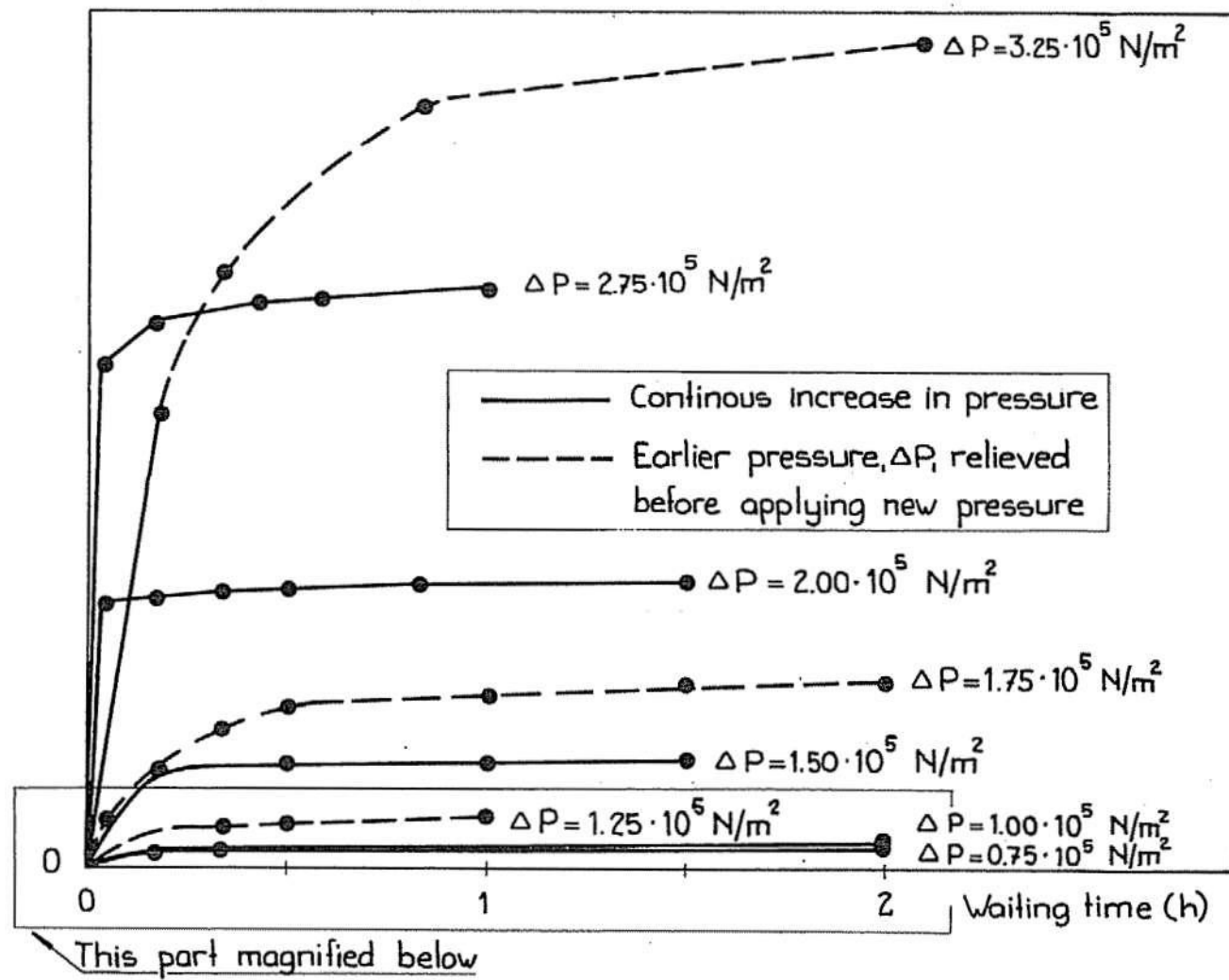
0   1   2   Waiting time (h)

FIG 20 Effect on permeability of waiting-time at water-air displacement. Clay brick, size 30 cm², thickness 30 mm.

FIG 21 Effect of degree of saturation before test on flow-pressure
curves.

① Compressed dried air
② Pressure regulators
③ H_2O manometer
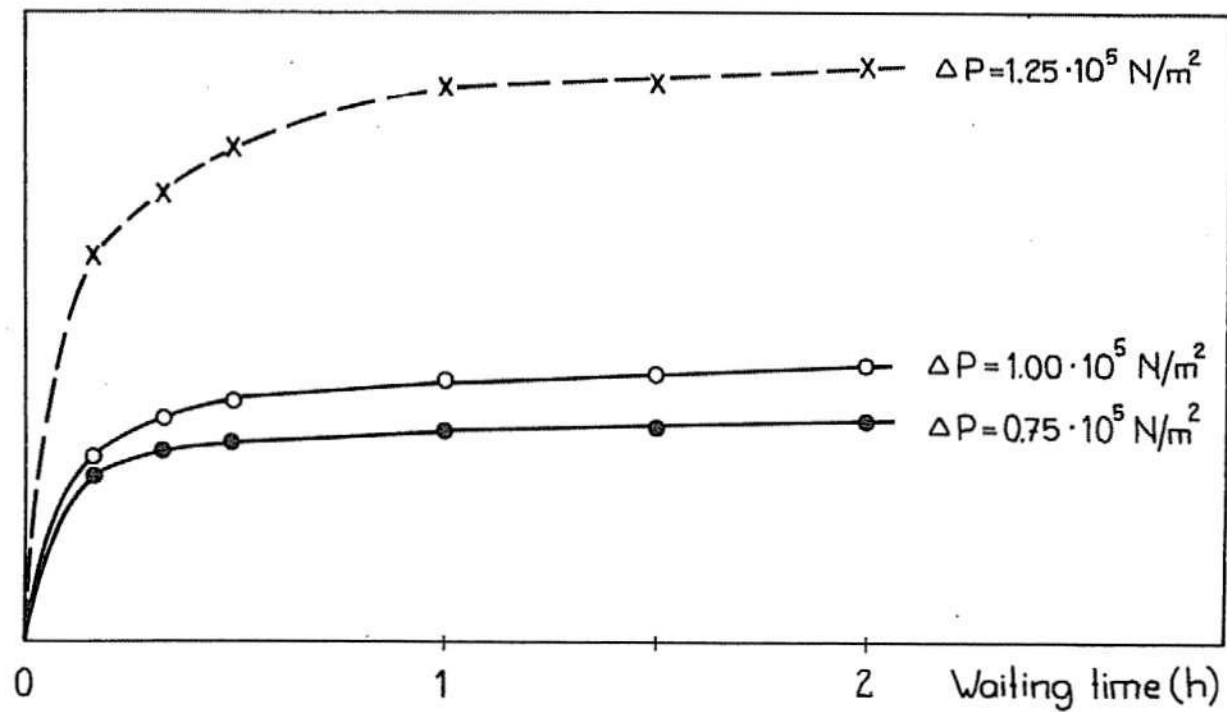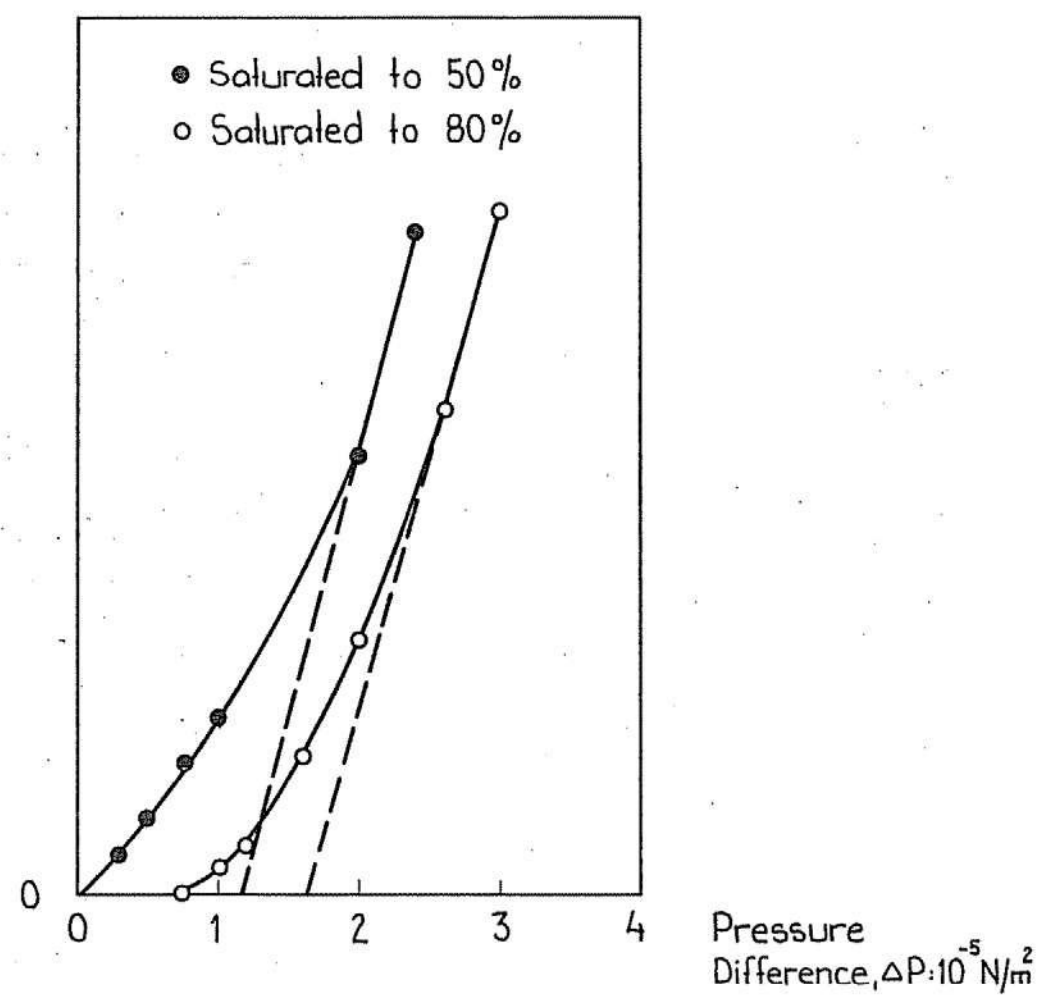④ Hg manometer
⑤ Precision manometer $0-4\cdot10^5 \, N/m^2$
⑥ Four ways valve
⑦ Containers for eventual liquid
⑧ Specimen holder. Stainless steel (See below)
⑨ Funnel for water filling
⑩ Isolated methanol filled container
⑪ Piston for lifting and lowering container
⑫ Burette $0-20 \, cm^3$
⑬ Burette $0-100 \, cm^3$
⑭ H_2O-manometer
⑮ Flow meters, two different ranges

FIG 22 Apparatus for displacement water-air. /12/

6 screws for tightning

6 screws for fastening of lid.

To ⑨

Water

Lid of PMMA partly covered by a plate of stainless steel

Wedges of stainless steel

Bottom of PMMA

Rubber packing   o-ring   Box of stainless steel

II

DETERMINATION OF PORE-SIZE DISTRIBUTION FROM FREEZING-POINT DEPRESSIONS

Contribution to RILEM committee
"Pore Structure and Properties of Materials"

by
Göran Fagerlund

CONTENTS

Lund, September 1972

1 INTRODUCTION

Capillary condensed water in the pore system of a porous material has been found to have the same freezing characteristics as ordinary water; for instance a 9 % increase in volume at transition to ice. This follows from the fact that at subfreezing temperatures "capillary condensation and menisci theories are operative and that a solid meniscus exist", Feldman /4/.

Hence there must be a connection between the pore water pressure and the freezing point depression of the pore water. Consequently the freezing point depression is a function of the pore radius, since there also exists a connection between pore water pressure and pore radius; This connection can be expressed as in eq (1)

$$\Delta p_{1g} = - \frac{2 \cdot \sigma_{1g} \cdot \cos \theta}{r_{1g}} \tag{1}$$

By measurements of the non-freezable water content at different temperatures it is therefore possible to calculate the pore-size distribution.

The determination of non-freezable water contents can also be made indirectly from the sorption isotherm or moisture equilibrium curve (=equilibrium moisture content as function of capillary rise or suction, pF). viz there exist connections between pore water pressure and relative vapour pressure or suction; eq (2)

$$\Delta p_{1g} = - \rho_1 \cdot g \cdot h = \frac{R \cdot T \cdot \rho_1 \cdot \ln(p/ps)}{M} \tag{2}$$

The expressions (1) and (2) are discussed somewhat more extensively in the contribution about suction porosimetry.

Determination of pore-size distribution from freezing point depressions is a method which is relatively unexploited. Any commersially manufactured apparatus are not available as far as we know.

2 THEORETICAL BACKGROUND

2.1 Theoretical expressions

The internal pressure of a small spherical crystal immersed in its own melt is according to eq (1)

$$\Delta p_{s1} = \frac{2 \cdot \sigma_{s1}}{r_{s1}} \tag{3}$$

On basis of eq (3) the following expression can be derived for the equilibrium of the spherical crystal in its own melt. See for instance Sill & Skapski /18/

$$\frac{\Delta T}{T_0} = \frac{2 \cdot \sigma_{s1} \cdot M}{\rho_s \cdot \Delta H} \cdot \frac{1}{r} \tag{4}$$

Williams /23/ derive the following somewhat different expression for the freezing point of a crystal. A similar expression is stated by Helmuth /7/

$$\ln \frac{T_0 - \Delta T}{T_0} = -\omega \cdot \frac{2 \cdot \sigma_{s1} \cdot M}{\rho_1 \cdot \Delta H} \cdot \frac{1}{r} \tag{5}$$

where ω is a shape factor that adopts values between $1,1 < \omega < 1,3$ for different crystal shapes.

Eq (5) is supposed to be valid over a greater temperature span than eq (4). At small freezing point depressions they coincide.

Blachere & Young /2/ add a term to eq (4) where consideration is taken even to the occurence of a liquid-vapour interface. The influence is expressed in terms of a relative humidity of the pore water

$$\Delta T = \frac{2 \cdot \sigma_{s1} \cdot M}{\rho_s \cdot \Delta s_f \cdot r} - \frac{R \cdot T}{\Delta s_f} \left(1 - \frac{\rho_1}{\rho_s}\right) \ln(p/p_s) \tag{6}$$

Since $\rho_1/\rho_s > 1$, an interface water-vapour evidently increases the freezing point. This depends on tensile stresses in the water decreasing the pressure in the ice crystal.

The second term is small compared to the first (≈ 9 % of ΔT /2/) and almost constant with temperature.

Williams /23/ on the other hand takes consideration to the occurence of a solid-gas meniscus which seems more reasonable than the water-gas meniscus. The general equation for freezing point depression then gets the form

$$\ln \frac{T_0 - \Delta T}{T_0} = -\omega \cdot \frac{2 \cdot \sigma_{s1} \cdot M}{\rho_1 \cdot \Delta H} \cdot \frac{1}{r_{s1}} + \left(\frac{1}{\rho_1} - \frac{1}{\rho_s}\right) \cdot \frac{2 \cdot \sigma_{sg} \cdot M}{\Delta H} \cdot \frac{1}{r_{sg}} \tag{7}$$

Since $\frac{1}{\rho_1} < \frac{1}{\rho_s}$ an interface solid gas decreases the freezing point. This is an effect of an extra pressure in the ice crystal caused by the interface ice-gas. If the sample is completely saturated $r_{sg} = \infty$ and the second term is equal to 0. If the sample is not completely saturated the first

ice formed creates solid menisci within the specimen. In this case the second term in eq (7) must be considered.

By combination of eq (3) for the internal pressure in the ice crystal and eq (5) or (4) for freezing point depression, it is possible to calculate the following connection between pressure in the ice and the freezing point

$$\Delta p_{s1} = - \frac{\Delta H}{M} \cdot \rho_1 \cdot \ln \left(\frac{T_0 - \Delta T}{T_0} \right) = \frac{\Delta H}{M} \cdot \rho_s \cdot \frac{\Delta T}{T_0} \qquad (8)$$

Where the secondterm is valid at temperatures around 0^oC. This equation indicates that the ice is under hydrostatic pressure.

Schofield /16/ assumed that the ice first formed was under ordinary atmospheric pressure while the water was under reduced pressure as indicated by eq (1).
This assumption leads to eq (9)

$$\Delta p_{1g} = - \frac{\Delta H}{M} \cdot \frac{\Delta T}{T_0} \cdot \rho_1 \qquad (9)$$

This equation is normally expressed in terms of "suction" by insertion of eq (2) for the pressure difference Δp_{1g}

$$h = \frac{\Delta h}{g} \cdot \frac{\Delta T}{T_0} \qquad (10)$$

Several investigators, for instance Schofield & da Costa /17/ and Williams /23/, have proved experimentally that eq (10) is valid for the initial freezing points for different soil samples with various moisture contents. The fact that eq (10) is applicable indicates that "the equilibrium freezing temperature associated with a particular (unfrozen) water content is not greatly affected, if at all, by the amount of ice (formed at higher temperatures) already present", and "that the unfrozen water content for a soil at a given negative temperature is independent of the total (water and ice moisture content (so long of course, as the total moisture content is not less than the appropriate unfrozen water content", (Williams /23/).

As mentioned earlier the equation gives the freezing point depression for water in contact with ice under atmospheric pressure. This is a connection which can be assumed to be valid for a granular material where the ice often is formed in ice lenses considerably largerthan the pores. In this case the radius of the ice crystal is large and the ice pressure is almost equal to the atmospheric.

For a solid material the size of ice bodies are limited by the width of the pores since an ice lense could not be formed. In this case eqs (3)-(8) ought to be valid.

Kubelka /9/ discuss however the possibility of not using σ_{sl} and ρ_s in those equations at calculation of freezing point depressions in porous inert materials but instead the values σ_{lg} and ρ_l; This would mean considerably greater freezingpoint depressions than those predicted by eqs (4, 5, 6, 7). viz $\sigma_{sl} < \sigma_{lg}$. The following values have been published

/6/ $\quad \sigma_{lg} = 75,64(1 + 1,84 \cdot 10^{-3} - 0,40 \cdot 10^{-6}) \cdot 10^{-3}$ \hfill (11)

/8/ $\quad \sigma_{sl} = 30,5(1 - 0,93 \cdot 10^{-2} \cdot \Delta T) \cdot 10^{-3}$ \hfill (12)

/2/ $\quad \sigma_{sl} = 40 \cdot 10^{-3}$ \hfill (13)

Eqs (4) and (5) are now changed to eq (14)

$$\frac{\Delta T}{To} = -\ln \frac{To-\Delta T}{To} = \frac{2 \cdot \sigma_{lg} \cdot M}{\rho_l \cdot \Delta H} \cdot \frac{1}{r} \tag{14}$$

By insertion of eqs (1) and (2) in eq (14) Shofield´s eq (9) is obtained. This means that Kubelka /9/ takes over the assumptions made by Schofield and apply them even to a solid porous material.

This is justified by experiments (for cement paste) made by Powers & Brownyard /13/. See below.

Williams /23/ has performed freezing experiments with soils. Some of them are shown in fig 1 together with the two curves eq (5) and (14). The experimental results fall beteen the two theoretical curves. Blachere & Young /2/ on the other hand have proved the correlation between eq (6) and the mean pore radius of glass powders.

By kombination of eq (14) and Kelvin´s law for capillary condensation as expressed in eq (2) it is possible to calculate a connection between the freezing point depression of the water in a pore and the relative humidity for capillary condensation in the same pore

$$-\frac{\Delta T}{To} \propto \ln \frac{To-\Delta T}{To} = -\frac{1}{\omega} \frac{R(To-\Delta T)}{(\Delta H)_{To-\Delta T}} \cdot \ln(p/p_s)_{To-\Delta T} \tag{15}$$

Where indici $(To-\Delta T)$ indicates the temperature for which p/p_s and ΔH should be valid.

The freezing point depression can also be calculated from the sorption isotherm determined at another constant temperature T. In this case the connection gets the form

$$-\frac{\Delta T}{T_0} \approx \ln \frac{T_0 - \Delta T}{T_0} = -\frac{1}{\omega} \cdot \frac{R(T_0 - \Delta T)}{(\Delta H)_{T_0 - \Delta T}} \cdot \frac{(\sigma_{lg})_{T_0 - \Delta T}}{(\sigma_{lg})_T} \cdot \frac{(\rho_l)_T}{(\rho_l)_{T_0 - \Delta T}} \cdot \ln(p/p_s)_T \quad (16)$$

An equation like (16) was suggested by Powers & Brownyard /13/ at their comparison between non freezable water content of cement paste and the sorption isotherm.

Eq (5) can also be transformed to a form similar to that of eq (15) by insertion of eqs (1) and (2)

$$\ln \frac{T_0 - \Delta T}{T_0} = -\frac{1}{\omega} \cdot \frac{R(T_0 - \Delta T)}{(\Delta H)_{T_0 - \Delta T}} \cdot \left(\frac{\sigma_{sl}}{\sigma_{lg}}\right)_{T_0 - \Delta T} \cdot \ln (p/p_s)_{T_0 - \Delta T} \quad (17)$$

2.2 Semiempirical expressions

In a fine porous material water and ice co-exist in the pore system since evidently a fraction of the water remains unfrozen even at low temperatures. Washburn /21/ has derived an expression for the connection between the vapour pressure of ice, vapour pressure of supercooled bulk water and temperature

$$^{10}\log \frac{p_i}{p_s} = -\frac{1,1489 \cdot \Delta T}{T_0 - \Delta T} + 1,33 \cdot 10^{-5}(\Delta T)^2 + 9,084 \cdot 10^{-8}(\Delta T)^3 +$$

$$+ 1,08 \cdot 10^{-9}(\Delta T)^4 \quad (18)$$

At the freezing point the evaporable water and the ice are at equilibrium. Hence

$$^{10}\log p/p_s = \text{eq } (18) \quad (19)$$

Washburn´s expression is semiempirical since it is based upon empirical data for the specific heats of ice and super-cooled water. Washburn /21/ states however that calculated vapour-pressures according to eq (18) agree extremely well with measured values. At -16^0C the difference $(p_i - p_s)$ between calculated and measured values is only 0,004 mm Hg. Another connection between the vapour-pressure of ice and water and the temperature has been used by Puri et al /15/.

$$-\ln p_i/p_s = 0,9686 \cdot 10^{-2}\Delta T - 0,56 \cdot 10^{-6}(\Delta T)^2 + 0,72 \cdot 10^{-8}(\Delta T)^3 \quad (20)$$

And similar to the derivation of eq (19)

$$-\ln p/p_s = \text{eq (20)} \qquad (21)$$

Hence by knowledge of the sorption isotherm it is possible to calculate the amount of non freezable water at different temperatures not only through eqs (15), (16) or (17) but also through eqs (19) or (21) after adaptation of the isotherm to the actual temperature.

Both eq (19) and (21) can be used for an evaluation of pore-size distribution from freezing point depressions. This is done by combining eq (19) or (21) with Kelvin´s law eq (2).

For instance a combination of eq (19) with eq (2) (and (1)) gives the expression

$$r_K = \frac{2 \cdot \sigma_{lg} \cdot M}{\rho_1 \cdot R(T_o - \Delta T) \cdot 2,303} \cdot \frac{1}{\frac{1,1489 \Delta T}{T_o - \Delta T} - 1,33 \cdot 10^{-5}(\Delta T)^2 - 9,084 \cdot 10^{-8}(\Delta T)^{3-}}$$

$$\cdot \frac{1}{-1,08 \cdot 10^{-9} \cdot (\Delta T)^4} \qquad (22)$$

At the calculation of pore-size distribution it is also necessary to make corrections for non-freezable water between the ice body in a pore and the pore wall. See 2.4.

2.3 Comparison between different expressions for freezing-point depression

One of the major problems at use of the theoretical expressions in section 2.1 at evaluating freezing point depressions is that little is known about the variation of the heat of fusion with temperature.

The formula for this variation of bulk water is

$$\Delta H = M \left\{ 333700 - \int_o^{\Delta T} (C_w - C_i) \cdot dT \right\} \qquad (23)$$

Only the variation of C_i with temperature is well known /6/. However if data of C_w in the range $0 - -5^\circ C$ is used the following expression is obtained

$$\Delta H = M \left\{ 333700 - \int_o^{\Delta T} 2190 \, dT \right\} \qquad (24)$$

According to this equation $\Delta H = 0$ at $-152^\circ C$. Hence it must be limited to moderate freezing point depressions.

ΔH according to eq (24) has been inserted in eqs (15) and (17). Eqs (11) and (12) are used for surface tensions. Then these equations are drawn in fig 2 together with the semiempirical eqs (19) and (21).

Evidently the exact eq (15) (with ΔH according to eq (24)) and the semi-empirical equations (19) and (21) give approximately the same result down to a freezing-point of -30°C. After that, certain deviations occur, probably depending on different estimations of the heat of fusion at low temperatures.

The approximate eq (15) differs from the exact already at -10°C. The deviations are however relatively small for moderate freezing-point depressions.

eq (17) based on surface tension solid-liquid gives a freezing-point depression-relative pressure curve quite different from the other equations.

By equaling the theoretical exact equation (15) with the semiempirical equations (19) or (21) it is possible to calculate the heat of fusion on which eq (19) and (21) are based.

A combination of eq (15) with eq (19) gives a heat of fusion

$$\Delta H = M(333700 - 2000\Delta T) \qquad (25)$$

which is approximately the same result as the theoretically derived eq (24).

Powers & Brownyard /13/ used eq (19) at calculation of non-freezable water content in cement-paste. The agreement between measured and calculated values is rather good down to -30°C. See table 1.

TABLE 1

Temp °C	Non-freezable water-content expressed as number of molecular layers on the internal surface		
	Observed	Calculated	Ratio
-12	4,00	3,72	1,08
-20	3,70	3,25	1,13
-30	3,20	2,93	1,09

Eqs (15) and (21) will evidently give the same good agreement.
The authors used the absorption isotherm at their calculation since they
regarded melting of ice in a material a process of absorption. viz the
observed non-freezable water contents were determined by melting-experi-
ments.

Probably the correlation between measured and calculated values should
have been less satisfactory if the desorption-isotherm had been used as
the basis of calculation.

No evidence have been found in literature where an equation of type (17)
have proved the same good agreement with experimental data as eqs (15),
(19) and (21).

Hence since it is such a good correlation between eq (15) and the semi-
empirical eq (19) which in turn has been succesfully used by Powers &
Brownyard, as mentioned above, it is suggested that the following expres-
sions are used at the calculation of pore-size distribution from freezing-
point depressions

$$r_K = - \frac{2 \cdot \sigma_{lg}}{\rho_1 \cdot \Delta H} \cdot \frac{M \cdot 1}{\ln(\frac{T_0 - \Delta T}{T_0})} \tag{14'}$$

or for smaller freezing-point depressions

$$r_K = \frac{2 \cdot \sigma_{lg} \cdot M}{\rho_1 \cdot \Delta H} \cdot \frac{T_0}{\Delta T} \tag{14''}$$

where $\underline{\Delta}H$ is obtained from eq (24). σ_{lg} from eq (11) and ρ_1 from eq (26)

$$\rho_1 = 1000 - 0,26 \cdot \Delta T \tag{26}$$

A simplified function in the range $0 \leq \Delta T \leq 50^0C$ is

$$r_K = \frac{1}{8,061 \cdot 10^6 \Delta T - 6,12 \cdot 10^4 (\Delta T)^2 + 2 \cdot 10^2 (\Delta T)^3} \tag{27}$$

The function (14') is shown in figure 3.

2.4 Adsorbed non freezable water

Water close to the pore-walls does not freeze at normal temperatures.
Williams /23/ states that the thickness of this layer on clay particles
is about 70 A at temperatures around 0^0C. Feldman /4/ gives the value
50 A of the thickness of the adsorbed layer on glass. Loewenstein /11/
reports an adsorbed water film on glass fibres of 25 molecules which is
about 77 A. However the thickness ought to diminish rapidly at decreasing
temperatures.

At an evaluation of the pore-size distribution consideration must be taken to the thickness of the adsorbed layer. It is assumed that the pore-radius is composed of two parts. See fig 4.

$$r = t + r_K \tag{28}$$

r_K is obtained from eq $(14')$
t is obtained from eq (29) (Wheeler /22/)

$$t = -d\left(\frac{5}{\ln p/p_s}\right)^{1/3} \tag{29}$$

where $d = 3,5 \cdot 10^{-10}$ (m)

By using eq (15) it is possible to calculate a connection between the thickness of the adsorbed layer and the freezing-point depression

$$t = 28,5 \cdot 10^{-10} \cdot \sqrt[3]{\frac{1}{\Delta T}} \tag{30}$$

At $\Delta T = 0,05^{\circ}C$ $t = 77$ A and at $\Delta T = 0,1^{\circ}C$ $t = 61$ A values that are in accordance with the values stated above.

In order to get an idea of the accuracy of eq (30) a comparison is made between the absorption isotherm of cement-gel according to Powers & Brownyard /13/ and eq (30). Cement-gel is a material with extremely small pores.

TABLE 2

ΔT ($^{\circ}C$)	p/p_s	$\frac{t}{d}$		Difference Δt (A)
		eq (30)	isotherm /13/	
5	0,95	4,75	3,15	5,6
11	0,90	3,65	2,78	3,0
17	0,85	3,17	2,60	2,0
23	0,80	2,84	2,44	1,4
30	0,75	2,62	2,35	0,9
39	0,70	2,40	2,22	0,6
47	0,65	2,26	2,12	0,5
60	0,60	2,08	2,00	0,3
75	0,55	1,93	1,90	0,1

Obviously eq (30) gives somewhat greater values of t than the measured. However at smaller pores the difference is rather small. The difference may depend on restrictions of adsorption caused by limited pore-sizes.

2.5 Calculation of pore-size distribution

It is assumed that the non freezable water content in the material has been determined as function of temperature. Perhaps this has been done by use of a calorimeter (see part 4.3 below).

Consider a hypothetical curve $W_{nf} = f(\Delta T)$ (figure 5).

The pore-size distribution is calculated in accordance with the method by which a pore-size distribution is calculated from a sorption-isotherm. See for instance /5/.

$(r_k)_n$ and t_n at temperature $To-\Delta T_n$ are obtained from eq (14') and (30) respectively

$$(\Delta V_p)_n = (\Delta V_k)_n \cdot \left(\frac{r_{n-1} + r_n}{(r_k)_{n-1} + (r_k)_n}\right)^2 \qquad (31)$$

$$(\Delta V_k)_n = (\ (W_{nf})_{n-1} - (W_{nf})_n) \cdot \frac{1}{\rho_n} - (\Delta V_t)_n \qquad (32)$$

$$r_n = (r_k)_n + t_n \qquad (28')$$

$$(\Delta V_t)_n = (t_{n-1} - t_n) \cdot \sum_{0}^{n-1} (\Delta S)_i \qquad (33)$$

$$(\Delta S)_i = \frac{4 \cdot (\Delta V_p)_i}{r_{i-1} + r_i} \qquad (34)$$

Successive insertion of eq (32), (28'), (33) and (34) in eq (31) gives

$$(\Delta V_p)_n = \left\{[(W_{nf})_{n-1} - (W_{nf})_n] \cdot \frac{1}{\rho_n} - 4(t_{n-1} - t_n) \cdot \sum_{0}^{n-1} \frac{(\Delta V_p)_i}{r_{i-1} + r_i}\right\} \cdot$$

$$\left[\frac{r_{n-1} + r_n}{(r_k)_{n-1} + (r_k)_n}\right]^2 \qquad (35)$$

It is assumed that all pores are cylindrical.

3 DISCUSSION OF THE METHOD

3.1 Generally

An advantage of the method is that it is very fast and cover a large pore-size range (=40Å - 5000Å). A calorimetric determination of freezable water takes only a few hours while a determination of pore-size distribution from for instance a water vapour isotherm is an affair of weeks.

Another advantage is that the medium of measurement is water.

The method has however many disadvantages. The first one is of pure
theoretical nature. It lies in defining a true connection between pore-
size and freezing point depression and has been discussed above in sec-
tions 2.1 and 2.2.

Other difficulties will be discussed below.

3.2 Water content required at the test

If the method is to be useful it is necessary that the pore-water is in
thermodynamic equilibrium before (and after) the freezing. Besides the
moisture ratio has to be great enough to ensure that all pores with radii
less than about 1 µm are filled with water. Those demands may of course
be fulfilled by using specimens which from the beginning have been comple-
tely saturated, for instance by vacuum-treatment, after which they have
passed through a successive emptying of pores at a determination of pore-
size distribution by a sort of suction-measurement.

The effect of not using a completely saturated specimen can be estimated
from eqs (6) and (7).

3.3 Displacement of water at freezing

Water expands about 9 % volume at freezing. This is according to Feldman
/4/ even valid for capillary condensed water. That fact bring about cer-
tain displacements of non-frozen water within the specimen. The recipients
for that water are previously empty pores and the surface of the material.
At the same time non-freezable water from narrow pores migrates to ice-
bodies in the coarser pore where it freezes. The latter fenomenon is a sort
of drying process which is especially pronounced at very fine-porous ma-
terials as for instance cement-pastes with w/c-ratio less than about
0,55 /10, 12/.

However those displacements have evidently not had any greater signifi-
cance at the experiments on even dense cement-pastes performed by Powers
& Brownyard (table 1).

3.4 Deformation of the specimen at freezing

Because of the swelling of the water at freezing the specimen may sustain
such big deformations that its tensile strength is exceeded at certain
points at which the porosity-conditions are changed. However at the mo-
derate degrees of saturations needed in a specimen at the experiment
(c.f. point 3.2) above) the swelling will probably be insignificant and

above all reversible at the melting of ice. Besides unpublished results
at our institution as well as results published by Powers and Helmuth /12/
indicate that specimen frozen at "moderate" degrees of saturation rather
shrink than swell.

As an example is assumed a specimen with the open porosity 40 %. The pores
are filled to 80 % at the beginning of the freezing. It is assumed that
90 % of the water is freezable at the lowest temperature used. This must
be considered an extreme material.
The maximum swelling under the assumption that no water is displaced from
its original locus is

$$\frac{\Delta V}{V} = \frac{0,09 \cdot 0,4 \cdot 0,8 \cdot 0,9}{1} = 0,0259$$

Under the assumption that all the swelling is plastic or viscous, that
is, non-reversible at the melting, a highly unlikely assumption, and that
the pore-walls are incompressible, the increase in total pore-volume is

$$\frac{\Delta V_p}{V_p} = \frac{0,0259}{0,40} \cdot 100 = 6,5 \ \%$$

Therefore the errors dependent on deformation of a normal specimen must
be small.

3.5 Salts in the pore-water

Occurence of salts in the pore-water influences the freezing point de-
pressions. However the same problems exist when pore-size distributions
are evaluated from water-vapour sorption-isotherm. Figure 6 shows some
examples of the influence of salt concentration in the pore-water on the
absorption-isotherm, Vos & Tammes /19/.
The final melting-point of the pore-water is a measure of the concentra-
tion of salts provided that the biggest water-filled pores are numerous
and represent negligible freezing point depressions.

Powers & Brownyard /13/ measured final melting points on cement-pastes.
They found values of final melting points between $-0,05^o$C and $-1,60^o$C.
The value $-0,05^o$C is valid for cements with low percentage of alkalies.
A simple calculation shows that under the reasonable assumption that
the pore-water always is a saturated solution of $Ca(OH)_2$ the final mel-
ting point ought to be around $-0,05^o$C. The value $-1,60^o$C represents a
cement with a high percentage of soluble alkalies (Na_2O and K_2O). The
results also show that specimen with the same cement but different

w/c-ratios had different final melting-points. The higher the w/c-ratio, the closer to $0^{o}C$ was the final melting point which probably depends on leaching out of alkalies during the 28 days water storage before the test. A high w/c-ratio signifies a high permeability and a high rate of leaching. Therefore, in order to avoid influence of salts on the freezing-point depressions a practicable way can be to use water-stored specimen.

3.6 Hysteresis between ice-formation and ice-melting

Powers & Brownyard /13/ showed the existence of a certain hysteresis between ice-formation and ice-melting in cement-pastes. According to them ice-formation is similar to a process of desorption while ice-melting is rather a process of absorption.

Helmuth /7/ has explained the hysteresis by geometrical properties of the pore-system. Ordinary water does not freeze at the ordinary freezing-point but is super-cooled to a temperature dependent on the amount of water. At the occurence of impurities in the water. Bigg /l/ has found the connection between mean freezing-temperature and the size of the water droplet indicated in figure 7.

Since the pores in ordinary building materials are small the fenomenons of super-cooling can be considerable. However the super-coolings occuring are in most cases relatively small, normally less than $5^{o}C$ since the number of pores are large and therefore the probability of an early freezing in any pore is relatively great. See figure 8 from Bigg /l/. This figure shows the frequency-curve of freezing temperatures of a certain water-dropsize. Similar functions are valid for other sizes.

However, large super-coolings may occur in isolated pores for the following reason. When the ice-formation after a slight super-cooling is initiated in one point in a material it propagates very fast through all pore-water freezable and reachable at the actual temperature. This has been shown by Helmuth /7/ who even states a rate of propagation of the ice-front of about 10 mm/s. However, the ice-front may not propagate into water which is certainly freezable at the actual temperature but which is enclosed by pores so narrow that its water is not yet freezable. Freezing of this enclosed water can not occur until the temperature is low enough to make it possible for the ice-front to propagate the pore-openings (c.f. eq (14$^{'}$)) or the water in those pores freezes by "self-nucleation".at about $-40^{o}C$. Therefore it can not be expected that for instance the same amount of water is frozen at $-10^{o}C$ when the minimum

freezing temperature is exactly -10°C as when the specimen is thawed to -10°C from a lower temperature. A hysteresis between ice-melting and ice-freezing occurs This is exemplified in figure 9 which shows an example of the authors determination of non-freezable water at -10°C in a cellu-lar concrete frozen to -12,5^{o}C and to -25°C.

Cement-paste has been considered as a material composed of more or less isolated capillary pores in which the water is freezable at ordinary tem-peratures. The capillaries are embedded in a matrix composed of a very fine-porous gel with non-freezable water. The capillary pores are forming an interconnected network only at w/c-ratios larger than about 0,55-0,60 /14/. According to this model a dense cement-paste ought to be a material where the above-mentioned effect of super-cooling is great. According to Winslow & Diamond /24/ there exist threshold diameters in cement-paste at determination of pore-size distributions by mercury-intrusion. Below the threshold diameter the greatest portion of intrusion commences. Above the treshold diameter the intrusion is very small.

The threshold diameter is about 0,08 µm at w/c= 0,40 and 0,10 µm at w/c = 0,60, if the pastes are well hydrated. These two values represent freezing-point depressions of only about 3,3^{o}C and 2,6^{o}C respectively according to eq (14$^'$) and eq (30) (consideration taken to adsorbed water). However probably other "threshold diameters" exist in cement-paste that cause hysteresis in ice-formation and ice-melting even at lower tempera-tures.

Therefore to avoid the effect of hysteresis and super-cooling it is pro-posed that the specimen is frozen to at least -50°C ä -60°C before the test and that the test is performed as a thawing-test. Powers & Brown-yard /13/ performed their determinations of freezable water content in cement-paste on specimen frozen to -78°C.

4 METHODS OF MEASUREMENTS

4.1 Determination of initial freezing temperatures

Eq (10) shows the connection between the initial freezing temperature and the suction (capillary rise) of the material.

Croney et al /3/ advise a simple calorimeter for determination of the initial freezing temperature. This method can however be used only for suctions of $3 \leqslant pF \leq 4$ that is for pore radii $0,15\mu \leq r \leq 1,53\mu$ and freezing-point depressions of $0,1^oC \leq \Delta T \leq 0,8^oC$.

4.2 Dilatometric method

As mentioned in the introduction capillary condensed water is assumed to
expand ≈ 9 % at freezing, just as bulk water. Then the amount of ice for-
med or melted can be determined by measurements of the volume change of
a saturated sample. This method was used by Powers & Brownyard /13/ at
their determinations of non freezable water contents of portland cement-
paste.

The specimen was crushed into granules which were water saturated. The
granules were put in a glass-bulb and frozen to $-78^{\circ}C$ in a mixture of
solid CO_2 and alcohol. Then the air in the bulb was evacuated and toluene
let into it. On the top of the bulb was a calibrated glass capillary,
also filled with toluene.

The temperature was raised after the dilatometer was put in a cryostat
and the level of the meniscus in the capillary read. Powers & Brownyard
give the equation for calculation of amount of ice formed or melted.
It is necessary to compensate for the presence of toluene and its effect
on the water vapour pressure. This can be done through eq (35)

$$\frac{\Delta T}{\Delta T_t} = \frac{\sigma_{wa}}{\sigma_{wt}} \approx 2 \qquad (35)$$

Some results are already shown in table 1. As predicted by the reasoning
in section 3.6 the authors found a hysteresis ice-formation – ice-mel-
ting.

4.3 Calorimetric methods

Blachere & Young /2/ used DTA-technique for determination of freezing-
and melting-curves of saturated glass-powders.

Williams /23/ describe a calorimeter by which freezing as well as melting
experiments can be done.

At our institution we have used a simple type of calorimeter built at the
institution. Figure 10.

It consists of an ordinary freezing-box capable of reaching $-30^{\circ}C$. In
the box there is placed a cylindrical vessel of copper. The specimen with
size $30 \times 30 \times 120$ mm^3 is wrapped in aluminum foil and placed in a
specimen-holder made of aluminum which in turn is placed centrically
in the copper vessel. The specimen-holder is provided with a 220 ohms
heating-coil of nichrome. On the outer surface of the specimen-holder

as well as on the inner surface of the copper-vessel there are placed two 120 ohm resistance-thermometers. Two thermocouples are placed within the specimen, one at the top and one in the center. One thermocouple is placed at the surface of the specimen-holder and two at the surface of the copper-vessel.

The heating-coil is connected to a stabilized DC-aggregate with variable voltage.

The resistance thermometers are connected to a tyristorized temperature regulator. This senses the temperature-difference between the copper-vessel- and specimen-holder-surfaces. If there is a difference the regulator corrects this by changing the voltage on 6 lamps of 200W each.

The four resistance thermometers are not quite alike either in resistance or in temperature-coefficients. Therefore the regulation must be adjusted to give fair results. This is done by thawing test on a container with a known amount of water and on prisms of metals with known heat capacities. The adjustment is performed by changing the resistance of one thermometer-branch by the aims of a precision potentiometer.

The specimen is adapted to a suitable amount of water (c.f. 3.2 above). It is provided with thermocouples and placed in the specimen-holder. This in turn is placed in the copper-vessel. The whole assembly is frozen to $-25^{\circ}C$ during about 16 hours. The DC-aggregate is adjusted to a suitable voltage dependent on the heat capacity of the specimen. The rate of temperature-rise ought to be alike for all specimen. The temperature of the specimen gradually increases which means that the temperature-regulator gradually increases the voltage on the 6 lamps, so that the temperature-difference between the surfaces of the copper-vessel and the specimen-holder is minimized, = adiabatic conditions.

The results of the test is registrated on the recorder.

When corrections are made for eventual errors dependent on imperfect regulation the result is a curve; Specimen-temperature as function of supplied energy to the specimen. See figure 11.

Provided that the total specific heat of the dry specimen and the specimen-holder is a constant in the interval $-25^{\circ}C - +5^{\circ}C$ the freezable water at temperature θ_n is (c.f. figure 11)

$$\frac{(W_f)_{n+1} \left\{ \Delta h_n + \frac{1}{2} (\theta_{n+1} - \theta_n) \cdot (C_w - C_i)_n \right\} + W_{n+1} - W_n - C \cdot (\theta_{n+1} - \theta_n)}{\Delta h_n - \frac{1}{2}(\theta_{n+1} - \theta_n) \cdot (C_w - C_i)_n} = (W_f)_n \quad (37)$$

where $\Delta h_n = 333700 + 2190 \cdot \theta_n$ (24')

and $(C_w - C_i)_n = -9,9 \cdot \theta_n + 2107$ (38)

The non-freezable water-content at each temperature is obtained from

$$(w_{nf})_n = w_e - (w_f)_n \qquad (39)$$

After calculation of the non-freezable water-content the pore-size distribution can be calculated from eq (35).

The calculation are very well suited for a computer.

In figure 12 there is shown the pore-size distribution in the range 200 A-5000 A for a certain sand-lime brick. One of the two distribution-curves is calculated according to eq (35), on basis of a calorimeter experiment the other is measured by Hg-porosimeter at the State Institute for Technical Research in Finland.

The specimen-size is 120 cm^3 at the determination from freezing-point depressions and only 0,61 cm^3 at determination by Hg-porosimeter. Therefore the latter is less representative especially since this type of sand-lime brick contains coarse quartz-grains. However there is a godd correspondence between the two curves at pore-radii smaller than 200 A and coarser than 2000 A. The deviation is considerably greater for pore-radii between those two values. Probably this is an effect of hysteresis since the Hg-porosimeter is a method based upon absorption. In the other method the water is already present in the pores at the test. Therefore a method of mercury absorption overrates the smaller pores since a pressure correspondant to a smaller pore is needed in order to penetrate the "bottleneck" of a relatively coarse pore.

Of course it is desirable to have an adiabatic calorimeter with greater precision and capable of reaching a lower temperature than that used at our institution.

However it is not quite necessary to have an adiabatic calorimeter at all. At our institution we have also built a very simple difference calorimeter for specimen size 30 x 30 x 120 mm^3. Figure 13.

It consists of an outer jacket of brass. Within this a centrically situated inner-jacket of phenolic plastics. The specimen is placed in the inner-jacket. Between the two jackets there is placed a heat insulation of foamed poly-urethane. It is shaped so as to direct the heat flow

manily angular to the length-axis of the specimen. Both the inner- and outer-jackets are provided with resistance-thermometers of thin copper-wire completely covering the areas"hit" by the heat flow. The assembly is immersed in a kerosene-bath of -30°C. The outer thermometer immidiately adopts this temperature. The inner thermometer gradually gets colder. The difference in resistance between the outer and inner thermometer is· measure of the heat flow through the insulation. The connection between difference in resistance and amount of heat· flow (the calorimeter-constant) is calibrated by exchanging the specimen to a heating coil which generates different effects.

Three thermocouples in the specimen and the heat flow through the insulation is registered on a 12-point recorder. Freezing as well as thawing experiments can be performed.

A test can be divided in time-elements. The result can be plotted as sum of energy transported through the insulation as function of sum of temperature-difference between the outer and inner resistance thermometers, Vuorinen /20/. See figure 14.

5 SYMBOLS

C	total specific heat of an unfrozen specimen and specimen-holder at a thawing experiment $(\frac{j}{^oC})$
C_i	specific heat of ice $(\frac{j}{Kg \cdot ^oC})$
C_w	specific heat of water $(\frac{j}{Kg \cdot ^oC})$
M	molecular weight $(\frac{Kg}{Kmole})$
R	gas constant $(\frac{j}{Kmole\ ^oK})$
S	surface area of the pores (m^2)
T	absolute temperature (^oK)
To	freezing point of bulk pure water (^oK)
V	volume of specimen (m^3)
V_k	"Kelvin pore-volume" = volume inside the adsorbed layer (m^3)
V_p	pore-volume (m^3)
V_t	volume of adsorbed water (m^3)
W	total energy supplied to a specimen at a thawing experiment (j)
d	diameter of water molecule (m)
g	gravity acceleration $(\frac{m}{S^2})$
h	capillary rise (m)
p	vapour pressure of evaporable water in a material $(\frac{N}{m^2})$
p_i	vapour pressure of ice $(\frac{N}{m^2})$
p_s	vapour pressure of bulk water $(\frac{N}{m^2})$
r	radius of capillary or radius of crystal (m)
r_k	Kelvin radius. Definition eq (28) (m)
t	thickness of water layer adsorbed on the pore-wall (m)
w_e	total evaporable water content (Kg)
w_f	freezable water content (Kg)
w_{nf}	non-freezable water content (Kg)

Δh heat of fusion $(\frac{j}{Kg})$

ΔH molar heat of fusion $(\frac{j}{Kmole})$

Δp pressure difference across curved interface (N/m^2)

ΔSf molar entropy change of fusion $(\frac{j}{(Kmole\ ^oK)})$

ΔT freezing point depression (^oC)

ΔT_t freezing point depression at freezing in toluene (^oC)

ρ density $(\frac{Kg}{m^3})$

σ surface tension $(\frac{N}{m})$

θ temperature (^oC)

θ contact angle   (radians)

ω shape factor of crystal (1)

indici:
1   liquid
lg   liquid-gas
s   solid
sl   solid-liquid
sg   solid-gas
wa   water-air
wt   water-toluene

6 LITERATURE

1 Bigg E K — The Supercooling of Water. Proc Phys Soc, London B66 (1953), pp 688-694.

2 Blachere J R
Young J E — The Freezing Point of Water in Porous Glass. J Amer Ceram Soc 55 (1972), pp 306-308.

3 Croney D
Coleman J D
Bridge P M — The Suction of Moisture Held in Soil and Other Porous Material. Road Res Techn Paper No 24, London, Her Majesty's Stat office 1952.

4 Feldman R F — Length Change-Adsorption Relations for the Water-porous Glass System to $-40^{\circ}C$. Canad J of Chem 48(2) 1970.

5 Gregg S J
Sing K S W — Adsorption, Surface, Area and Porosity. Academic Press, London 1967.

6 — Handbook of Chemistry and Physics. 45th Edition 1964-65. The Chemical Rubber Co.

7 Helmuth R A — Capillary Size-Restrictions on Ice-Formation in Hardened Portland Cement-Pastes. Proc Vol II, IV, Int Symp Chem of Cements, Washington D C 1960, pp 855-869.

8 Hesstvedt E — The Interfacial Energy Ice/Water. Norwegian Geotechnical Institute, publ No 56, Oslo 1964, pp 7-10.

9 Kubelka P — Über den Schmelzpunkt in sehr engen Kapillaren. Ztschr Elektrochem Bd 38 Nr 8a, 1932, pp 611-614.

10 Litvan G G — Phase Transitions of Adsorbates: IV Mechanism of Frost Action in Hardened Cement Paste. J Amer Ceram Soc 55 (1972) pp 38-42.

11 Loewenstein K L — Glass Systems. Composite Materials, pp 129-220. Elsevier Publ Comp; Amsterdam/London/New York 1966.

12 Powers T C
Helmuth R A — Theory of Volume Changes in Hardened Portland Cement-Paste during Freezing. HRB Proceedings 32 (1953).

13 Powers T C
Brownyard TC — Physical Properties of Cement-Paste. Res Labs Port Cem Ass Bulletin 22, Chicago 1948.

14 Powers TC
Copeland L E
Hayes J C
Mann H M — Permeability of Portland Cement-Paste. Proc Amer Concr Inst 51 (1954-55) pp 285-298.

15 Puri B R
Sharma L R
Lakhanpol K L — Freezing-Point of Water held in Porous Bodies at different Vapour Pressures. J Phys Chem 58 (1954) pp 289-292.

16 Schofield R K — The pF of Water in Soil. 3 rd Int Congr Soil Sci, 1935, 2 (1935), pp 37-48; 3 (1935), pp 182-86.

17 Schofield R K
da Costa J V B — The Measurement of pF in Soil by Freezing-Point. Agric Science 28 (1938), pp 645-53.

18 Sill R C   Method for the Determination of the Surface Tension
   Skapski A S   of Solids from their Melting Points in thin Wedges.
                    J Chem Phys 24 (1956), pp 644-51.

19 Vos B H   Moisture and Moisture Transfer in Porous Materials.
   Tammes E   Report No BI-69-96. TNO Delft 1969.

20 Vuorinen J   On Use of Dilation Factor and Degree of Saturation
                    in Testing Concrete for Frost-Resistance.
                    Nordisk Betong 1970:1, pp 37-63.

21 Washburn E W   The Vapour Pressure of Ice and of Water below the
                    Freezing Point. Monthly Weather Rev, Oct 1924,
                    pp 488-490.

22 Wheeler A   Reaction Rates and Selectivity   in Catalyst Pores.
                    Catalysis Part II. Ed P H Emmett Rheinhold Publ
                    Corp N Y 1955, pp 105-165.

23 Williams P J   Properties and Behaviour of Freezing Soils.
                    Norwegian Geotechnical Institute. Publ No 72,
                    Oslo 1967.

24 Winslow D N   A Mercury Porosimetry Study of the Evaluation of
   Diamond S   Porosity in Portland-Cement. J of Materials, vol 5,
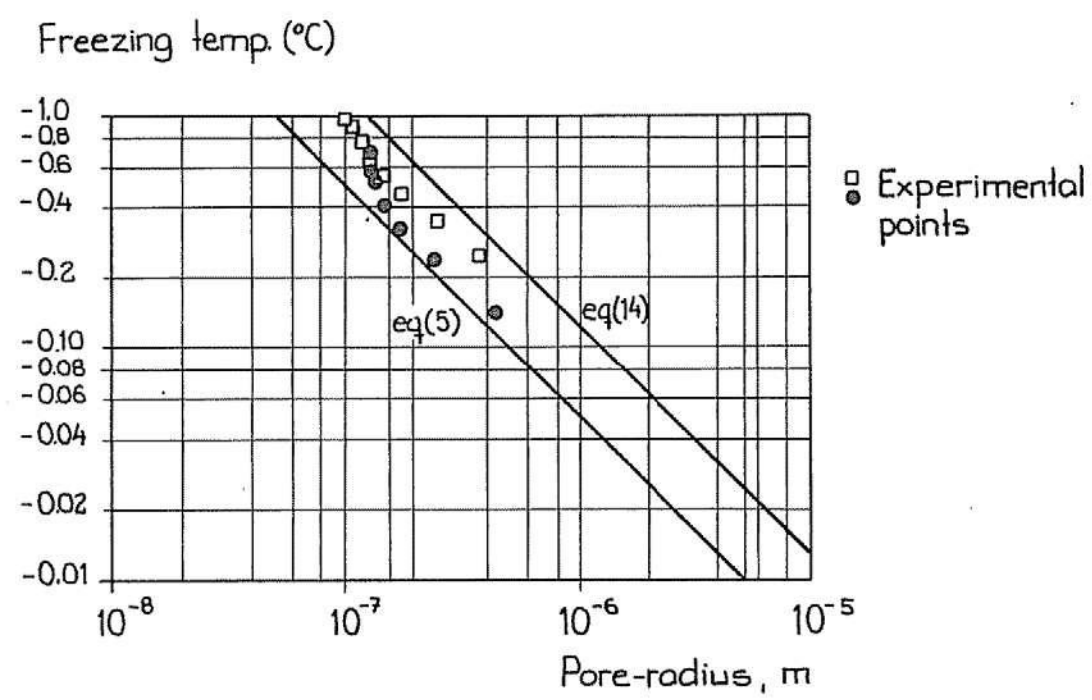   No 3, Sept 1970, pp 564-585.

Freezing temp. (°C)

FIG 1 Experimentally determined freezing point depressions
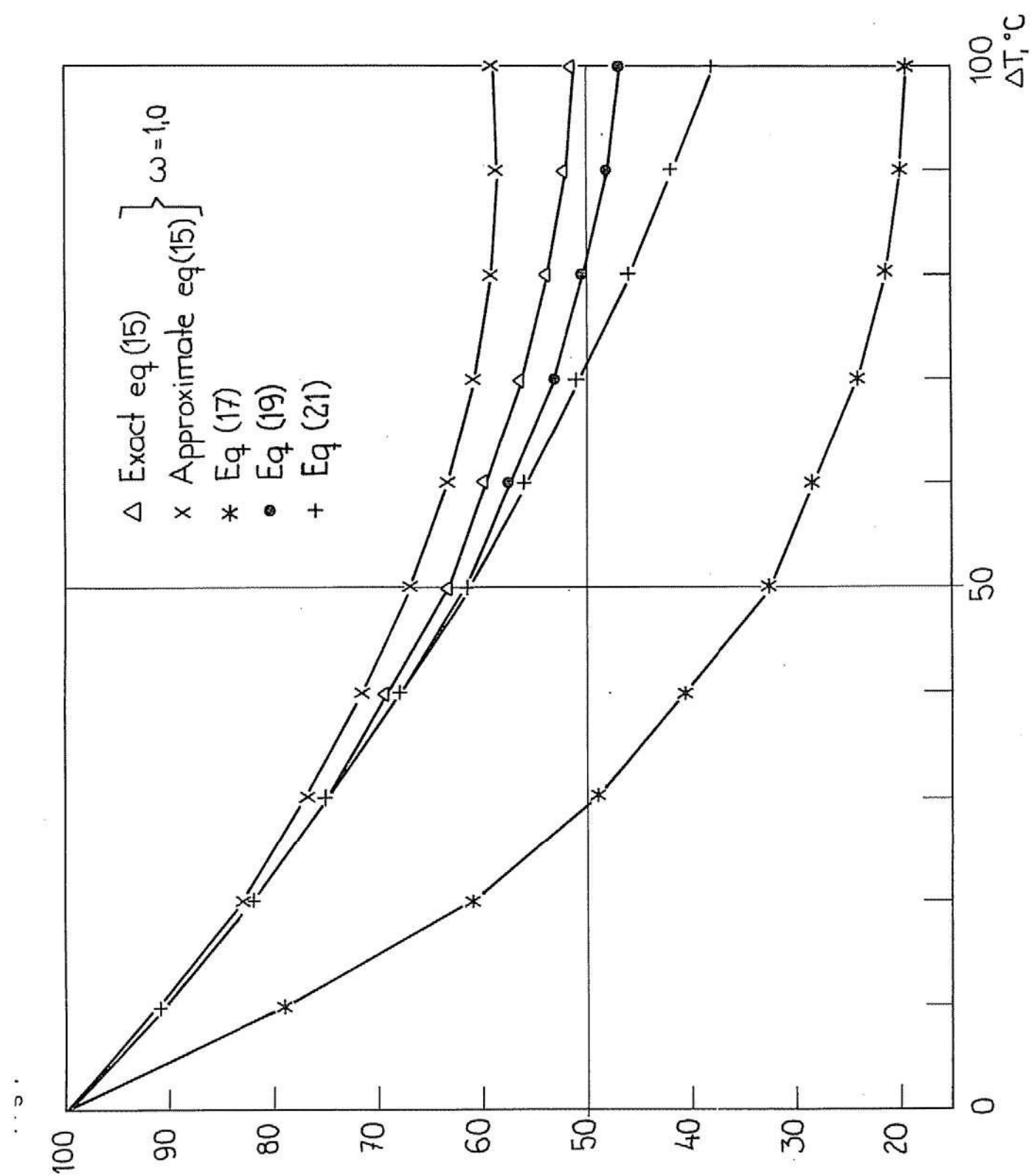together with theoretical curves eq (5) and eq (14). /23/

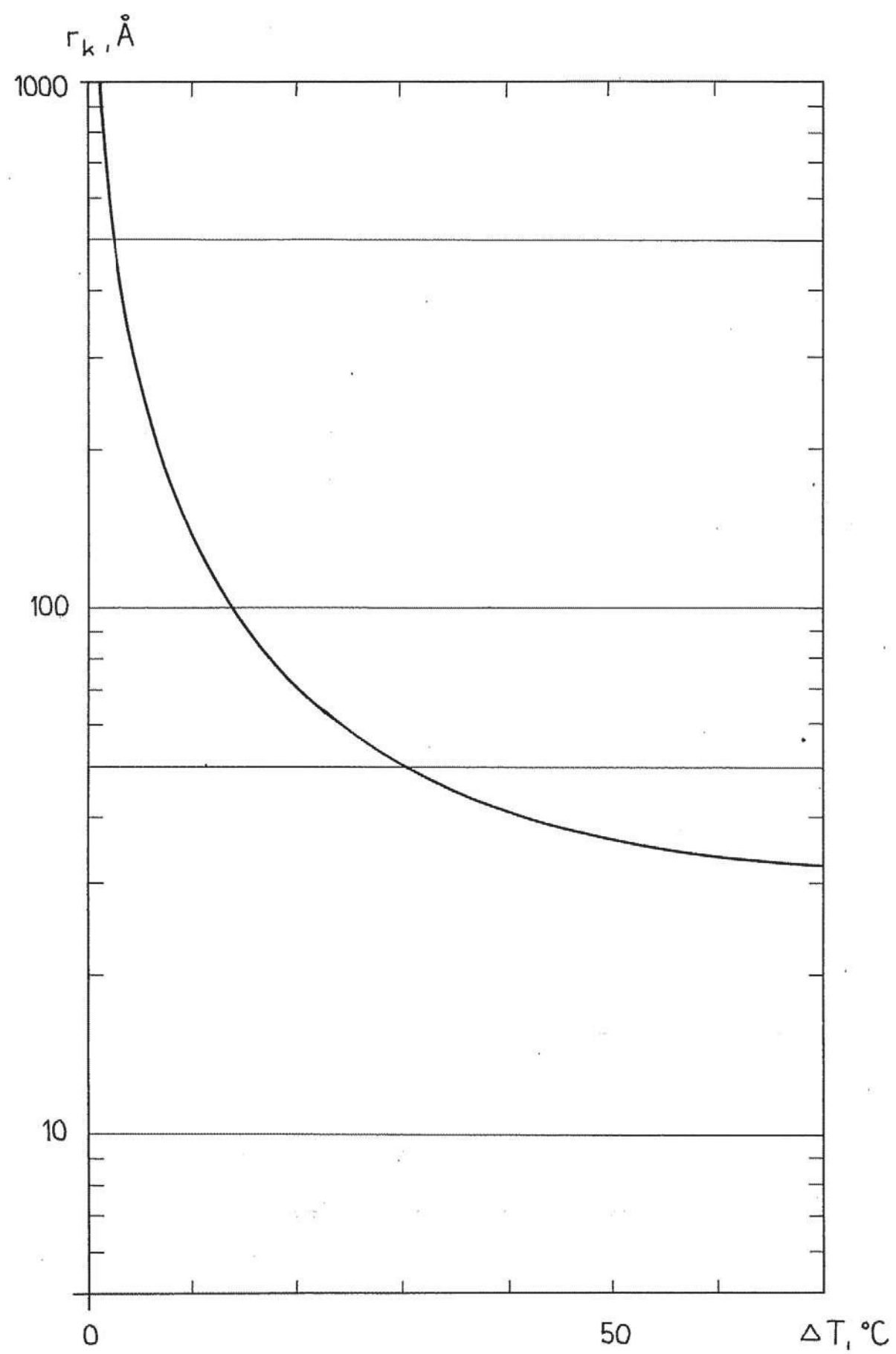FIG 2 Different expressions for freezing point depressions.

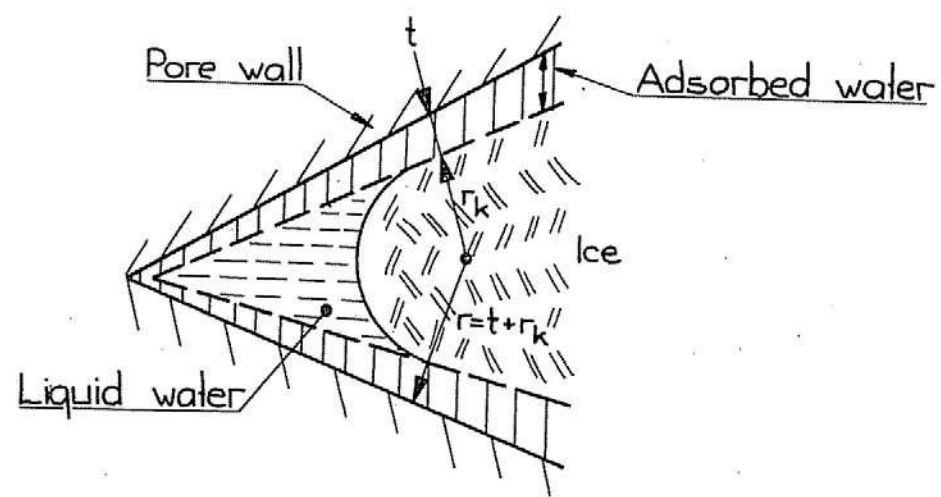FIG 3 Freezing point depression as function of the Kelvin-radius eq (14').
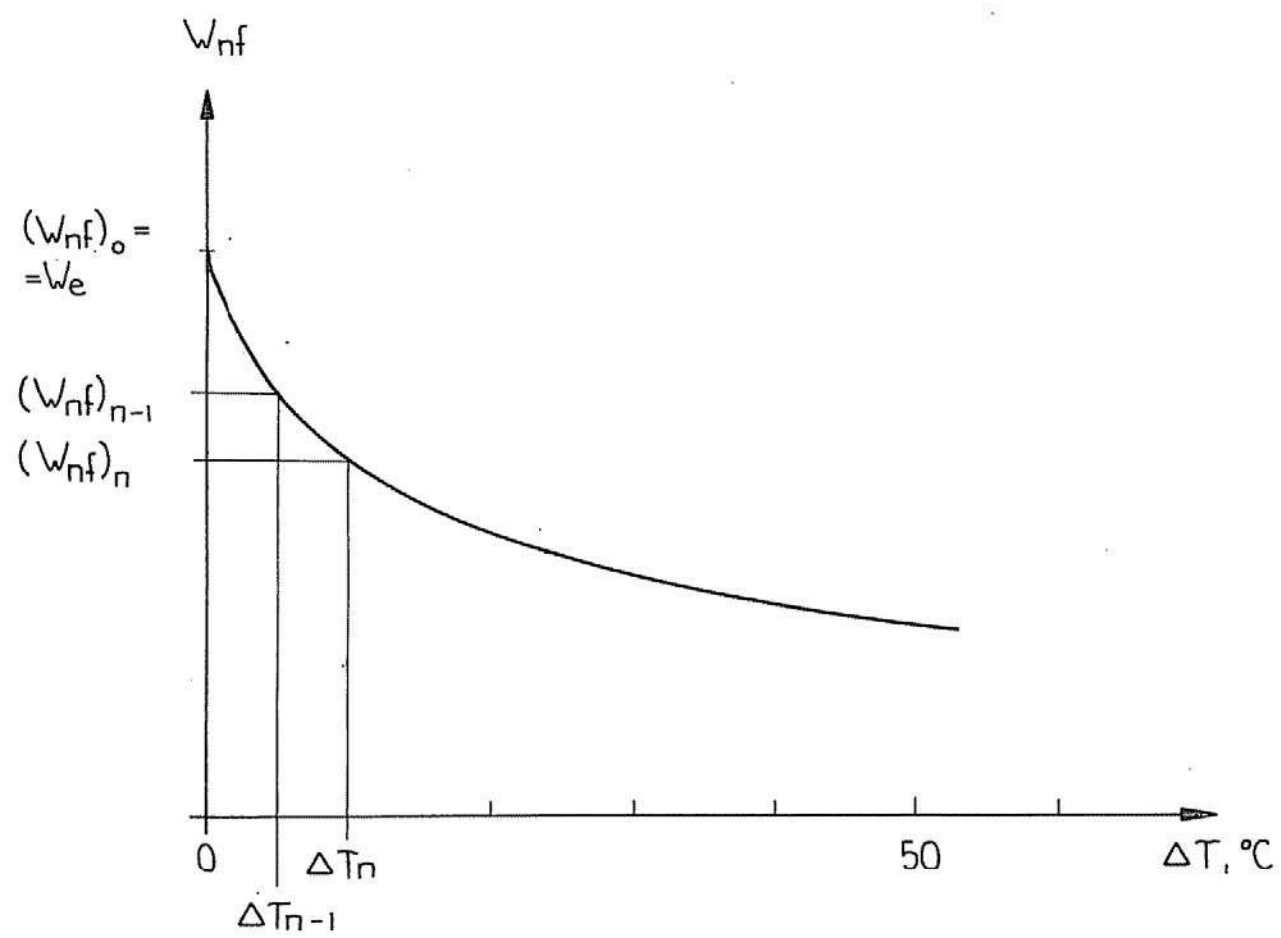
FIG 4 Freezing in a conical pore.

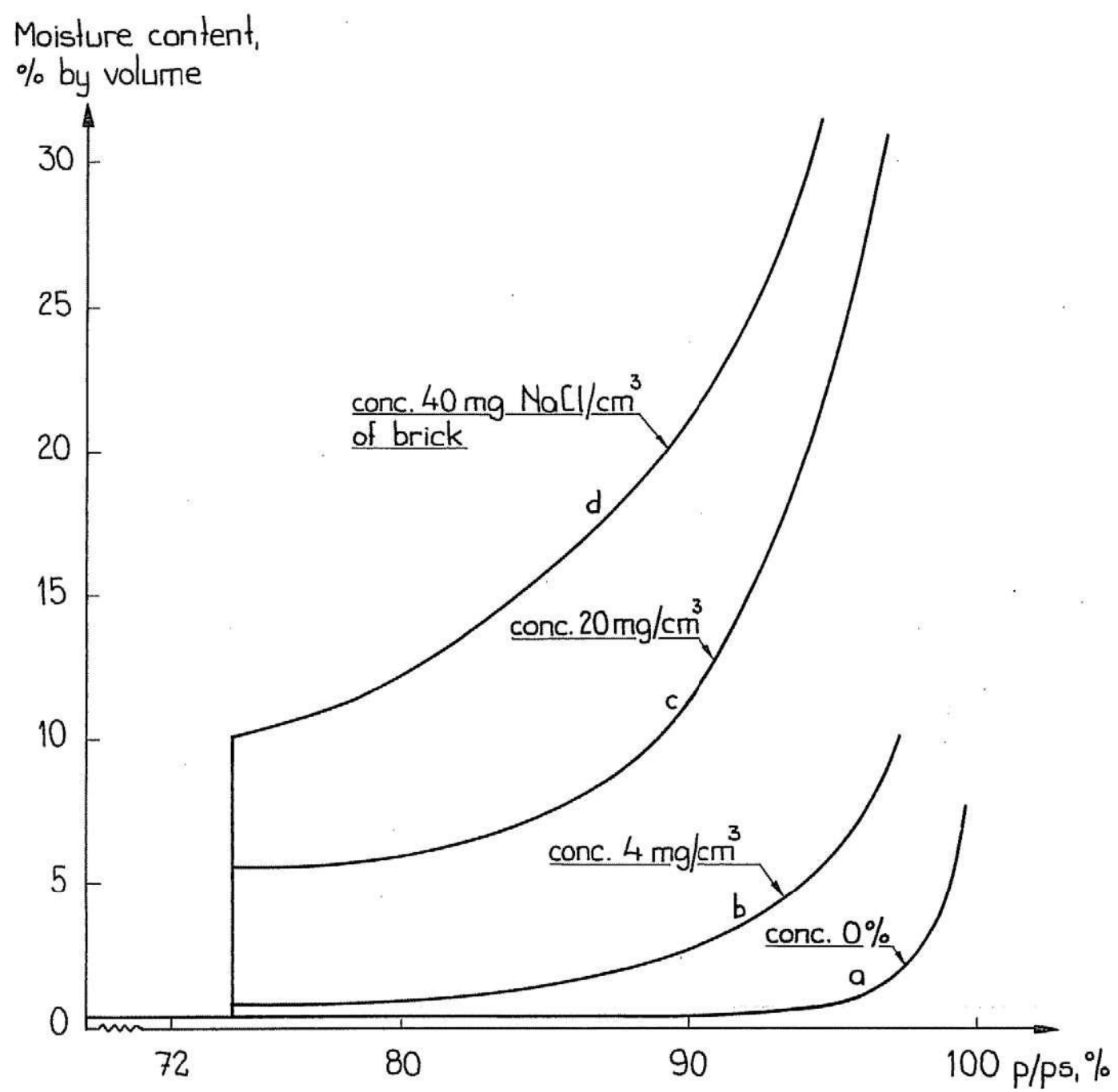FIG 5 Hypothetical connection between non-freezable water and temperature.

FIG 6 Influence of salts in the pore-water on the sorption iso-
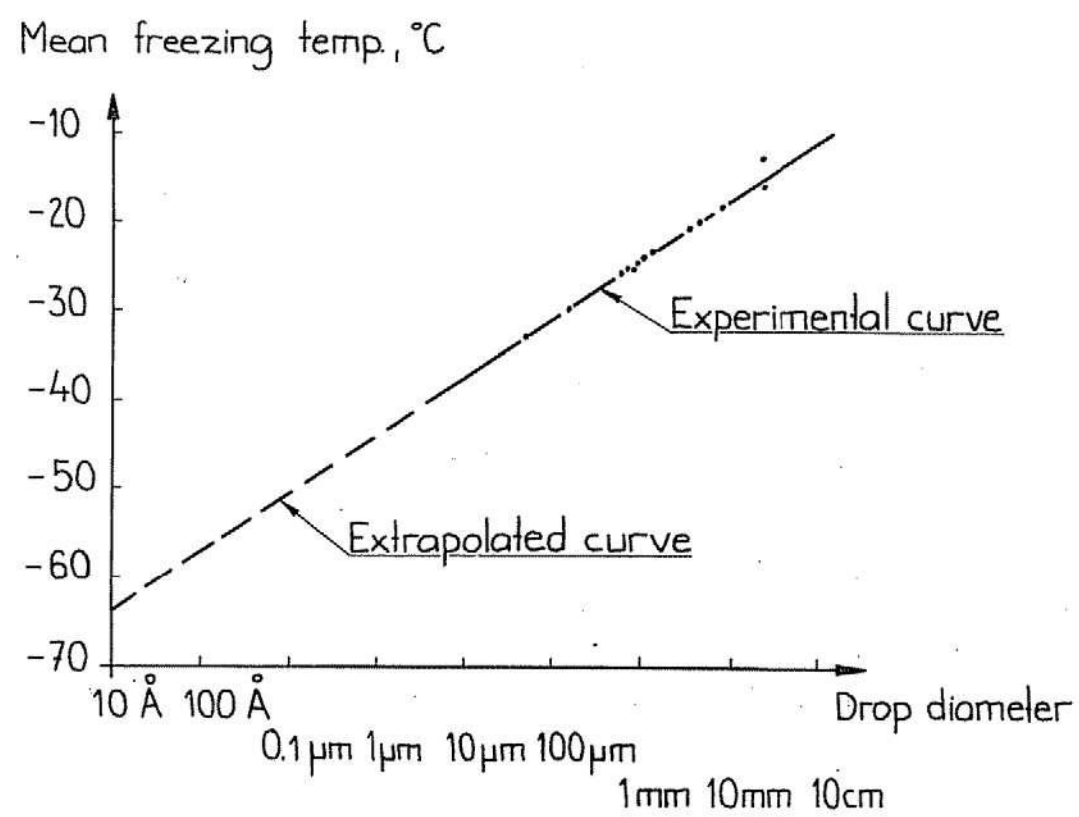therm of a brick /19/.

Mean freezing temp., °C

-10
-20
-30   Experimental curve
-40
-50
-60   Extrapolated curve
-70
     10 Å 100 Å   Drop diameter
        0.1 μm 1μm 10μm 100μm
                          1mm 10mm 10cm

FIG 7 Mean freezing temperature as function of drop diameter. /1/

Relative frequency of freezing

100
 50
  0
    -20   -22   -24   -26   -28
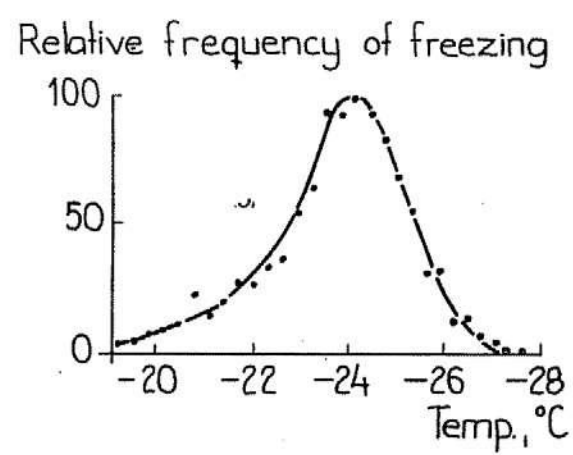   Temp., °C

FIG 8 Relative frequency of freezing as a function of temperature
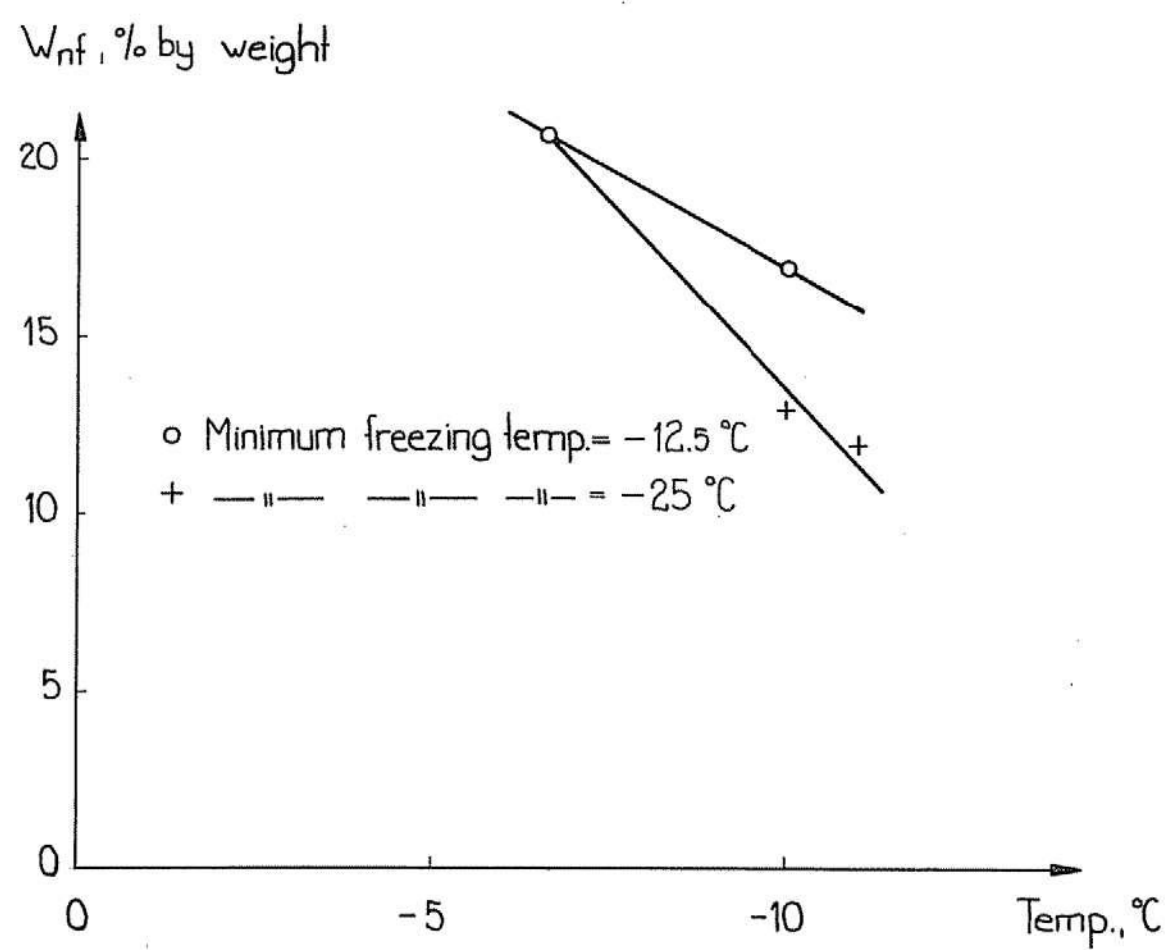   for 1 mm drops. /1/

FIG 9 Effect of minimum temperature on non-freezable water content. Cellular concrete.
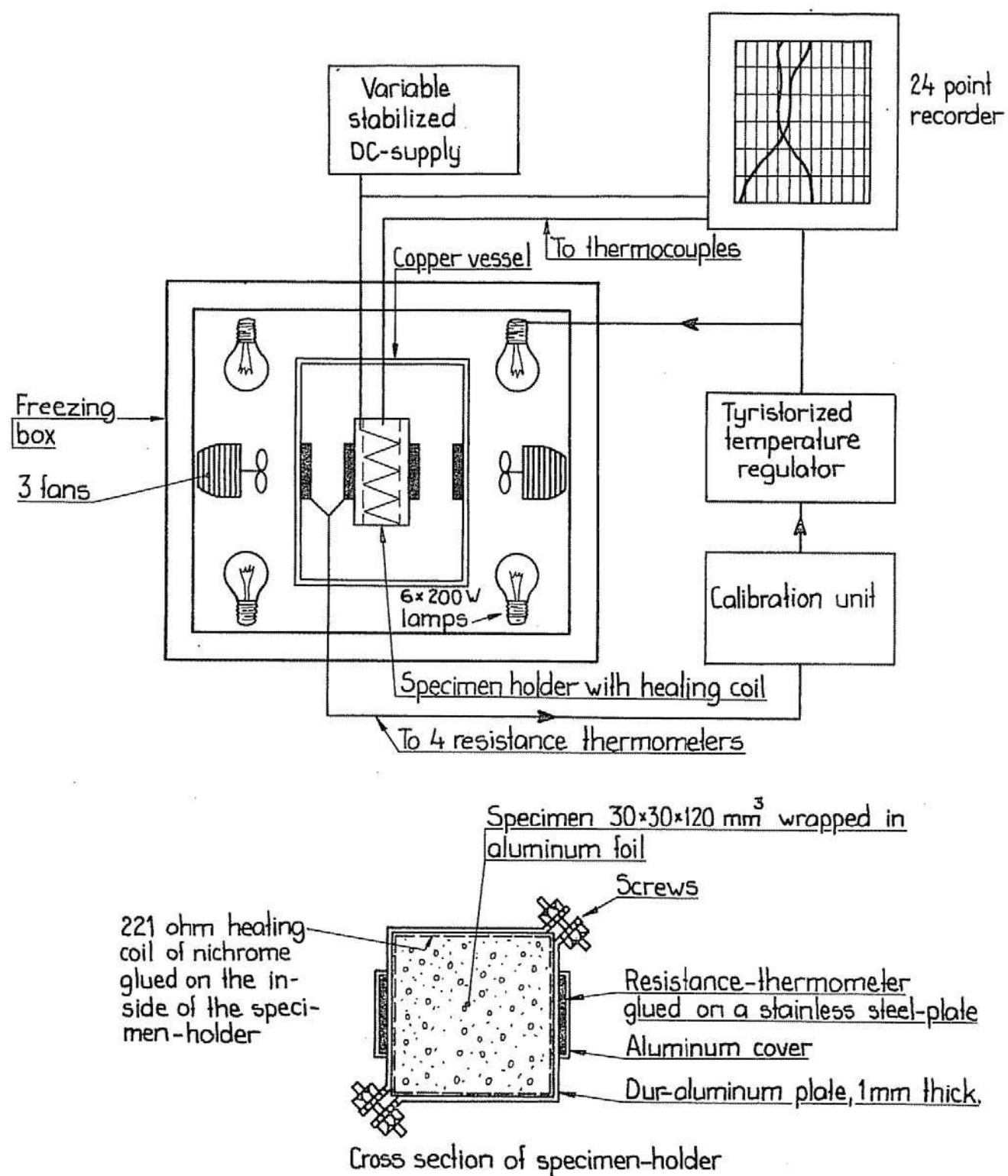
FIG 10 Adiabatic calorimeter for determination of non-freezable
        water content.

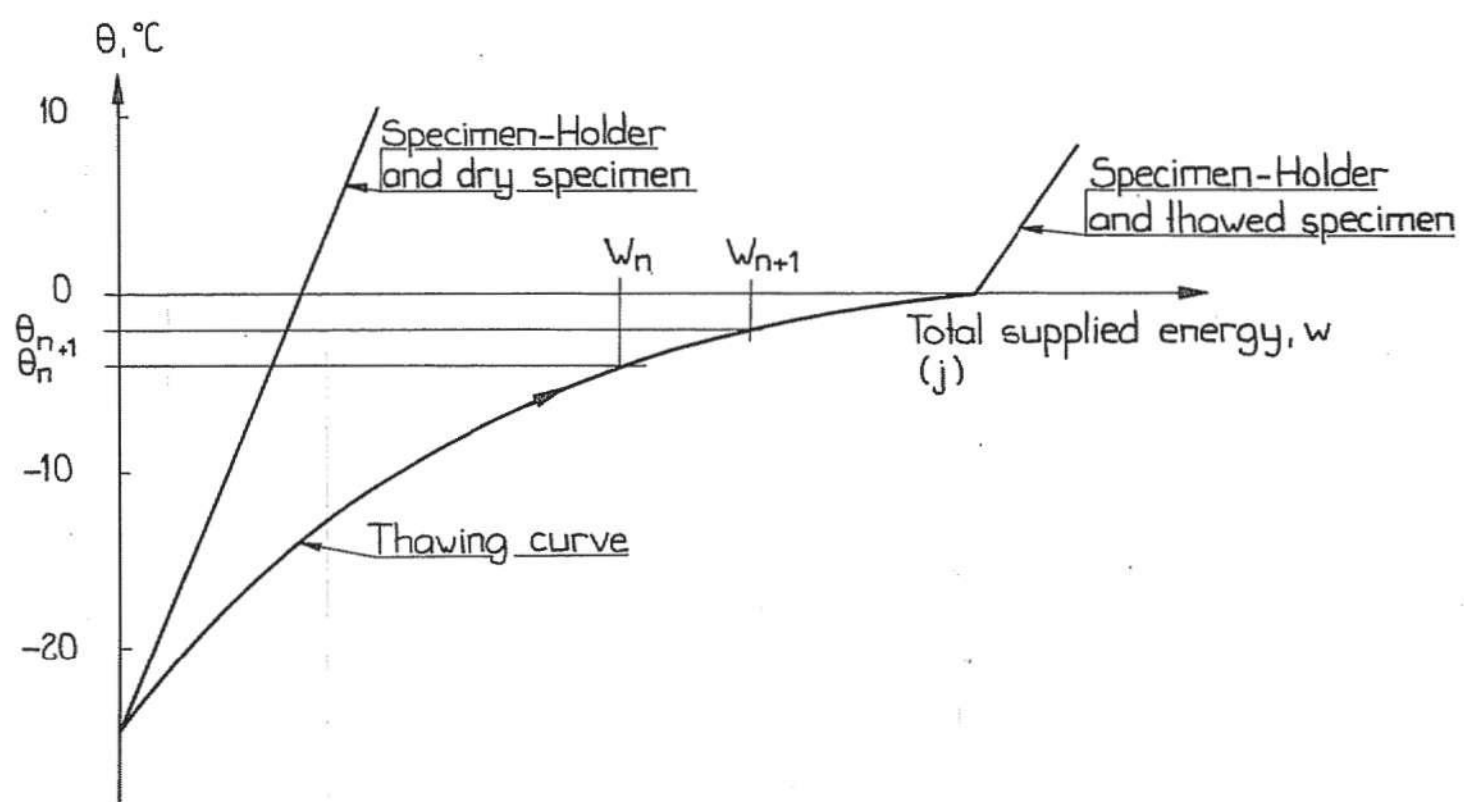FIG 11 Calculation of non-freezable water content from the thawing
curve obtained in the adiabatic calorimeter in FIG 10.

Sum pore volume, %
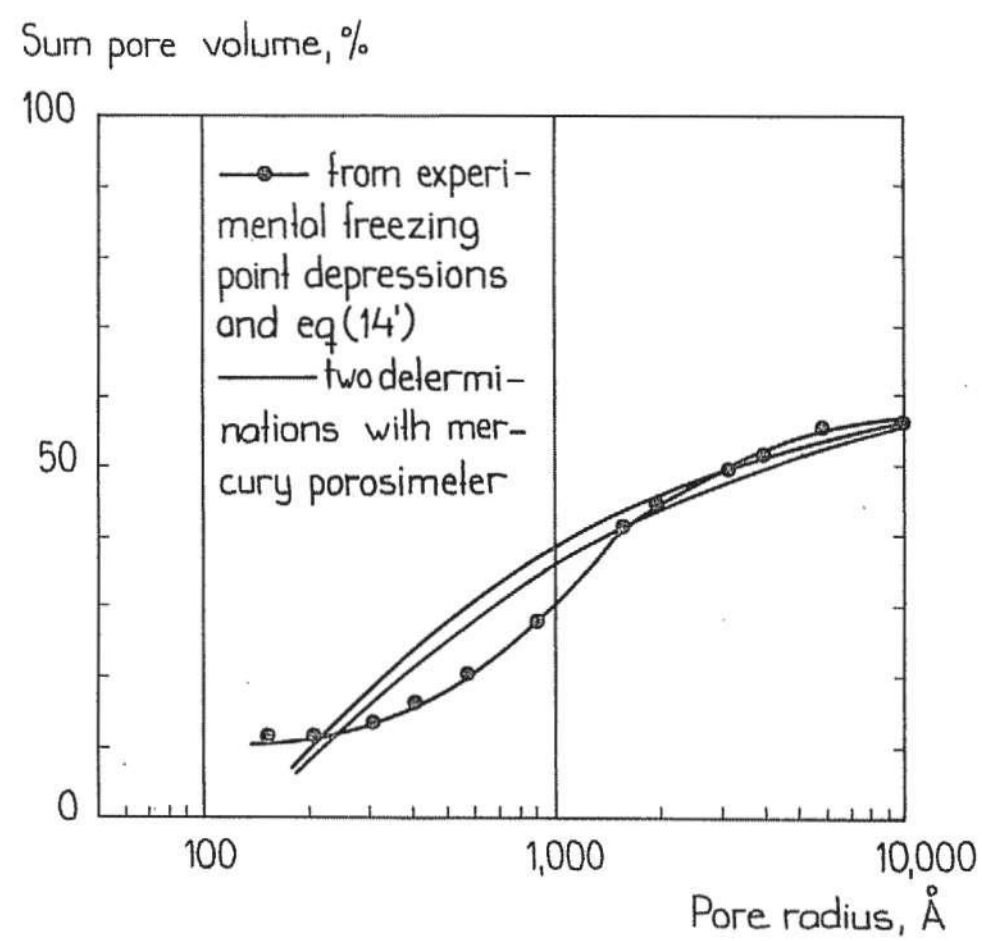
FIG 12 Comparison between pore size distribution determined by
experimental freezing point depressions and by mercury
porosimeter. Sand lime brick.
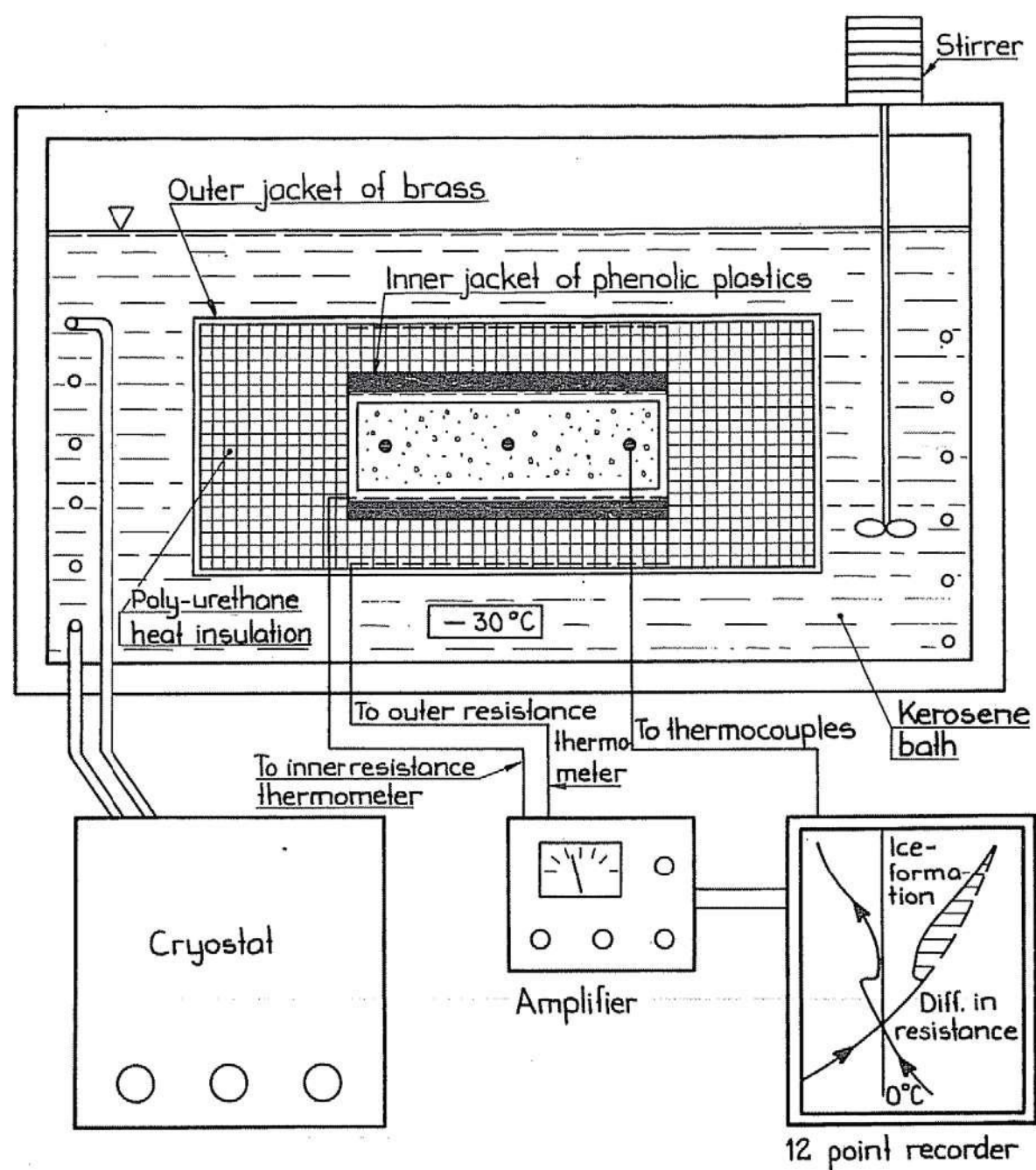
FIG 13 Difference-calorimeter for determination of ice formed and
ice melted at different temperatures.

Sum of energy leaving calorimeter

Thawing

Freezing

Extrapolated curve

Measure of frozen water at temp. θ_n.

Sum of resistance
difference between
outer and inner
resistance thermometer

+ 0 θ_n $-\theta_1°C$

Specimen temperature

FIG 14 Evaluation of a determination of non-freezable water content
by the difference-calorimeter in FIG 13.

III

DETERMINATION OF SPECIFIC SURFACE BY THE BET-METHOD

Contribution to RILEM committee

"Pore Structure and Properties of Materials (PM)"

by
Göran Fagerlund

CONTENTS

Lund, September 1972

1. BRIEF THEORETICAL BACKGROUND

The BET-theory was originally elaborated by Brunauer, Emmett and Teller /10//9/. A modern summary and discussion of the theory is given in Gregg & Sing /19/.
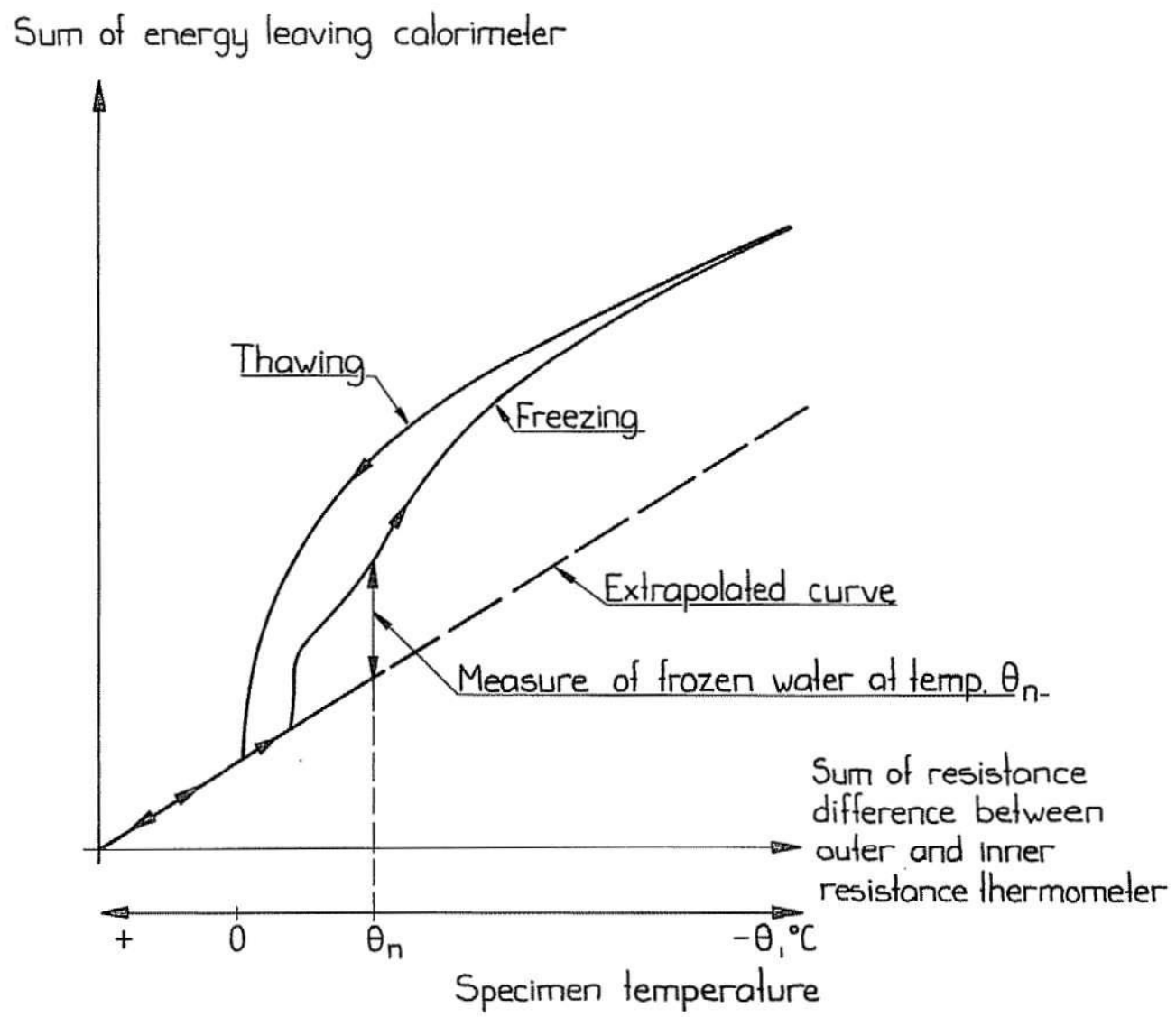
The determination of specific surface by means of the BET-theory is based upon the phenomenon physical adsorption of gases on the external and internal surfaces of a porous material.

Such a material which is surrounded by and in equilibrium with a certain gas which has a certain temperature, T, and relative vapour pressure, p/p_0, adsorbes physically a certain amount of gas. The amount of adsorbed gas is dependent on its relative vapour pressure and is proportional to the total external and internal surface of the material.

The connection between relative vapour pressure and amount of adsorbed gas at a constant temperature is called an "adsorption isotherm.

The isotherm of physical adsorption can be divided in 5 types. See fig 1. The isotherms of type II and III are from a theoretical point of view only valid for nonporous solids but are often applicable even to porous solids. The majority of building materials seems to have isotherms of type II, at least when the adsorbate is water vapour.

Isotherm of type IV and V are valid only for porous materials. They are modifications of isotherms of type II and III respectively. The modifications at high relative vapour pressures are dependent on the restrictions laid upon adsorption by the width of the pores. The ordinary building materials have such a great amount of large pores that this restriction is negligable why the distignation between isotherm II and IV (or III and V) is without practical significance in the low pressure range. On the other hand the phenomenon capillary condensation occurs in the porous material when the adsorbate is thick enough to form a curved meniscus in the pore. Therefore the isotherm of a porous material in the high pressure range differs from that of a nonporous material. However this is of no importance at calculation of specific surfaces according to the BET-theory.

The type I isotherm is hardly applicable to building materials. It is valid only for a solid with extremely narrow pores like som gels.

The exact form of the isotherm of a certain material is strongly affected
by the choice of adsorbate. The influeace of the adsorbate may also be
of such a character that the specific surface calculated from the isotherm
may be dependent on the choice of adsorbate. This will be discussed fur-
ther on in section 3.

The basic equation for calculation of specific surface from adsorption
data is

$$S = \frac{Xm}{M} \cdot N \cdot Am \tag{1}$$

The main obstacle at use of eq (1) lies in the estimation of Xm. It is
in determination of this quantity the BET-theory has proved utterly suc-
cessful. Besides it is especially successful in calculation of Xm from
isotherms of type II and IV, that is from isotherms applicable to the
majority of building materials.

Brunauer, Emmett & Teller / 10 / based their theory on the following main
assumptions.

- The surface of the material consists of a great number discrete equiva-
  lent adsorption sites (a homogeneous surface).
- At a certain vapour pressure a varying number of molelcules are adsorbed
  on any one site. They are stacked on the top of each other to form a
  number of layers.
- The heats of adsorption and the condensation constants (the fraction
  of arriving molecules per second actually condensating on empty sites)
  in all layers above the first are the same and equal to those of bulk
  liquid. This is a most important assumption.
- At saturation the amount of layers become infinite. As a consequence
  the theory is from a theoretical point of view only valid for a non-
  porous material.cf page 2.
- A molecule covered by another molecule cannot evaporate. This is another
  assumption of great importance.
- There is no interaction "horizontally" between molecules in different
  sites.
- At dynamic equilibrium the number of molecules evaporating from a
  layer is equal to the number condensating on the layer below (conden-
  sation constants = evaporation constants).

Many of these assumptions have been criticized by many authors.

The treatment leads to the following well-known equation

$$\frac{X}{Xm} = \frac{C(p/p_o)}{(1-p/p_o)(1+(C-1)p/p_o)} \tag{2}$$

This equation is given in a more general form by Hill /24/.

Eq (2) can be rewritten in the form of eq (3):

$$\frac{p}{(p_0 - p)} \cdot \frac{1}{X} = \frac{1}{Xm \cdot C} + \frac{C - 1}{Xm \cdot C} \cdot \frac{p}{p_0} \qquad (3)$$

where $C = \dfrac{\tau_1}{\tau_2}$ \qquad (4)

Thus C expresses the relative lifetime of molecules in condensed state
in the first layer and in the second or higher layers. The latter is in
turn approximated to the lifetime of molecules in bulk liquid. The value
of C can be used as a guide at determination of the heat of adsorption

$$E_1 - L = R \cdot T \cdot \ln C \qquad (5)$$

This equation is very rough. However a large C signifies at large heat
of adsorption of the first layer.

It can be shown mathematically that the sorption isotherm according to
eq (3) will be of type II or III. Type III isotherm is valid only for
$C \leq 2$.

Therefore the isotherm has an inflection point, (see fig 1). It can be
proved that this point is close to the point where $\frac{X}{Xm} = 1$, that is where
the first monolayer is completed. At C = 9 and when $C \to \infty$ the inflection
point is equal to $\frac{X}{Xm} = 1$. För values of C, $9 < C < \infty$, the inflection point
is up till 20 % larger than the point p/p_0 where $\frac{X}{Xm} = 1$. For values of
C < 9 the inflection point is less than the point, p/p_0, where $\frac{X}{Xm} = 1$.

However the value $\frac{X}{Xm} = 1$ must not necessarily mean that the first mono-
layer is completed since adsorption into the second or higher layer occurs
before the first is quite complete.

The difference between $\frac{X}{Xm} = 1$ and the completion of the first monolayer
is smaller the more sharp the distinction is between the first and sub-
sequent layer adsorptions, that is the higher the value of C. This is the
basis of the so called B-point-method. At a high value of C the experi-
mental isotherm often has a relatively long linear part. See fig 2. The
point where The linear part begins is termed the B-point. The adsorption
at the B-point can be regarded as the monolayer capacity Xm. At low values
of C (isotherm type III) adsorption in the second layer occurs simlulta-
nously with in the first. Hence the B-point is difficult to discern and
the monolayer capacity is uncertain.

According to Gregg & Sing /9/ the difference between monolayer capacity
calculated from the B-point and from the BET-theory can differ as much

as $0,75 \leq Xm/X_B \leq 1,53$. Anderson /2/ states: "It cannot be too strongly recommended that, for any given type of adsorbent, the coincidence of point B and the BET-monolayer values should be established before proceeding to use the latter method for routine measurements."

Theoretically the isotherm of a <u>porous material</u> is of type IV or V. The main difficulty at use of these isotherms is that they normally exhibit hysteresis between adsorption and desorption. This depends on the occurence of capillary condensation in pores so small that the adsorbate is thick enough to form a curved meniscus.

However, the part of the isotherm used for calculation of specific surface, from zero pressure up till the point where the first monolayer is completed (approximately at the inflection point), is without hysteresis adsorption - desorption in most cases.

Therefore the same procedure can be used at calculation of specific surface from type IV isotherms as from type II isotherms.

Equation (3) forms a straight line when $\frac{P}{(P - P)} \cdot \frac{1}{X}$ is plotted as function of P/P_o. A hypothetical isotherm is plotted in fig 3. The curve of nitrogen adsorption is normally linear in the range of monolayer adsorption that is in the low pressure range, $0,05 \leq P/P_o \leq 0,30$ according to Anderson /2/. At higher pressures the experimental curve often deviates from the line.

The slope of the line is s and the intercept is i. Fig 3.

$$s = \frac{C - 1}{Xm \cdot C} \tag{6}$$

$$i = \frac{1}{Xm \cdot C} \tag{7}$$

From these expressions the values of Xm and C can be calculated.

$$Xm = \frac{1}{s + i} \tag{8}$$

$$C = \frac{s}{i} + 1 \tag{9}$$

Insertion in the basic equation (1) gives

$$S = \frac{1}{s + i} \cdot \frac{N \cdot Am}{M} \tag{10}$$

The value Am can be calculated form the density of the adsorbate according to eq (11).

$$Am = 1,091 \cdot (\frac{M}{\rho \cdot N})^{2/3} \tag{11}$$

This equation assumes a certain packing of molecules Gregg & Sing /19/.

As mentioned earlier the BET-theory as represented by eq (2) has been criticized because it is based upon oversimplified assumptions.

This has led to the derivation of modified BET-equations. Such equations have been suggested for instance by Anderson /1/, Hüttig /25/, Dole /13/, Halsey /21/, Fergusson & Barrer /16/ och Theimer /37/. The modified equations are discussed in contribution 3.2.1.2 "Determination of specific surface by adsorption methods other than the BET-method[x]."

The modified BET expressions lead to adsorption isotherm of all five types.

Despite the fundamental deficiencies of the assumptions behind the BET-theory is has proved utterly successful. According to Theimer /37/ "the reason for this is that when the factor C>>1 (which is normally the case) the value of X/Xm given by the BET-formula (eq (2)) does not vary appreciably with the parameter C. Hence the only remaining parameter essential for the adsorption at higher pressures is the area of adsorbing surface."

2 METHODS OF DETERMINATION OF BET-SURFACE

2.1 Introduction

The BET-method as it is normally used can be regarded as a static method since it requires knowledge of the sorption isotherm, that is, the amount of adsorbate taken up at equilibrium with different relative vapour pressures. Hence it is a relatively slow method when it is used in the way outlined above on page 5, eq (10).

Therefore also fast dynamic adsorption methods have been elaborated that make rapid determinations of specific surfaces possible. The dynamic methods treated in this contribution are principally based upon the BET-theory. However since the theory is used in special ways they deserve their own treatment.

---

x) Another contribution to the work within the RILEM committee written by J M Haynes.

2.2 Static methods; Determination of adsorption isotherms

Adsorption isotherms of a certain material can easily be determined
experimentally. Methods of determination are not shown in detail here.
Comprehensive such informations are provided for instance in Gregg & Sing
/19/, Gål /17/ and Joy /27/. In this report only the principles of de-
termination are given. The influence of adsorbate is not discussed but
literature references are provided in section 3.

2.2.1 Outgassing

Before accurate measurements can be made any gas already adsorbed on the
surface has to be removed.

According to Joy /27/ adsorbed impurities does not affect the BET-surface
area but may alter the heat of adsorption as long as

$$\frac{T_b}{T_a} > 3 \tag{12}$$

If $T_b/T_a < 3$ the adsorbed impurity affects both the area and the heat of
adsorption (C-value). See also section 3.

The method of outgassing must therefore be choosen with care. Joy writes
/27/ "For more accurate work it is necessary to use the most drastic
means permissible without causing decomposition, sintering or transfor-
mation of the material".

Normally vacuum is used, eventual in combination with elevated temperature.
Gregg & Sing /19/ consider a vacuum of 10^{-5} torr to be sufficient. The
rate of outgassing is substantially increased at use of elevated tempe-
rature. According to Joy /27/ the time needed at $450^{\circ}C$ is 8 % of the time
needed at $100^{\circ}C$.

2.2.2 Volumetric methods

A typical apparatus for nitrogen adsorption is shown in fig 4 /14/.
Joy writes /27/ "Adsorbate gas is taken into the burette. Its pressure
is read on the manometer. The stopcock between the sample and the burette
is then opened and the new pressure is read after allowing time for
equilibrium to be established.

The volume of gas admitted to the sample bulb is proportional to the
difference in the pressures before and after opening the stopcock;
This latter pressure is the equilibrium adsorption pressure. The volume

adsorbed is equal to the volume admitted less the volume of gas required to fill the "dead space" in the sample bulb and burette connections. Thus the volume adsorbed together with the equilibrium pressure gives one adsorption point. Further points are obtained by admitting more and more gas into the burette. The apparent dead space can be calculated or can at each pressure be readily obtained by repeating the experiment with a relatively nonadsorbable gas(at the temperature used),such as helium.

A disadvantage of this adsorption procedure is that the total volume admitted is formed by summing the separate doses, so that errors are cumulative."

Many other apparatus˝ and modifications have been described /17, 19, 27/. Much of the modifications are dependent on different gases used.

2.2.3 Gravimetric methods

In the gravimetric methods the amount of gas adsorbed is measured by weighing.

The measurements are done by some sort of a balance. The most widely used balance are the coil spring, for instance made by fused silica-spring and the beam balance.

The silica-spring has a linear elastic deformational behaviour (no hysteresis loading-unloading). Its sensitivity is determined by eq (12), /19/.

$$\sigma = \frac{4 \cdot b^3 \cdot n}{z \cdot a^4} \qquad (12)$$

Maximum sensitivity of the silica-spring is 10^{-4}.

The beam balance has a greater sensitivity, 10^{-5} g is detectable in the best balances, appeared in literature. In /17, 19 / are provided extensive reviews of different beam balance systems.

The method of measurement is simple. After each increase in gas pressure the weight gain of the specimen is measured.

The main advantage of the gravimetric methods is,that the volume of the adsorption system is without importance. Besides the gas adsorbed can be observed directly as a weight gain of the specimen. The calibration of the weighing unit is simple and normally valid for a long time.

The sensitivity of the balance must be considered. It depends on the precision wanted and the surface of the material. The expression of sensitivity is:

$$\sigma_r = S \cdot q_s \cdot \alpha \qquad (13)$$

or

$$\sigma_a = S \cdot W \cdot q_s \cdot \alpha \qquad (14)$$

q_s, the weight of adsorbate on 1 m^2, is $0,28 \cdot 10^{-6}$ kg for nitrogen at -195^oC /19/. Thus at a precision, α, of 1 % and a total surface area of 1 m^2 a weight change of $2,8 \cdot 10^{-9}$ g must be detected.

This seems impossible but the problem can be solved by increasing the total mass of the specimen according to equation (14).

2.3 Dynamic methods

2.3.1 Method according to Innes

Innes /26/ has developed an apparatus for continous adsorption measurements. Fig 5.

The apparatus is not described in detail only the principles of measurement.

The starting-point is the following connection between surface area and adsorbed amount of gas:

$$S = k \cdot \frac{1}{\rho} \cdot X_{0,2} \qquad (15)$$

where $k = 3,50 \cdot 10^9$ ã $3,68 \cdot 10^9$

This expression is directly taken from the BET-theory eq (2) at $P/P_o = 0,20$. It assumes that the gas used is nitrogen. $k = 3,50 \cdot 10^9$ corresponds to a size of the nitrogen molecule of 15,4 A^2 and $k = 3,68 \cdot 10^9$ to a size of 16,2 A^2. According to eq (2) it is impossible to use an expression like (15) for all values of the constant C. Therefore a correction factor dependent on C must be introduced. See fig 6.

The dried sample is placed in a special tubing immersed in liquid nitrogen whereupon it is outgassed to a pressure of 0,3 mm Hg or less. Then the sample is exposed to a constant slow flow of nitrogen. Some of the nitrogen is adsorbed and some fill up the adsorbent tubing. Because of the slow flow, equilibrium pressures are assumed during the process. The time needed in order to reach a relative pressure of $P/P_o = 0,20$ is a

measure of the specific surface of the sample. The time is recorded auto-
matically.

The specific surface is obtained from a modified eq (15):

$$S = 3,5 \cdot 10^9 \; \frac{r \cdot t_{0,2} + \Delta_v}{W} \qquad (16)$$

The term Δ_v is introduced to correct for the volume of the tubing not
occupied by solid material but filled with nitrogen of relative pressure
$p/p_0 = 0,20$.

Innes gives an expression for calculation of Δ_v.

According to Innes the surface area results can be expected to be within
5 % of those of the BET-method and to be reproducible within 3 %. A weak-
ness of the method is that the calculation is based upon one measurement
only.

The author extends the method to determinations of porosity.

Bini & Disch jr /6/ state that the Innes˜ method give reasonable agreement
with the BET-method for materials having a surface area of about 5000 m^2/kg
or higher. For lower values the authors propose a modification.

The reason for the modification is that the value Δ_v in eq (16) must be
known with greater accuracy at small surface areas than is proposed in
Innes˜ theory. The authors derive a new expression for Δ_v which takes into
account nonideal behaviour of the nitrogen at 78°K and variations in the
volume of the sample tube.

Experiments have proved that for materials with low areas the modified
method gives results in much closer agreement with the BET-method than
does the original Innes˜ equation.

Later on the Innes˜ method has been further developed. Lange /28/ has
made a modification towards very low flowing rates which makes determina-
tions of complete adsorption isotherms possible. Therefore more accurate
BET-areas can be calculated.

2.2.2 Method according to Nelson & Eggertsen /30/

Nelson & Eggertsen /30/ (see also /35, 38/) have devised an elegant method
of determination of specific surfaces. It can be regarded as a gas chro-
matograpic method. The sample is exposed to a continuous stream of a he-

lium-nitrogen mixture of certain relative pressures. The amount nitrogen adsorbed is determined by measurements of the nitrogen concentration of the flowing gas.

The specific surface is calculated according to the BET-theory.

The sample is dried and put in a sample-tube. A dry mixture of helium and nitrogen, where the nitrogen has a certain pressure, flows through the sample. The thermal conductivity of the gas mixture is measured and recorded automatically. An apparatus is shown in fig 7.

When the sample is at room temperature no adsorption occurs. The thermal conductivity is constant. Then the sample tube is immersed in liquid nitrogen and an adsorption of nitrogen occurs. This is registered as a change in thermal conductivity. See fig 8. When the adsorption is completed the conductivity is the same as before adsorption. A peak in the conductivity is created. The sample tube is finally removed from the bath and allowed to warm up. A desorption occurs which is indicated as an opposite change in thermal conductivity, that is in a new peak in the diagram.

The area of the peaks must be the same since it represents the total amount of gas adsorbed and desorbed. The area is multiplied by a calibration constant which is obtained from measurements of the change in conductivity of injections of a known charge of nitrogen to the nitrogen-helium mixture.

The method is rapid. By increasing the nitrogen pressure a complete adsorption and desorption isotherm can be obtained which makes calculations of pore size distributions possible.

The accuracy of the method is excellent compared to normal BET-calculations from sorption isotherms. It is especially useful at small surface areas because of the high sensitivity of the thermal conductivity detection

Modifications of the method are described in Gregg & Sing /19/. A general discussion of methods based upon gas chromatography is given by Scholl /35/.

2.2.3 Method according to Haul & Dümbgen /22/

Haul & Dümbgen /22/ have elaborated a simple method for determination of adsorption of nitrogen. The specific surface is again calculated by means of the BET-theory. An apparatus is shown in fig 9.

The dry sample is placed in a tube. It is heated in nitrogen for a short time and then cooled to room-temperature. A second tube with the same volume as the sample tube is filled with nitrogen with the same pressure. Both tubes are immersed in liquid nitrogen. The porous sample adsorbs nitrogen which means a decrease in pressure in the sample tube in comparison to the pressure in the empty tube. The pressure difference between the two tubes is measured with a differential manometer. It is a measure of specific surface of the sample.

The absolute pressure at equilibrium is measured with an ordinary manometer.

The method is a one-point method why it is necessary to keep the relative pressure p/p_0 withing the BET-range, but as high as possible;

$$p/p_0 \lesssim 0,30.$$

An expression for calculation of adsorbed amount of gas from the differential and absorbate pressure is given in the original report and is not cited here.

The monolayer capacity is calculated from eq (2) with $C \gg 1$ after which the specific surface is obtained from eq (1). A nomogram for calculation is presented by Gall /18/.

The method gives reproducable values which are normally 5 à 10 % smaller than those obtained from an ordinary BET-plot.

Commercial instruments based on this principle are described by Guyer Jr & Böhlen /20/ and Gall /18/.

3 APPLICATIONS OF THE BET-THEORY

The BET-theory has found widespread applications even within the field of building materials. In fact one of the first successful applications was made by Powers & Brownyard /32/ at their fundamental studies of hardened Portland cement pastes.

The BET-theory is from a theoretical point of view applicable if the isotherm is of type II or IV. In the rare case of an isotherm of type I,

III or V the BET-equation is abandoned in favour of another suitable ex-
ression. Examples of such expressions are given in another contribution
(3.2.1.2 "Determination of specific surface by adsorption methods other
than the BET-method"[x] References are given on page 6 above.
In the case of an isotherm of type I, that is for a microporous solid,
special theories for calculation of specific surfaces have been elabora-
ted. These are described by Gregg & Sing /19/.

The isotherm is plotted according to eq (3). Normally a straight line is
obtained in the low pressure range $0,05 \lesssim P/P_o \lesssim 0,30$, that is in the range
of monolayer adsorption when nitrogen is used as adsorbate, Anderson /2/.
The intercept i and the slope s of the line is determined.

The monolayer capacity is calculated from eq (8) and the specific surface
from eq (10).

Eventually the monolayer capacity can be obtained from the B-point of the
isotherm according to what is discussed in section 1.

The first question arising at the determination is the choice of adsorbate.
It is essential to use an adsorbate that gives an isotherm of type II or
IV. Hence the value of C must be high which means a well-defined B-point.
The most common adsorbates are:

- Nitrogen at low temperature (nitrogen vapour). Gregg & Sing /19/,
  Barrett et al /4/, Guyer Jr & Böhlen /20/ and Joy /27/.
- Krypton at low temperatures. Gregg & Sing /19/, Haynes /23/, Rosenberg
  /33/, Beebe et al /5/, Sing & Swallow /36/ and Joy /27/.
- Kr^{85}, a radioactive isotope. Clarke /12/, Aylmore & Jepson /3/ and
  Gregg & Sing /19/.
- Water vapour, Powers & Brownyard /32/ and Gål /17/.
- Hydrocarbons of different types. Gregg & Sing /19/.
- Other adsorbates are for instance inert gases like helium, xenon, argon;
  Gregg & Sing /19/. Phenol; Boehm & Gromes /7/.

The specific surface calculated is often dependent on the adsorbate
choosen. So for instance there is an interesting and informing debate
going on concerning the true specific surface of portland cement pastes.
There is much evidence that specific surfaces calculated from watervapour
isotherms are substantially greater than those calculated from adsorption
of nitrogen, Powers /31/. Feldman & Sereda /15/ claim that the nitrogen-
surface is true and that the great adsorption of water-vapour is due to
"interlayer water" within the solid crystals. This is rejected by Bru-
nauer et al /11/ on the following very important grounds.

x) Another contribution to the work within the RILEM committee written
   by J M Haynes.

Firstly, the pastes used by Feldman & Sereda were not properly dried.
The drying was so called P-drying which means equilibrium with the
vapour pressure of magnesium perchlorate dihydrate and tetrahydrate,
which is $8 \cdot 10^{-3}$ mm Hg, whereas a proper drying of cement paste, D-drying,
means equilibrium with the vapour pressure of ice at -78° C which is
$5 \cdot 10^{-4}$ mm Hg. This small difference in drying conditions has a substan-
tial effect on the adsorption. D-drying corresponds to complete dryness.

Secondly, the pore structure of the paste is such, that the nitrogen mole-
cule cannot penetrate into many large pores and cover the total surface,
Mikhail et al /29/. The difference between the penetration abilities of
nitrogen and water depends partly on the size of the molecules (the water
molecule is smaller) but is also dependent on the fact that the water
molecule has a strong dipole which is strongly attracted to the ionic
surfaces of the compounds in hydrated cements. The nitrogen molecule is
nonpolar. Besides the occurence of constrictions in the necks of the
pores present an energy barrier to the diffusion of the adsorbate mole-
cules into the pores. If the energy of activation of this diffusion is
considered equal for both adsorbates (it is probably smaller for water
vapour because of its smaller size) the water molecule should pass over
the energy barrier about 50 times as rapidly as the nitrogen molecule
viz, the temperature of water is $= 298^{\circ}$K while the temperature of nitro-
gen is $= 77^{\circ}$K.

Hence, since it takes 2 or 3 weeks to reach equilibrium at water adsorp-
tion it would take years for nitrogen to equilibrate.

Even once the proper adsorbate is choosen and a correct isotherm is de-
termined some additional problems arise:

- The saturation pressure, P_o, of some adsorbates may be uncertain.
  This problem is discussed by Haynes /23/ and Sing & Swallow /36/ in
  connection with adsorption of argon.
- The value Am, that is the area occupied per molecule of adsorbate,
  must be known but is often uncertain. Eq (11) is not always applicable.
  The exact value of Am is mainly dependent on the net heat of adsorp-
  tion. When this is very large the adsorbate is more like a solid than
  a liquid for which reason eq(11) is no more valid. The "problem Am" is
  discussed in detail in Gregg & Sing (19) and in Broekhoff /8/.

4 SYMBOLS

Am	area occupied per molecule of adsorbate in the completed monolayer (m^2)
C	constant, defined in eq (4)
C_i	C of the i-th layer (see eq (4))
E_1	heat of adsorption of the first layer $(\frac{j}{K\ mole})$
E_1-L	net heat of adsorption of the first layer $(\frac{j}{K\ mole})$
L	heat of condensation $(\frac{j}{K\ mole})$
M	molecular weight of adsorbate (Kg/K mole)
N	Avogadro's constant $(\frac{1}{K\ mole})$
R	gas constant $(\frac{j}{K\ mole \cdot {}^oK})$
S	specific surface (m^2/Kg material)
T	absolute temperature (^oK)
T_a	temperature of adsorption measurement (^oK)
T_b	boiling point of an adsorbed gaseous impurity (^oK)
W	dry weight of porous sample (Kg)
X	amount of adsorbed vapour (Kg/Kg material)
Xm	amount of adsorbate in a completed monolayer (Kg/Kg material)
$X_{0,2}$	amount of adsorbate at P/p_o = 0,20 (Kg/Kg material)
a	radius of silica fibre in coil spring (m)
b	radius of coil spring (m)
i	intercept of line of eq (3)
k	constant in eq (15). Its value depends on size of adsorbing molecule $(\frac{1}{m})$
n	number of runs of coil spring
p	actual vapour pressure of adsorbate (N/m^2)
p_o	vapour pressure of adsorbate at saturation (N/m^2)
p/p_o	relative vapour pressure
q_s	mass of one monolayer adsorbate on 1 m^2 surface (Kg/m^2)
r	rate of flowing nitrogen, eq (16). (m^3/s)
s	slope of line of eq (3)
$t_{0,2}$	time needed to reach the relative pressure P/p_o=0,20, eq (16)(s)

z	torsional modulus of silica (N/m^2)
α	precision in measurements (Kg/Kg)
Δ_v	correction term in eq (16) (m^3)
ρ	density of adsorbate (Kg/m^3)
σ	sensitivity of adsorption spring balance (m/N)
σ_a	<u>absolute</u> sensitivity of adsorption beam balance (Kg)
σ_r	<u>relative</u> sensitivity of adsorption beam balance $(Kg/Kg$ material$)$
τ_1	lifetime of a molecule in condensed state in the first layer (s)
τ_2	lifetime of a molecule in condensed state in the second or higher layer or in bulk liquid (s)

5 LITERATURE

1   Anderson R B   J Amer Chem Soc 68(1948) p 686.

2   Anderson P J   Introduction to the Physical Chemistry of Ceramic Surfaces. Trans Brit Ceram Soc 3(1966) p 423.

3   Aylmore D W   "Technique Using ^{85}Kr-labelled Krypton for Surface
    Jepson W B   Area Measurements." J Sci Instr 38(1961) p 156.

4   Barrett E P   "The Determination of Pore Volume and Area Distri-
    Joyner L G   butions in Porous Substances. I Computations from
    Halenda P P   Nitrogen Isotherms." J Amer Chem Soc 73(1951) p 373.

5   Beebe R A   "The Determination of Small Surface Areas by Kryp-
    Beckwith J B   ton Adsorption at Low Temperatures." J Amer Chem
    Honig J M   Soc 67(1945) p 1554

6   Bini L   "Modification of the Innes Equation for Determining
    Disch R L   Surface Areas of Low-Area Solids." Anal Chem 31(1959)
    p 1404.

7   Boehm H-P   "Bestimmung der Spezifischen Oberfläche hydrophiler
    Gromes W   Stoffe aus der Phenol-Adsorption." Angew Chem
    71(1959) p 65.

8   Broekhoff J C P   "Adsorption and Capillarity." Waltman Delft 1969.

9   Brunauer S   "The Adsorption of Gases and Vapours." Princeton
    Univ Press, 1943.

10   Brunauer S   Adsorption of Gases in Multimolecular Layers."
    Emmett P H   J Amer Chem Soc 60(1938) p 309.
    Teller E

11   Brunauer S   "The New Model of Hardened Portland Cement Paste."
    Odler I   Highway Res Record No 328(1970) p 89.
    Yudenfreund M

12   Clarke J T   "Surface Area Measurement of Graphite Using the
    γ-Radiation of Kr^{85}." J Phys Chem 68(1964) p 884.

13   Dole M   "Statistical Thermodynamics of the Sorption of Va-
    pours by Solids." J Chem Phys 16(1948) p 25.

14   Emmett P H   "Physical Adsorption in the Study of the Catalysts
    Surface." 12th Rep of the Committee on Catalysts.
    J Wiley & Sons, N. Y. 1940.

15   Feldman R F   "A new Model for Hydrated Portland Cement and its
    Sereda P J   Practical Implications." Eng J Aug/Sept 1970 p 53.

16   Fergusson R R   "Derivation and Development of Hüttig's Multilayer
    Barrer R M   Sorption Isotherm." Trans Farad Soc 46(1950) p 400.

17   Gál S   "Die Methodik der Wasserdampf-sorptionsmessungen."
    Springer-Verlag Berlin, Heidelberg,New York 1967.

18   Gall L   "Über ein neues Gerät zur Schnellen Bestimmung
    Spezifischer Oberflächen." Angew. Mess+Regeltechn.
    4(1964) p a107.

19 Gregg S J   "Adsorption, Surface Area and Porosity."
   Sing K S W   Academic Press, London and New York 1967.

20 Guyer Jr A   "Methoden der Mikrostrukturbestimmung poröser
   Böhlen B   Stoffe." Chimia 17 (1963) p 82.

21 Halsey G   "Physical Adsorption on Non-Uniform Surfaces."
                  J Chem Phys 16(1948) p 931.

22 Haul R   "Vereinfachte Methode zur Messung von Oberflächen-
   Dümbgen G   grössen durch Gasadsorption." Chemie-Ing Techn
                  32(1960) p 349.

23 Haynes J M   "Use of Krypton for Surface Area Measurements."
                  J Phys Chem 66(1962) p 182.

24 Hill T L   J Chem Phys 14(1946) p 263.

25 Hüttig   Monatsch 78 (1948) p 177.

26 Innes W B   "Apparatus and Procedure for Rapid Automatic Ad-
                  sorption, Surface Area and Pore Volume Measurement."
                  Anal Chem 23(1951) p 759.

27 Joy A S   "Methods and Techniques for the Determination of
                  specific Surface by Gas Adsorption."
                  Vacuum Vol III(1953) p 254.

28 Lange K R   "Adsorption Isotherms by a Rapid Flow Method."
                  J Colloid Sci 18(1963) p 65.

29 Mikkail R   "Pore Structures and Surface Areas of Hardened Port-
   Copeland L E   land Cement Pastes by Nitrogen Adsorption.
   Brunauer S   Canad   J of Chem 42(1964) p 426.

30 Nelson F M   Analyt Chem 30(1958) p 1387.
   Eggertsen F T

31 Powers T C   "Physical Properties of Cement Paste." Proc 4th Int
                  Symp on the Chemistry of Cement. Nat Bureau of
                  Standards. Wash DC 1960.

32 Powers T C   "Studies of the Physical Properties of Hardened
   Brownyard TL   Portland Cement Paste." Res Lab Portland Cement Ass
                  Bull 22. 1948.

33 Rosenberg A J "Rapid Precise Measurements of Krypton Adsorption
                  and the Surface Area of Coarse Particles."
                  J Amer Chem Soc 78(1956) p 2929.

34 Ross S   "Physical Adsorption by Homogeneous and Hetero-
                  geneous Solid Surfaces." Fundamental Phenomena in
                  Materials Sci. Vol 2. Plenum Press N.Y. 1966.

35 Scholl F   "Bestimmung der Oberflächengrösse und der Ober-
                  flächeneigenschaften   von Festkörpern mit Hilfe
                  Gaskromatografischer Verfahren. Proc VIII Int Ceram
                  Congr Copenhagen 1962 p 75.

36 Sing S W   "The Determination of Specific Surface Area by
    Swallow D   Low-Temperature Krypton Adsorption." Proc Brit
                    Ceram Soc (1965) p 39.

37 Theimer O   "On Multilayer Adsorption Isotherms." Trans Farad
                    Soc 48(1952) p 326.

38 Winter D G   "A Simple Apparatus for the Evaluation of Pore Size
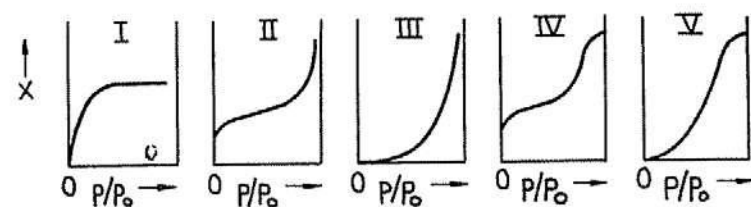   Distribution." Chem & Ind 22(1969) p 233.

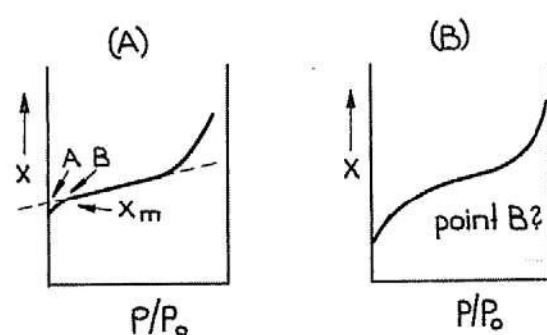FIG 1   The five isotherm types according to Brunauer classification.

FIG 2   The type II isotherm with high (A) and low (B) C-values.
Only (A) gives a well defined "B-point".   /2/
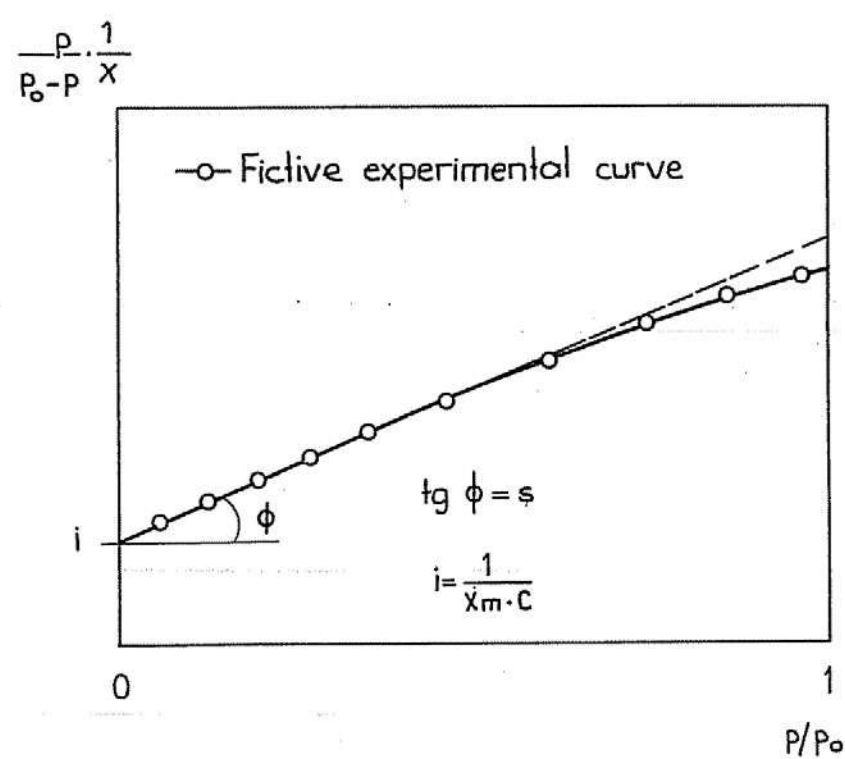
FIG 3   Graphical representation of the BET-equation (3).
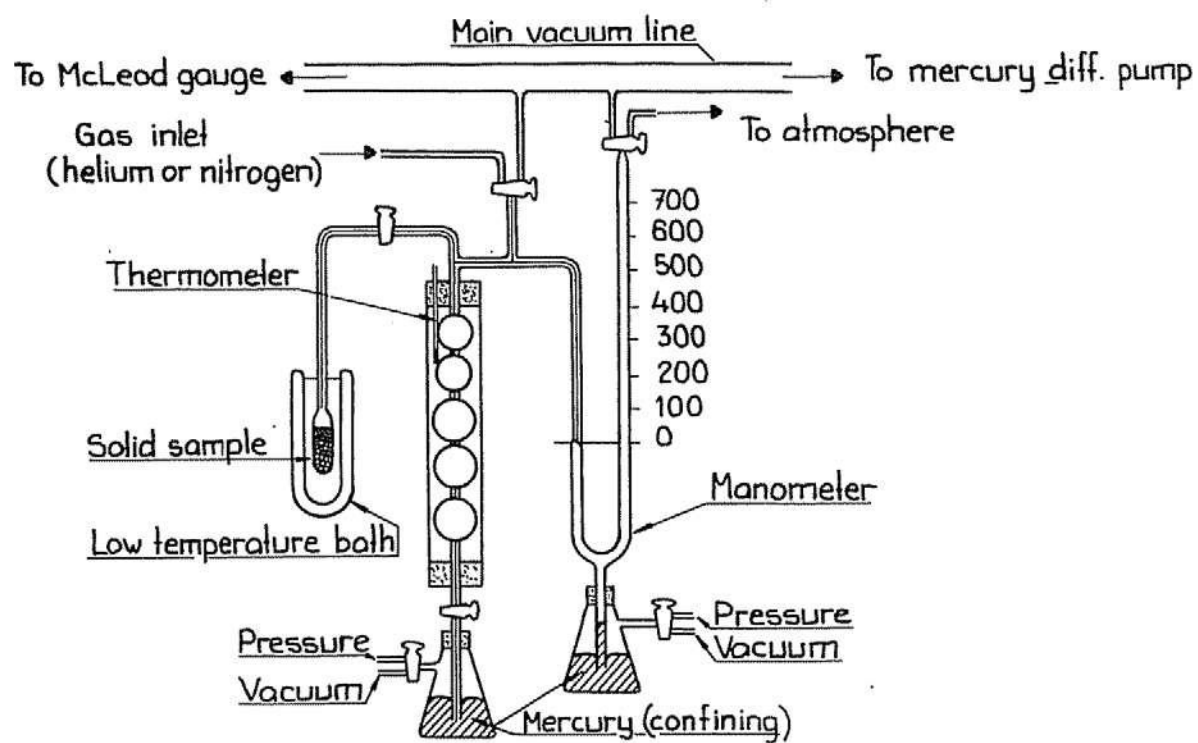
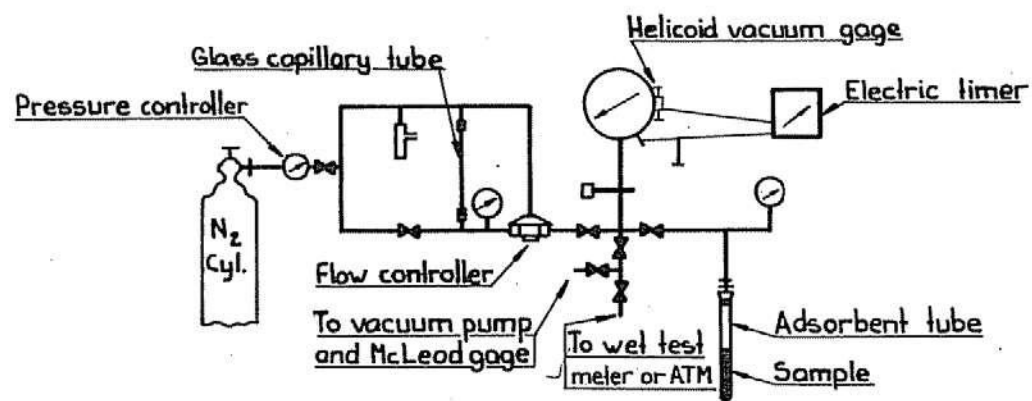FIG 4 The volumetric absorption apparatus of Emmett /14/.

FIG 5 Apparatus for continuous absorption, surface area and pore volume
       measurement. Innes /26/.
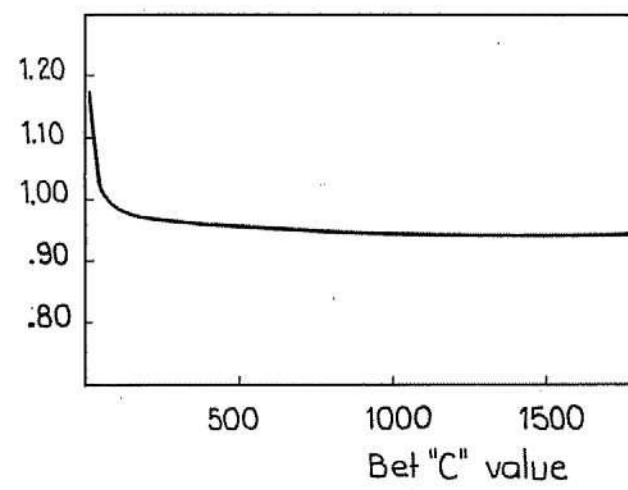
Correction factor

FIG 6   Correction factor for calculating BET surface area from Innes
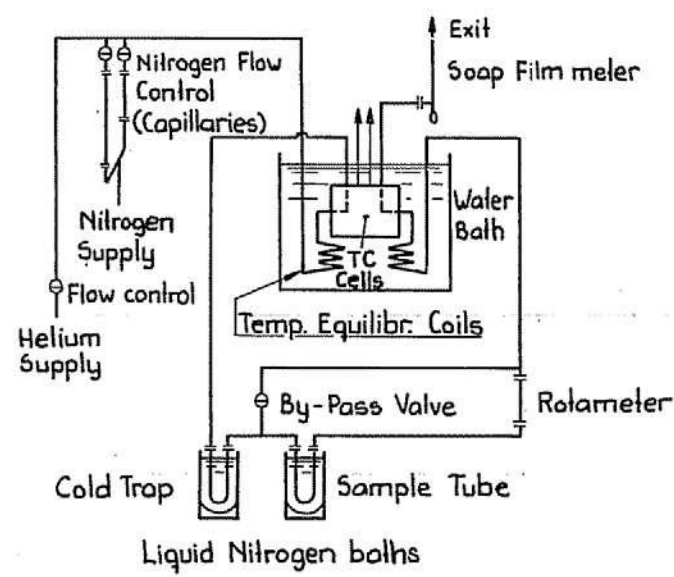   surface area eq (15)   /26/

FIG 7   Schematic diagram of surface area apparatus according to Nelson &
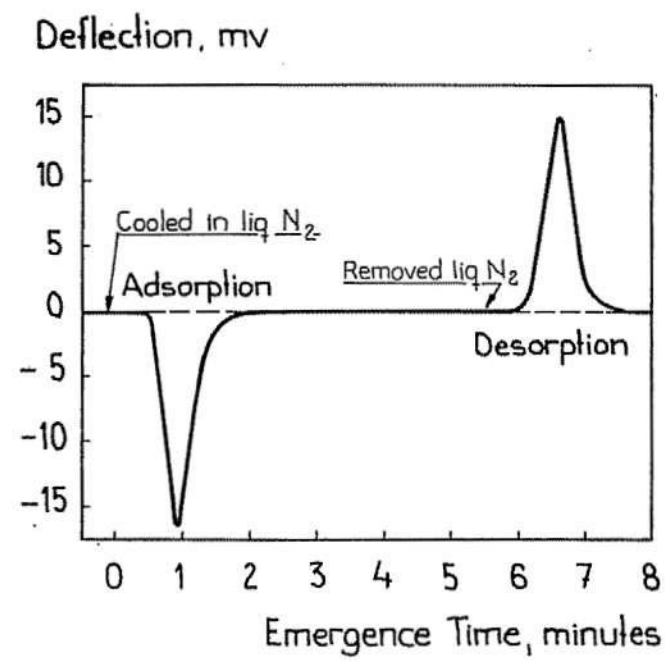   Eggertsen /30/.

FIG 8 Nitrogen absorption and desorption curves at use of apparatus
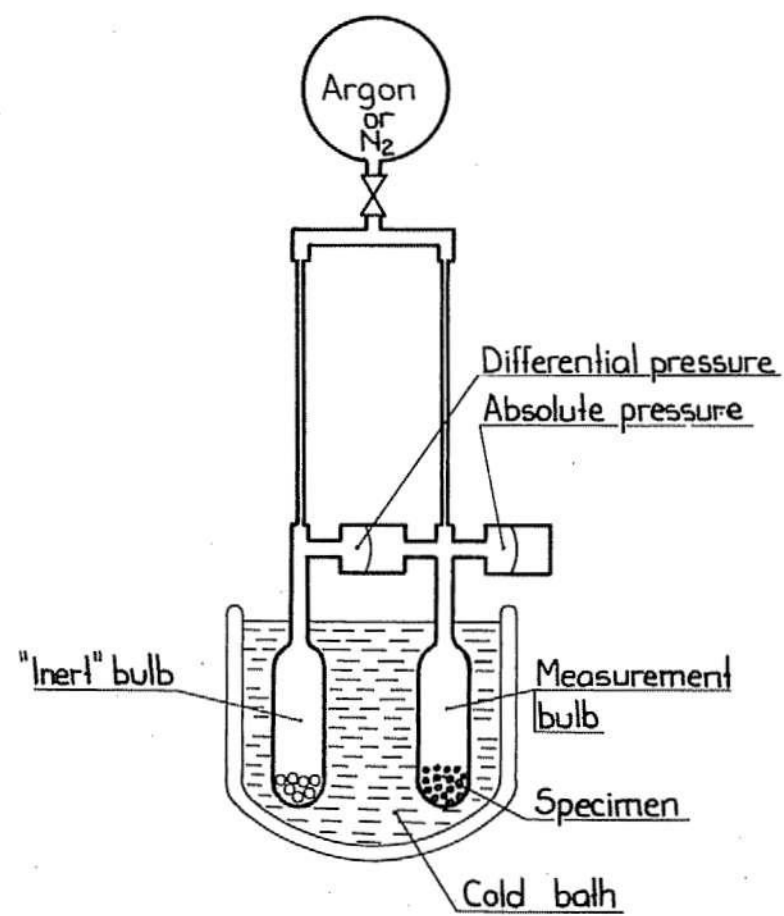according to FIG 7 /30/.

FIG 9 Schematic picture of apparatus based upon principles of Haul
& Dümbgen; Guyer & Böhlen /20/.

Publikationer från Institutionen för Byggnadsteknik vid
Tekniska Högskolan i Lund

Bulletiner

1. Halvorsen, Ulf A. Korrosion och kalkurlakning vid sprickor i betongkonstruktioner. Lund 1966.
2. Lindblad, Sven. Impact sound characteristics of resilient floor coverings. A study on linear and nonlinear dissipative compliance. Lund 1968.
3. Nielsen, Anders. Byggnadsmaterials reologi. Problemställningar och litteratur. Lund 1968.
4. Nielsen, Anders. Krypning hos högtrycksånghärdad gasbetong. Lund 1968.

Interna rapporter

1. Bankvall, Claes G. Principer för teoretisk behandling av konvektionsförloppet i en sluten värmeisolerad konstruktion. Lund 1966.
2. Ahlgren, Lennart. Grundläggande lagar för fuktvandring i porösa byggnadsmaterial. Lund 1966.
3. Ahlgren, Lennart. Uppföljning av uttorkningsförloppet hos golvbetong. Lund 1967.
4. Nielsen, Anders. Orienterande undersökning av krypning hos högtrycksånghärdad gasbetong. Lund 1967.
5. Nielsen, Anders. Orienterande undersökning av krypning under uttorkning hos högtrycksånghärdad gasbetong. Lund 1968.
6. Nielsen, Anders. Lättbetong internationellt sett. Engelska forskningsinstitut. Intryck från London 27-30 maj 1968. Lund 1968.
7. Cronström, Örjan & Forssander, Tom. Undersökning av polyetylenglykolstabiliserat trä. Lund 1968.
8. Åkerlund, Sture. Egentyngdens inverkan på brottrisken - några räkneexempel. Lund 1968.
9. Grönqvist, Nils-Ove. Utmattningshållfasthet hos armeringsstänger. Lund 1968.
10. Grönqvist, Nils-Ove. Statisk hållfasthet hos armeringsstänger tidigare utsatta för pulserande last. Lund 1969.

Rapporter

11. Bankvall, Claes G. Temperaturbestämning och värmeisole-

ringsundersökning genom strålningsmätning. Byggnads-
tekniska tillämpningar av IR-kameran. Lund 1969.

12. Bankvall, Claes G. Research in heat transfer. Lund 1969.
13. Bankvall, Claes G. Porositet och porstorleksfördelning.
Metoder att studera och kvantifiera porositet och por-
storleksfördelning. Lund 1969.
14. Bankvall, Claes G. Ensidig, evakuerbar och roterbar platt-
apparat för värmeisoleringsundersökningar. Lund 1970.
15. Bankvall, Claes G. Värmetransport i fibrösa material.
Lund 1970.
16. Sandberg, Per Ingvar. Icke stationär fukttransport. Be-
räkningar med dator. Lund 1970.
17. Åkerlund, Sture. Säkerhetsproblem vid takkonstruktioner
av trä. Textdel och figurdel. Lund 1970.
18. Jonasson, Hans. The propagation of sound over ground with
and without acoustic barriers. Lund 1971.
19. Bomberg, Mark. Water flow through porous materials. Part 1:
Methods of water transport measurements. Lund 1971.
20. Bomberg, Mark. Water flow through porous materials. Part 11:
Relative suction model. Lund 1971.
21. Bomberg, Mark. Water flow through porous materials. Part 111:
Applications of the relative suction model. Lund 1972.
22. Beständighet, reologi, fukt. En redovisning till Statens
Råd för Byggnadsforskning över forskningen vid avd. bygg-
nadsmateriallära, LTH åren 1968-1971. Lund 1971.
23. Hellsten, Mikael & Toolanen, Bengt. Trä impregnerat med
polyetylenglykol och melaminharts. Lund 1971.
24. Snödjup och vattenvärde. Lund 1971.
25. Bankvall, Claes G. Värmetransport i fiberisolerade konstruk-
tioner. Den naturliga konvektionens betydelse. Lund 1971.
26. Fagerlund, Göran. Samband mellan porositet och materials
mekaniska egenskaper. Lund 1972.
27. Sandberg, Per Ingvar. Samtidig ångdiffusion och luftström-
ning genom ett poröst material. Lund 1971.
28. Nilsson, Leif. Utredning och förslag till provningsmetoder
för korrugerade takplattor av asbestcement. Lund 1971.
29. Samband mellan struktur och egenskaper hos byggnadsmaterial.
Lund 1972.
30. Under publicering.
31. Degerman, Tryggve. Gipsregelväggars funktion som vind-
stabiliserande element. Krafter och deformationer vid

lastupptagning genom skivverkan i gipsplattor. Lund 1972.

32. Boija, Jan, Larsson, Per-Robert & Sandberg, Bengt. Egenskapernas variation med djupet hos ensidigt vakuumbehandlade plattor av stor tjocklek. Lund 1972.

33. Examensarbeten 1966-71. Sammanställning av examensarbeten utförda vid byggnadsmateriallära, LTH. Lund 1972.

34. Fagerlund, Göran. Kritiska vattenmättnadsgrader i samband med frysning av porösa spröda material. Lund 1973.

35. Bodlund, Kaj. Punkt-till-punkt korrelation i efterklangsrum och i väggar monterade i reduktionslaboratorium. Lund 1972.

36. Ahlgren, Lennart. Fuktfixering i porösa byggnadsmaterial. Lund 1972.

37. Under publicering.

38. Bankvall, Claes G. Natural convective heat transfer in insulated structures. Lund 1972.

39. Bankvall, Claes G. Heat transfer in insulation and insulated structure. Lund 1972.

40. Fagerlund, Göran. Significance of critical degrees of saturation at freezing of porous and brittle materials. Lund 1973.

41. Fagerlund, Göran. Methods of characterization of pore structure. Lund 1973.